SPECTRODIRECTIONAL GROUND-BASED REMOTE SENSING USING DUAL-VIEW GONIOMETRY

FIELD BRF RETRIEVAL AND ASSESSMENT OF THE DIFFUSE IRRADIANCE DISTRIBUTION IN SPECTRODIRECTIONAL FIELD MEASUREMENTS

Dissertation

zur

Erlangung der naturwissenschaftlichen Doktorwürde
(Dr. sc. nat.)

vorgelegt der

Mathematisch-naturwissenschaftlichen Fakultät

der

Universität Zürich

von

Jürg Thomas Schopfer

aus

Gsteig b. Gstaad BE

Promotionskomitee
Prof. Dr. Klaus I. Itten (Vorsitz)
Dr. Stefan Dangel
Dr. Mathias Kneubühler

Zürich, 2008

Summary

Earth Observation (EO) data provide information of the surface characteristics with regard to the spatial, spectral, temporal and directional dimensions. In spectrodirectional Remote Sensing the Earth's surface reflectance characteristic is studied by means of its directional (angular) dimension. Almost all natural surfaces exhibit an individual anisotropic reflectance behaviour, which is described by the bidirectional reflectance distribution function (BRDF). BRDF effects in remotely sensed data occur in dependence on the specific observation-illumination geometry present for each pixel of the image during data acquisition. Various applications, such as BRDF correction of remote sensing data and quantitative retrieval of vegetation or soil parameters therefore require accurate knowledge of spectrodirectional surface reflectance properties. However, the target specific bidirectional reflectance factors (BRF) cannot directly be measured but need to be retrieved from spectrodirectional measurements usually performed with goniometer systems either in the field or in a laboratory environment. Field goniometry has the advantage that the target is left in its natural environment, including the natural illumination by the sun. The major disadvantage, however, is that atmospheric effects and undesired time variations of the illumination have to be taken into account. Laboratory goniometry on the other hand allows for a better control of environmental conditions but measurement results are subject to conical illumination geometry and the inhomogeneity of the illuminated area. Therefore, the directly measured quantities for field and laboratory goniometry are only approximations to the real target BRF. The most exact BRF retrieval (correction of the diffuse illumination due to the atmosphere) from field goniometer measurements can be achieved by following the procedure proposed by Martonchik et al. (1994) provided that the incoming diffuse radiation is observed as a function of the observation angles. However, most goniometer measurement setups do not account for this. Others do so, but only over a limited spectral extent (multispectral) or are not yet operational. Consequently, prior to the study at hand, no operational hyperspectral goniometer system, which is able to characterize the angular distribution of the reflected and incoming radiation field, existed.

The presented dissertation primarily focuses on field goniometry and the assessment of the diffuse influence in spectrodirectional field measurements. The main research questions are 1) how can the required input quantities for the BRF retrieval be accurately measured, 2) to what extent are traditional field reflectance measurements influenced by the diffuse irradiance and 3) to what extent do directional effects influence vegetation parameters derived from ground-based and spaceborne multiangular measurements.

Results consist of the development and characterization of the first *hyperspectral* dual-view field goniometer system (dual-view FIGOS), which is able to *simultaneously* obtain the reflected *and* the incoming diffuse radiation at high angular resolution. A reliable characterization of the angular distribution of the incoming diffuse illumination is presented for several atmospheric conditions and the performed field BRF retrieval for an artificial, as well as a natural target led to a reasonable assessment of the diffuse influence. Furthermore, this study clearly demonstrated the necessity of accounting for atmospheric changes during the measurement period. The direct comparison of multiangular spaceborne and ground-based measurements revealed that forward scattering reflectance

is especially sensitive to target heterogeneity and associated canopy element scales, which both strongly affect the distribution of illuminated and shadowed surface areas.

The dual-view FIGOS showed a stable and reliable performance during several extensive measurement campaigns and strongly supports future surface BRF generation being used for e.g. model validation and inversion purposes as well as for albedo calculations. Additionally, its combined use with multiangular spaceborne or airborne data acquisition provides the possibility of improved directional calibration instead of using nadir-view ground-truth measurements.

Zusammenfassung

Unter Einsatz von Erdbeobachtungsmitteln werden eine Vielzahl von Daten erhoben, welche Informationen zur Charakterisierung der Erdoberfläche liefern. Dabei spielen nicht nur räumliche, zeitliche und spektrale, sondern auch direktionale (richtungsabhängige) Aspekte eine wichtige Rolle. Die meisten natürlichen Oberflächen weisen ein für sie typisches anisotropes Reflektanzverhalten auf, welches sich physikalisch durch die so genannte bidirektionale Reflektanz Verteilungsfunktion (BRDF = "bidirectional reflectance distribution function") beschreiben lässt. Solche BRDF Effekte entstehen in Fernerkundungsdaten während der Datenerhebung, da jedes einzelne Bildelement (Pixel) einem leicht anderen Beobachtungswinkel unterliegt. Anwendungen, welche auf Erdbeobachtungsdaten basieren, wie z.B. die Abschätzung von Vegetations- und Bodenparametern oder aber auch die BRDF Korrektur von Bilddaten, profitieren somit von genauen Kenntnissen der direktionalen Oberflächen–Reflektanzeigenschaften. Um diese Eigenschaften zu messen, werden in der Praxis oft Goniometersysteme eingesetzt, und zwar sowohl unter Labor- als auch unter Feldbedingungen. In beiden Fällen können nur Annäherungen an die tatsächlichen bidirektionalen Reflektanzfaktoren (BRF = "bidirectional reflectance factor") gemessen werden. Spektrodirektionale Feldexperimente besitzen den Vorteil, dass das Messobjekt in seiner natürlichen Umgebung belassen werden kann und einer natürlichen Einstrahlung durch die Sonne ausgesetzt ist. Erschwerend kommt hinzu, dass atmosphärische Einflüsse (Wolken, Aerosole, etc.) sowie sich zeitlich ändernde Einstrahlungsverhältnisse (Bewegung der Sonne) berücksichtigt werden müssen. Laborexperimente erlauben frei einstellbare Beleuchtungswinkel und werden unter kontrollierbaren Messbedingungen durchgeführt. Sie unterliegen aber einer nicht-parallelen und inhomogenen Beleuchtung des Messobjektes durch die verwendete Lichtquelle. Dementsprechend müssen sowohl Feldmessungen wie auch Labormessungen korrigiert werden, um die tatsächliche BRF der gemessenen Oberfläche zu erhalten (BRF "retrieval"). Das zurzeit exakteste BRF "retrieval" für spektrodirektionale Feldmessungen basiert auf einem Ansatz von Martonchik u.a. (1994). Diese Methode setzt voraus, dass nicht nur die reflektierte Strahlung sondern auch die einfallende diffuse Strahlung als Funktion der Beobachtungswinkel bekannt ist, resp. gemessen wird. Die meisten verwendeten Goniometersysteme sind dazu entweder nicht in der Lage, messen die einfallende diffuse Strahlung nur in selektiven spektralen Bändern (multispektral) oder sind noch nicht operationell. Es existierte bis anhin kein hyperspektrales Goniometersystem, welches die oben erwähnten Voraussetzungen erfüllte.

Die vorliegende Dissertation beschäftigt sich vor allem mit Feldgoniometrie und der Berücksichtigung des diffusen Einflusses auf spektrodirektionale Feldmessungen. Die Forschungsfragen konzentrieren sich auf: 1) wie können die erforderlichen Grössen für ein Feld BRF "retrieval" gemessen werden, 2) in welchem Ausmass sind herkömmliche Reflektanzmessungen von der diffusen Einstrahlung betroffen und 3) inwiefern sind Vegetationsparameter, welche von bodengestützten und satellitengestützten multiangularen Messungen abgeleitet werden, von direktionalen Effekten beeinflusst?
Die Resultate beinhalten die Entwicklung und Charakterisierung des ersten *hyperspektralen* Feldgoniometers ("dual-view FIGOS"), welches in der Lage ist *gleichzeitig* die vom Objekt reflektierte *und* die einfallende diffuse Strahlung mit einer hohen Winkelauflösung zu messen. Die

richtungsabhängige Verteilung der einfallenden diffusen Strahlung wird für verschiedene atmosphärische Zustände untersucht und das Feld BRF “retrieval” für eine künstliche sowie eine natürliche Oberfläche durchgeführt. Entsprechende Ergebnisse zeigen die Korrektur des diffusen Einflusses. Dabei wird auch aufgezeigt, inwiefern atmosphärische Veränderungen, welche während der Messperiode auftreten, berücksichtigt werden können. Der direkte Vergleich von multiangularen satellitengestützten und bodengestützten Messungen verdeutlicht, dass insbesondere die vorwärts gestreuten Reflektanzen von der Oberflächenheterogenität und damit einhergehenden Skaleneffekten beeinflusst werden.

Zusammenfassend sei hervorgehoben, dass das “dual-view FIGOS” während mehrerer ausgiebigen Feldkampagnen sehr zuverlässig funktionierte und in der Lage ist, auch für die zukünftige Herleitung von Oberflächen BRF geeignete Messungen zu liefern. Solche Daten können sowohl für die Validierung und Inversion von Modellrechnungen, als auch für Albedo Berechnungen verwendet werden. Die Kombination von multiangularen satellitengestützten und bodengestützten Messungen bietet desweitern Möglichkeiten zu verbesserten Kalibrationsmethoden basierend auf direktionalen Daten anstelle von herkömmlichen Nadirdaten.

Table of Contents

List of Figures

List of Tables

List of Abbreviations

ABRAMS	Automated Bidirectional Reflection Acquisition Measurement System
ADEOS	Advanced Earth Observation Satellite
ATCOR	ATmospheric CORrection model
AGS	Automated Goniometer System
ASD	Analytical Spectral Devices Inc.
AVHRR	Advanced Very High Resolution Radiometer
BCRF	Biconical Reflectance Factor
BHR	Bi-Hemispherical Reflectance
BRDF	Bidirectional Reflectance Distribution Function
BRF	Bidirectional Reflectance Factor
CARBON-3D	Earth Observation mission for mapping global biomass
CBD	Convention on Biological Diversity
CCD	Charge Coupled Device
CHARISMA	Coblentz Hemisphere based Angular Resolved and Integral Scattering Measurement Apparatus
CHRIS	Compact High Resolution Imaging Spectrometer
CLabSpeG	Compact Laboratory Spectro-Goniometer
CNES	Centre National d'Etudes Spatiales
DEM	Digital Elevation Model
DHR	Directional Hemispherical Reflectance
DLR	German Aerospace Center
DOY	Day of Year
DTM	Digital Terrain Model
EGO	Former European Goniometric Facility, today at Joint Research Centre, Ispra (I)
ER-2	NASA research aircraft used for AirMISR
ESA	European Space Association
FiGIFiGo	Finnish Geodetic Institute Field Goniospectrometer
FIGOS	FIeld Goniometer System of RSL
FOV	Field of View
FWHM	Full Width Half Maximum
FZA	Fly-by Zenith Angle
GCOS	Global Climate Observing System
GCP	Ground Control Point
GEO	Group on Earth Observation
GER3700	Spectroradiometer of Spectra Vista Corporation
GEOSS	Global Earth Observation System of Systems
GIFOV	Ground Instantaneous Field Of View
GMES	Global Monitoring of Environment and Security
GRASS	Gonio Radiometer Spectrometer System

GSFC	Goddard Space Flight Center
HCRF	Hemispherical Conical Reflectance Factor
HDRF	Hemispherical Directional Reflectance Factor
IAC ETH	Institute for Atmospheric and Climate Science at ETH, Zurich, Switzerland
IPCC	Intergovernmental Panel on Climate Change
IWMMM	International Workshop on Multiangular Remote Sensing, Measurements and Models
LAGOS	LAboratory Goniometer System of RSL
LAI	Leaf Area Index
LT	Local Time
MFR-7	Multi-Filter Rotating Shadowband Radiometer
MGS	Mobile Goniometer System
MISR	Multiangle Imaging Spectro Radiometer
MODIS	Moderate Resolution Imaging Spectroradiometer
MODTRAN	MODerate spectral resolution atmospheric TRANsmittance
MUFSPEM	Mobile Unit for Field Spectroradiometric Measurements
NASA	National Aeronautics and Space Administration
NDVI	Normalized Difference Vegetation Index
NIR	Near InfraRed
NPL	National Physical Laboratory of United Kingdom
ONERA	Office National d'Etudes et de Recherches Aérospatiales (National Aerospace Research Center, France)
PARABOLA	Portable Apparatus for Rapid Acquisition of Bidirectional Observations of Land and Atmosphere
POLDER	Polarization and Directionality of the Earth's Reflectances
PRI	Photochemical Reflectance Index
PROBA	Project for On-Board Autonomy
RAMI	Radiative Transfer Model Intercomparison
RS	Remote Sensing
RSL	Remote Sensing Laboratories, Institute of Geography, University of Zurich
RT	Radiative Transfer
SNR	Signal to Noise Ratio
SPECTRA	Surface Processes and Ecosystem Changes Through Response Analysis
SPECCHIO	Spectral database of RSL
SRTM	Shuttle Radar Topography Mission
SWIR	ShortWave InfraRed
TERRA	NASA EOS satellite platform (launched April 1999)
TUM	Technical University of Munich, Germany
UN	United Nations
UNEP	United Nations Environment Program

UNFCC	United Nations Framework Convention on Climate Change
VI	Vegetation Index
VIS	VISible spectral range
VNIR	Visible to Near InfraRed
WAAC	Wide Angle Airborne Camera
WMO	World Meteorological Organization

List of Symbols

E	Irradiance	$[Wm^{-2}]$
E_{dir}	Direct irradiance	$[Wm^{-2}]$
E_{diff}	Diffuse irradiance	$[Wm^{-2}]$
$E_{tot,\ mfr}$	Irradiance derived from MFR-7 measurements	$[Wm^{-2}]$
$E_{tot,\ asd}$	Irradiance derived from ASD measurements	$[Wm^{-2}]$
c_{mfr}	Intercalibration coefficient between MFR-7 sunphotometer and ASD FieldSpec F3 spectroradiometer	dimensionless
Δ	Deviation from Lambertian reflectance characteristic	dimensionless
δ	Fractional deviation	dimensionless
f_{diff}	Weight factor for diffuse incident radiance	dimensionless
f_{tot}	Weight factor for reflected radiance	dimensionless
L	Radiance	$[Wm^{-2}sr^{-1}]$
L^{inc}	Incoming radiance	$[Wm^{-2}sr^{-1}]$
L_r	Reflected radiance from the target	$[Wm^{-2}sr^{-1}]$
L_{ref}	Reflected radiance from the reference panel	$[Wm^{-2}sr^{-1}]$
L_{diff}	Upward (from the target) diffuse radiance	$[Wm^{-2}sr^{-1}]$
L_{diff}^{inc}	Incoming diffuse radiance	$[Wm^{-2}sr^{-1}]$
λ	Wavelength	[nm], [µm]
N	Number of measurements per goniometer dataset	dimensionless
R, ρ	Reflectance factor	dimensionless
R_{ref}	Reflectance factor of reference panel	dimensionless
ρ_{ls}	Albedo of Spectralon derived by Labsphere	dimensionless
θ_i, φ_i	Zenith and azimuth angle of the direction of illumination	[°]
θ_r, φ_r	Zenith and azimuth angle of the direction of reflection	[°]
$-\mu$, μ	Cosine of the view and solar zenith angle	[°]

Sub- and superscripts

diff	Diffuse
dir	Direct
inc	Incoming
ref	Reference
tot	Total
r	Reflected
i	Incident
ls	Labsphere

1 Introduction

1.1 Background and scientific setting

Knowledge of the status of the Earth and its environmental processes is becoming increasingly important and is providing the basis for the management of our environment and our ability to derive sustainable benefit from it. Growing populations and increasing human activities are having a profound impact on natural resources and are leading to a continuous change of our environment. Expressions thereof consist of deforestation, manipulation of hydrological resources, occurrence of man-made fires, fossil fuel burning, increasing urbanization, loss of biodiversity, etc. These types of environmental management occur at variable local and regional scales but will finally sum up to produce global changes with major influences on the Earth system (ESA, 2006).

The political awareness of global change and its effects is raised and expressed in several environmental conventions and intergovernmental treaties. In a broad thematic view environmental objectives are formulated within the UN Millenium Project Report to the UN Secretary-General (UN Millenium Project, 2005) as support for national implementation strategies. More concisely, Climate Change issues are addressed by the Intergovernmental Panel of Climate Change (IPCC) and the Kyoto Protocol to the United Nations Framework Convention on Climate Change (UNFCCC). The Kyoto Protocol also accounts for carbon sinks associated to vegetation growth and expansion. Systematic monitoring of land use change in this context becomes an important control mechanism and is part of the cooperation with the Global Climate Observing System (GCOS) secretariat of the World Meteorological Organization (WMO) (WMO, 2006). Another high-ranking issue in global environmental governance is biological diversity, which strongly interacts with relevant ecosystem characteristics such as structure, nutrient cycling, productivity and vulnerability. At the 1992 Earth Summit in Rio de Janeiro, Brazil, world leaders agreed on a comprehensive strategy for sustainable development formulated in the Convention on Biological Diversity (CBD) and in 2002, the Conference of the Parties to the CBD adopted a strategic plan including the target to achieve a significant reduction of the current rate of biodiversity loss at global, regional and national levels by 2010 (UNEP, 2002). Further environmental issues associated with global change are addressed by intergovernmental directives such as the UN Convention to Combat Desertification (UN, 1994) and the Ramsar Wetland Convention (UN, 1971). Hazardous environmental and technological events such as earthquakes, floods, forest fires and oils spills are also topics, which request accurate knowledge and monitoring of the Earth. In order manage large disasters the International Charter “Space and Major Disasters” was initiated by the European and French Space Agencies (ESA and CNES) in 1999 (International Charter, 1999). It aims at providing a unified system of space data acquisition and delivery to those affected by natural or man-made disasters and was declared formally operational in 2000.

In support of the implementation and surveillance of these policies the environmental state and its processes need to be assessed and continuously monitored. Remote Sensing (RS) from spaceborne, airborne and ground-based platforms is an excellent tool for monitoring such ecological processes at

various spatial and temporal resolutions. On a global level, the intergovernmental Group on Earth Observation (GEO) is leading a worldwide effort to build a Global Earth Observation System of Systems (GEOSS). It is based upon regional, national and international systems in order to provide comprehensive and coordinated Earth Observation data for a broad range of societal benefit areas (GEO, 2005). The main European contribution to GEOSS is the European initiative Global Monitoring of Environment and Security (GMES) which services, among others, cover mapping of the Earth surface and its land-use, supporting of emergency management in case of hazards and forecasting applied for marine zones, air quality or crop yields.
As a consequence, a large number of Remote Sensing systems are used to observe the Earth's surface from spaceborne as well as from airborne and ground-based platforms. Technical as well as operational requirements of such sensor systems strongly depend on their intended engagement and the thematic field to be monitored (land surface, atmosphere, ocean).

1.2 Spectrodirectional Remote Sensing

In spectrodirectional Remote Sensing the Earth's surface reflectance characteristics is studied by means of their angular dimension. Almost all natural surfaces exhibit an individual anisotropic reflectance behaviour due to the contrast between the optical properties of surface elements and background and the geometric surface properties of the observed scene. Basically it means that a target area under a certain illumination condition is seen differently when looking at it from one direction as when observing it from another direction. The underlying concept, which describes the reflectance characteristic of a specific surface area, is called the bidirectional reflectance distribution function (BRDF). On the one hand, optical sensors operate with a specific field of view (FOV) and thus, each pixel in a remotely sensed image is observed under a slightly different observation angle. Such BRDF effects affect all remotely sensed data and the quality of retrieved products to a certain extent and need to be accounted for (Beisl, 2001). On the other hand, BRDF effects can be studied to gain additional information for quantitative retrieval of e.g. vegetation (Strub et al., 2002; Weiss et al., 2000), snow (Painter, 2002) or soil (Gobron et al., 2000) parameters. Thus, no matter which strategy is followed accurate knowledge of the spectrodirectional behaviour of the targets of interest is essential.

Since the 1990s a data basis for such studies is being provided by various multiangular instruments on spaceborne and airborne sensor platforms (e.g. CNES POLDER on ADEOS, NASA MISR on TERRA, AirMISR on ER-2). Among them, the British CHRIS (Compact High Resolution Imaging Spectrometer, launched in 2001) instrument on board of the Belgian PROBA platform can be considered as the first full spectrodirectional spaceborne instrument (Schaepman, 2006). In addition, several ground-based field and laboratory goniometer systems have been developed over the years (e.g. AGS, MGS, FIGOS, LAGOS, GRASS etc). They allow for accurate validation of data derived from air- and spaceborne sensors and provide new insights by supporting current BRDF research. A comprehensive overview of various ground-based goniometer systems is given in Table 1.

Although the importance of the BRDF is known and is centrally represented in various data processing chains it is often neglected for many applications. Reasons for that are attributed to the complexity of

determining accurate surface BRF quantities as well as to the fact that current correction algorithms still base on coarse approximations of the true surface specific BRF. However, in 1996 a first International Workshop on Multiangular Remote Sensing, Measurements and Models (IWMMM-1) has been initiated and took place in Beijing, China. Many ideas for further cooperation and research were raised addressing topics such as the combination of ecological and radiation models (the studied canopy is an overlap area with "the same sun"), structure based vegetation classification, bridging the gap between the leaf and canopy level, development and comparison of model standards etc. Furthermore, it was noted that "point" spectrodirectional measurements of selected targets under laboratory and under field conditions provide valuable information for model development, validation and inversion techniques. With regard to the spatial dimension and target scales, "area" spectrodirectional measurements using ground-based, airborne and spaceborne sensors (AVHRR, POLDER, MODIS, MISR, Spot-Vegetation) were proposed.
In the following years a spectrodirectional research community was established and regular workshops were held in 1999 (IWMMM-2, Ispra, Italy), 2002 (IWMMM-3, Steamboat Springs, USA) and last but not least in 2006 (IWMMM-4, Sydney, Australia). The presented results cover a wide range of applications in order to estimate surface BRDFs from space as well as from airborne and ground-based measurements. Among that, a BRDF library of selected soil and vegetation targets was compiled (Schönermark et al., 2004) and a RAdiative transfer Model Intercomparison (RAMI) initiative was established[1] (Pinty et al., 2001; Pinty et al., 2004; Widlowski et al., 2007). However, some concerns about the future of multiangular remote sensing were also expressed. These concerns mainly base on the facts that currently no follow-on missions are planned for the leading multiangular spaceborne instruments MISR and CHRIS since similar projects for pointable instruments such as SPECTRA (Rast, 2004) or CARBON-3D (Hese et al., 2005) were not selected for further development by ESA and DLR, respectively. Therefore, a corresponding letter expressing the opportunities of multiangular remote sensing evolved from IWMMM-4 and has been sent to the nations, organizations, committees and individuals as well as to the US National Academy of Sciences Decadal Survey for Earth Science (Jupp et al., 2006).

1.3 Directional reflectance anisotropy

Causes for target specific reflectance anisotropy are related to e.g. specular surface reflectance, volumetric scattering and shadow casting which all together influence the measured signal from a complex natural surface. Various studies (Hapke et al., 1996; Kimes, 1983; Sandmeier et al., 1998a) showed that directional effects in vegetation canopies are primarily related to the distribution of shadow and can be explained by the *gap* and *backshadow* effect, respectively. The gap effect predominantly occurs for canopies with vertically oriented structures such as forests or wheat, which allows observing the lower and less illuminated levels. The backshadow effect occurs for sensor positions opposite of the illumination source from where the sensor observes the not illuminated "backside" of the target. However, for such observation directions the gap effect is typically lower and the combination of the two leads to a reflectance minimum for slightly forward scattering directions and a reflectance maximum for backward scattering directions. The special case where the

[1] http://rami-benchmark.jrc.it

illumination direction is identical to the observation direction is called the *hotspot*. Typically, measurements for the exact hotspot configuration cannot be done since either the sensor or the illumination source (laboratory) shadows the target area.

The observed contrast between illuminated and shadowed areas within a scene is mainly driven by absorption and multiple scattering processes inside the canopy architecture. With lower absorption there is more light available for multiple scattering and reflectance structures generally tend to be higher and more isotropic. The opposite is the case for high absorption where less light is available for further scattering. With regard to vegetation canopies this leads to most distinct directional effects in the RED whereas the same effects are less pronounced in the GREEN and especially in the NIR spectral region. It has been shown by simulations and measurements that the canopy architecture and multiple scattering are interrelated, such that an increasing number of canopy layers leads to increased multiple scattering (Camillo, 1987).

Typically, the total incident light in a natural environment consists of a direct irradiance component, which is incident from the exact sun view direction, and a diffuse component incident from all directions. The distribution and the amount of the incoming diffuse radiation depend on the zenith angle of the illumination source and on the atmospheric conditions (aerosol, clouds, etc). In a study described by Privette et al. (2004) the effect of various atmospheric conditions (clear, hazy) on the surface directional reflectance has been modeled for a vegetation target. It has been found that the backscattering and especially the hotspot reflectance is dominated by the amount of direct irradiance whereas the forward scattering is more related to the diffuse irradiance. For hazy atmospheric conditions (increased diffuse irradiance) the direct irradiance fraction is lower and consequently the directly illuminated facets in the backward scattering reflect slightly less light than on a clear day. On the other side, the hazy condition (more diffuse light) leads to an increased forward scattering reflectance. The reason is that each of the diffuse radiance beams creates a tiny hotspot reflectance peak for its respective incident direction (Lyapustin et al., 1999).

1.4 Directional reflectance terminology

Although a non-measurable theoretical quantity, the bidirectional reflectance distribution function (BRDF) f_r is a fundamental expression of the reflectance characteristic of a specific surface area. As defined by Nicodemus et al. (1977) it is the ratio of the reflected radiance L [Wm^{-2} sr^{-1} nm^{-1}] in one specific direction θ_r, φ_r to the incident irradiance E [Wm^{-2} nm^{-1}] from the direction θ_i, φ_i. and can be written as

$$f_r(\theta_i,\varphi_i,\theta_r,\varphi_r,\lambda)=\frac{dL_r(\theta_i,\varphi_i,\theta_r,\varphi_r,\lambda)}{dE(\theta_i,\varphi_i,\lambda)}. \quad (1)$$

However, for practical reasons the more common bidirectional reflectance factor (BRF) R is used to describe the surface reflectance anisotropy. It is defined as the ratio of the reflected radiance from the surface L_r into a specific direction to the reflected radiance from a lossless, Lambertian reference panel

L_{ref} measured under identical observation and illumination conditions. R_{ref} is the actual BRF of the reference panel and corrects the target BRF R for the loss and the non-Lambertian behaviour of the reference panel (see Chapter 4.5). The target BRF R is then written as

$$R\left(\theta_i,\varphi_i,\theta_r,\varphi_r,\lambda\right) = \frac{L_r\left(\theta_i,\varphi_i,\theta_r,\varphi_r,\lambda\right)}{L_{ref}\left(\theta_i,\varphi_i,\theta_r,\varphi_r,\lambda\right)} * R_{ref}\left(\theta_i,\varphi_i,\theta_r,\varphi_r,\lambda\right). \quad (2)$$

Along with the growing spectrodirectional research community and the evolvement of newer technological possibilities an increasing appreciation of the different reflectance quantities could be observed and has been strengthened over the past decade. It has also been noted that not only the illumination and observation direction influence the measured reflectance quantity but also the FOV of the particular sensor (Schaepman-Strub et al., 2006). Based on Nicodemus et al. (1977) the various reflectance quantities and their terminology are shown in Figure 1.

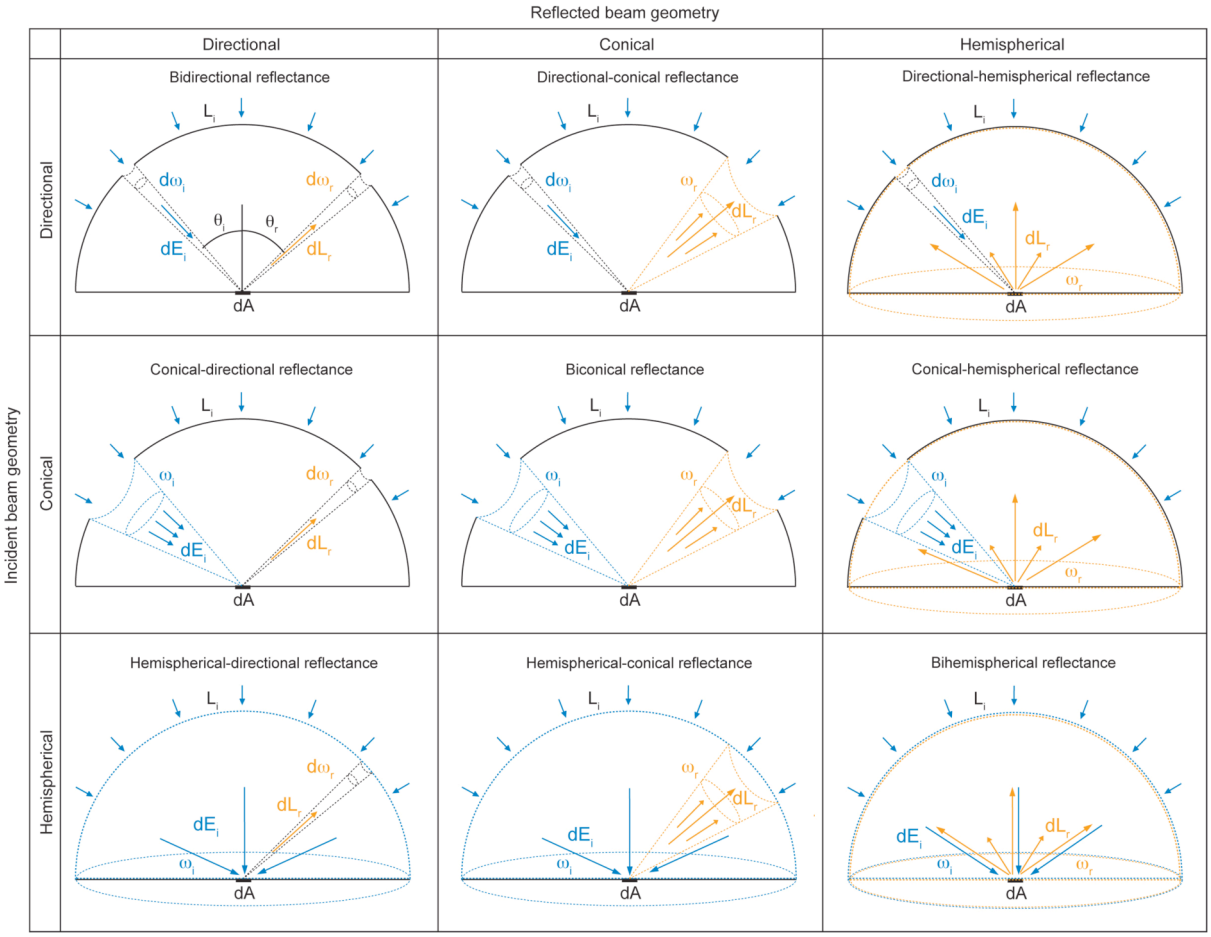

Figure 1: Overview of different reflectance quantities with respect to the incident and reflected beam geometry based on Nicodemus et al. (1977). Quantities of the incident and reflected radiation are represented by blue and orange colors, respectively.

The graphics in Figure 1 represent a thought experiment consisting of a large opaque hemisphere which is positioned over the target area dA in such a way that the target lies in the center of the base

area of the hemisphere. Outside the hemisphere there exists a field of radiation. Corresponding to the respective (incident and reflected) beam geometries, holes are cut in the spherical surface of the hemisphere in order to admit radiation from outside reaching the target area dA and being reflected towards the receiver, which is placed outside the hemisphere. The hemisphere is assumed so large compared to dA that only radially-directed rays of radiance $L_i(\theta_i,\varphi_i)$ can enter the opaque hemisphere. For all cases $L_i(\theta_i,\varphi_i)$ is assumed isotropic for all directions within the defined solid angle ω_i. Further in-depth information concerning this thought experiment can be found in Appendix B of Nicodemus et al. (1977).

In practice the target BRF can only be approximated by measurements since an infinitesimal small sensor FOV would be required. Knowing the respective surface BRF, all other quantities can be obtained by angular integration. Laboratory measurement results typically consist of biconical reflectance factors (BCRF) since both the illumination and observation geometries are conical. Measurement results obtained under hemispherical illumination conditions are called hemispherical conical reflectance factors (HCRF) corresponding to the respective geometries. However, the conicality is often neglected and corresponding results are called BRF and HDRF for the laboratory and the field case, respectively. For a small sensor FOV (< 3°) this might be acceptable.

Note, that by following the definition from Nicodemus et al. (1977) HCRF and HDRF are only defined for completely diffuse irradiance within the respective incident solid angle. However, this assumption does usually not correspond to an actual field measurement situation where direct and anisotropic distributed diffuse radiation is present. The reflectance quantity of the more general field case has been described by Martonchik et al. (2000) and Schaepman-Strub et al. (2006) and is graphically represented in Figure 2.

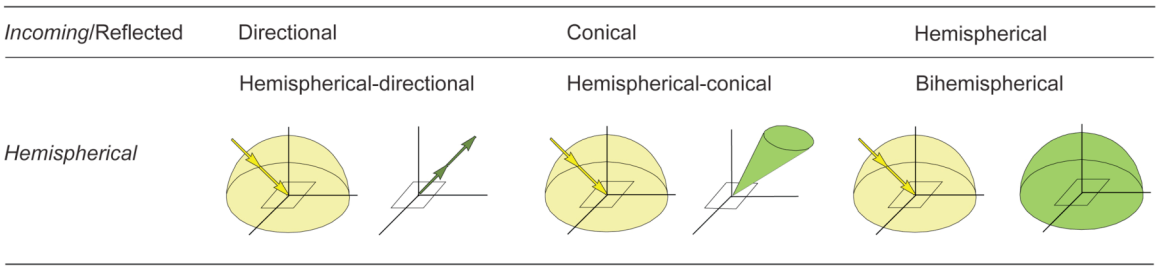

Figure 2: Reflectance quantities as obtained under actual field conditions where direct and diffuse radiation is present (Schaepman-Strub et al., 2006).

From Figure 1 and Figure 2 it can be identified that the same term “hemispherical” is used in an ambiguous way for the incident radiation characterization. This is often not recognized and, therefore, it is important to clearly characterize the reflectance quantity by means of the beam geometry and the radiation distribution within the solid angle of the incident beam. Furthermore, since the observation geometry also consists of a cone with a given solid angle corresponding to a sensor’s instantaneous field of view (IFOV), a sensor response function should be included, if the sensitivity of the sensor depends on the location within the rim of the cone (Schaepman-Strub et al., 2006).

In order to avoid misunderstandings the following definitions will be used throughout this work:

The laboratory case is called "BCRF" or "laboratory case" and the field case is called "field HCRF" or "field case".

1.5 Motivation and research questions

The presented research is related to the retrieval of the BRF from spectrodirectional field measurements. Ground level measurements of spectrodirectional surface reflectance properties can be performed using goniometer systems either in the field (Abdou et al., 2000; Sandmeier, 2000) or in a laboratory environment (Sandmeier et al., 1998b). However, there are obvious technical differences between the two concepts and corresponding measurements are not directly comparable (Dangel et al., 2005). Field goniometry has the advantage that the target is left in its natural environment, including the natural illumination by the sun. The major disadvantage is that atmospheric effects and undesired time variations of the illumination have to be taken into account. Laboratory goniometry on the other hand allows for a better control of environmental conditions but measurement results are affected by conical illumination geometry and the inhomogeneity of the illuminated area. In order to compare field and laboratory spectrodirectional measurements it is necessary to retrieve the BRF separately for each case for a specific target of interest. For the laboratory case an accurate BRF retrieval is described by Dangel et al. (2005). The most exact BRF retrieval from field goniometer measurements involves the correction of the diffuse irradiance and can be achieved by following the procedures proposed by Martonchik and others (Lyapustin et al., 1999; Martonchik, 1994). However, this implies accurate knowledge of the angular distribution of the incoming diffuse radiation at the same time as reflected radiances from the target are collected. With the Portable Apparatus for Rapid Acquisition of Bidirectional Observations of Land and Atmosphere (PARABOLA) such data can be collected to a certain degree, but over a limited spectral range only and under the assumption of an extensive homogeneous target area (Bruegge et al., 2000).

Currently, and prior to the study at hand, there existed no adequate instrument and measurement setup which was capable of observing the reflected and incoming diffuse radiation simultaneously at high angular *and* spectral resolution. As a consequence, no systematic comparison of retrieved BRF for both cases and the same target can be performed. Though, it is not known how field measurements can be transferred to laboratory measurements and for which targets a replacement of field by laboratory experiments is indeed feasible. Further, the magnitude of directional effects on various derived surface parameters is often unknown and their assessment requires accurate BRF knowledge of the corresponding surfaces (Diner et al., 1999; Verrelst et al., 2006). Such knowledge also provides valuable input to spectral databases and can be used for model development or model inversion techniques as well as for more accurate calibration and validation of reflectance data acquired with airborne and spaceborne sensor systems.

Within this research the abovementioned gaps are addressed and the first hyperspectral dual-view goniometer system is presented. The objectives of this work focus on 1) setting the stages to collect the

necessary spectrodirectional dataset in order to perform an accurate field BRF retrieval and to characterize the angular distribution of the incoming diffuse irradiance, 2) performing a BRF retrieval of selected targets and 3) investigating directional effects in derived surface parameters. The associated research questions and steps towards achieving these goals are outlined as follows:

1) How can the necessary input quantities for the BRF retrieval be accurately measured using the proven field goniometer system FIGOS? This involves constructional extensions to FIGOS as well as the choice of appropriate spectroradiometers and the determination of a measurement procedure for the simultaneous collection of direct, diffuse and reflected radiation quantities. The decision to rely on FIGOS is supported by the fact that the same system can also be used in a laboratory configuration as LAGOS and consequently the advantage of field – laboratory comparison measurements is still given. Prior to constructural activities a preliminary dual-view measurement setup was tested and is also presented here.

2) To what extent are traditional field measurements influenced by the diffuse irradiance and how accurately can the field BRF retrieval be performed using the retrieval algorithm proposed by Martonchik et al. (1994) and various goniometer datasets obtained with 1)? The field BRF retrieval is performed for an artificial inert target in order to not depend on target specific changes over time and the respective results are then compared to corresponding laboratory measurements where the diffuse irradiance is usually neglected. At the same time the angular distribution of the diffuse irradiance is investigated and comparisons to standard sunphotometer results are performed.

3) To what extent do directional effects influence vegetation parameters derived from ground-based and spaceborne multiangular measurements? Thereby, the retrieved BRF from ground-based spectrodirectional measurements is directly compared to spaceborne measurements performed with the Compact High Resolution Imaging Spectrometer CHRIS of the same surface area. As surface parameters two commonly used vegetation indices are derived from both datasets and are compared with regard to the magnitude of angular effects.

1.6 Structure of thesis

The thesis is located in the area of optical spectrodirectional Remote Sensing and aims at providing the necessary requirements in order to account for the diffuse influence in field reflectance measurements. The empirical study bases on ground-based goniometer measurements, which are used as input to an existing field BRF retrieval algorithm.

In the introduction section (Chapter 1) the study is positioned in the broader scientific context of Remote Sensing (RS). Thereby, important initiatives and treaties of inter-governmental organizations and scientific cooperation are briefly described highlighting the current and future focus of RS. A following subsection then discusses the potential of spectrodirectional RS along with the establishment of a "spectrodirectional" research community. Finally, some theoretical background as well as basic

reflectance definitions are given followed by the motivation and associated research questions, which led to this work.

Chapter 2 describes the complex of problems when performing ground-based directional measurements and gives a tabular overview of existing goniometers. In Chapter 3 the specific field and laboratory goniometer systems (FIGOS and LAGOS) are presented. A particular focus is laid on the development of the dual-view configuration of FIGOS (dual-view FIGOS), which provides the simultaneous spectrodirectional acquisition of radiation reflected from and incident to the surface, respectively.

Subsequently, the methodology to retrieve the surface BRF and to account for and characterize the diffuse irradiance are described in Chapter 4. Within that chapter a special subsection (Chapter 4.5) is dedicated to the determination of the reflectance characteristics of the Spectralon reference panel, which is used for field measurements in most cases. Chapter 5 describes the goniometer datasets which were acquired to a) test the dual-view configuration using a preliminary setup, to b) perform a BRF retrieval of an artificial target and compare it to spectrodirectional laboratory measurements and c) to determine the Spectralon reflectance characteristics.

The obtained findings are summarized in Chapter 6. They focus on the influence of the diffuse irradiance by comparing the field case to the laboratory case (no diffuse irradiance) and on a directional characterization of the diffuse irradiance for different atmospheric conditions. Furthermore, the results of the BRF retrieval for the artificial target are presented as well as the Spectralon BRF and its deviation from an ideal reflector (Lambert).

In Chapter 7 the field BRF retrieval is applied to first-time spectrodirectional dual-view FIGOS measurements of a natural vegetation surface. Thereby, the retrieved surface BRF is compared to multiangular spaceborne surface reflectances derived from CHRIS, and angular effects in derived surface parameters (vegetation indices) are investigated for both datasets.

Last but not least this study is concluded in Chapter 8 by relating the findings to the initially posed research questions, critically assessing the performance of the dual-view FIGOS and its potential for dual-view goniometer data collection and usage for combined ground-based and spaceborne multiangular data acquisition. At last, Chapter 9 gives an outlook of potential future steps to further improve spectrodirectional measurements and data quality, and to further contribute to the generation of concise BRF knowledge.

2 Ground-based Spectrodirectional Measurement Systems

2.1 Introduction

Basically, a goniometer is an instrument that either measures angles or allows an object to be rotated to a precise angular position. The term goniometry is derived from two Greek words, *gonia*, meaning angle and *metron*, meaning measure. Early scientific instruments, which based on the same principle of measuring angles consisted of the *astrolabe* and the *sextant,* both widely used for navigation and astronomy purposes[2]. Later, in the nineteenth century goniometers were extensively used in the discipline of crystallography for measuring angles between crystal faces (Grailich, 1857; Schabus, 1855). In its most simple design a goniometer looks like a well-known protractor with a turnable radius (Figure 3 left). Later versions already consisted of optical components allowing for a more accurate determination of the crystal face angles (Figure 3 right). Although these historic instruments were used for other applications and look quite old fashioned, some basic similarities to goniometer systems currently used in Remote Sensing cannot be overseen.

Figure 3: Two historic, scientifically used instruments for measuring angles versus the dual-view goniometer FIGOS. Left: Protractor with turnable radius to measure angles. Middle: Dual-view field goniometer FIGOS used for current Remote Sensing research. Right: Goniometer with two optics to observe a crystal, which is positioned in the center.

In the field of optical Remote Sensing ground-based goniometer systems are used to position a spectroradiometer into a specific observation position with respect to the target area. The goal is to directly measure the reflected or transmitted radiation from the target from various observation directions distributed over the whole hemisphere in order to describe the target specific directional reflectance characteristic at certain illumination conditions. Accurate knowledge of the scattering characteristics of specific targets plays a major role in various disciplines and consequently, several goniometers have been constructed and been used either in a field or a laboratory environment (Hosgood et al., 1999). In the laboratory, goniometer systems were used to measure reflectances of rock samples, soil powders and snow to explain the scattering properties of the surface of the moon (Coulson, 1965; Hapke et al., 1963; Oetking, 1966). The reflectance properties of single plant leaves

[2] http://www.britannica.com

were first studied using small target goniometers (Brakke, 1994; Brakke et al., 1993; Breece et al., 1971; Vanderbilt et al., 1985) and later, larger goniometers have been developed to investigate the reflectance characteristics of soil surfaces and vegetation canopies (Sandmeier et al., 1998a; Sandmeier et al., 1999). Other fields which make use of directional measurement systems include computer graphics where video cameras are used to study the visual appearance of real-world surfaces (Dana et al., 2004) and material sciences where knowledge of the spectral reflectance characteristic of e.g. reference panels is needed for calibration purposes of optical sensors. An interesting example of a goniometer like system (Meridian C-60) used in industry is found at Kaidan Ltd. (http://www.kaidan.com) and is used for e.g. positioning photographic cameras at different observation zenith angles.
Within this chapter an overview of existing goniometer systems used in optical Remote Sensing is given and important differences between the systems are discussed.

2.2 Goniometer systems

All measurements of the directional reflectance behaviour of specific surfaces are only approximations to the real surface BRDF (cf. Chapter 1.4). This is, on the one hand, due to limitations of the system and the sensor itself and on the other hand due to the complex structure of natural surfaces and the atmospheric influence. Although some limitations can be corrected during the post-processing of the observed data (e.g. illumination inhomogeneity in the laboratory) others remain (e.g. target heterogeneity) but are kept minimal by choosing an appropriate experimental setup. Important considerations for an appropriate spectrodirectional measurement setup include the relationship between the sensor observation geometry and the observed target type, the measurement environment (laboratory or field experiment) as well as goniometer specific characteristics.

2.2.1 Observation geometry versus observed surface area

The signal observed by the spectroradiometer consists of an integrated value over the sensor ground instantaneous field of view (GIFOV). The geometry of the GIFOV is defined by the sensor FOV, the observation distance and the observation angle. In this context the distribution of cast shadow and illuminated areas over the target is a critical factor. This is not only important when goniometer system results are directly compared to each other but also when ground-based spectrodirectional data are used for calibration purposes of airborne or spaceborne remote sensing data and in general, when up-scaling procedures are applied. Furthermore, the sensors GIFOV is changing while observing the target from different directions. If the target is nearly homogeneous and of sufficient extent this is not a problem. However, for laboratory spectrodirectional measurements this is often not the case since space is generally limited and the target needs to be manageably small. Consequently this may lead to the fact that within the GIFOVs for large off-nadir viewing directions different surfaces are observed and the recorded signal consists of fractions of both surfaces.

Another effect, which is closely related to heterogeneous surfaces within the sensor's GIFOV, may occur due to an unknown FOV non-uniformity. Until now the FOV non-uniformity is poorly

considered in field spectroscopy and manufacturer's specifications generally lack detail (Mac Arthur et al., 2007). Consequently, it may occur that surfaces outside the theoretical FOV influence the reflectance while some regions inside the FOV are not detected by any of the channels. This effect may strongly affect the recorded reflectance when looking at heterogeneous surfaces or surfaces, which are spatially defined by sharp boundaries (e.g. Spectralon panel on black background). Investigating the FOV non-uniformity Mac Arthur et al. (2007) found a substantial spatial dependency of the spectroradiometers' spectral response for each channel as pointed out in Figure 4.

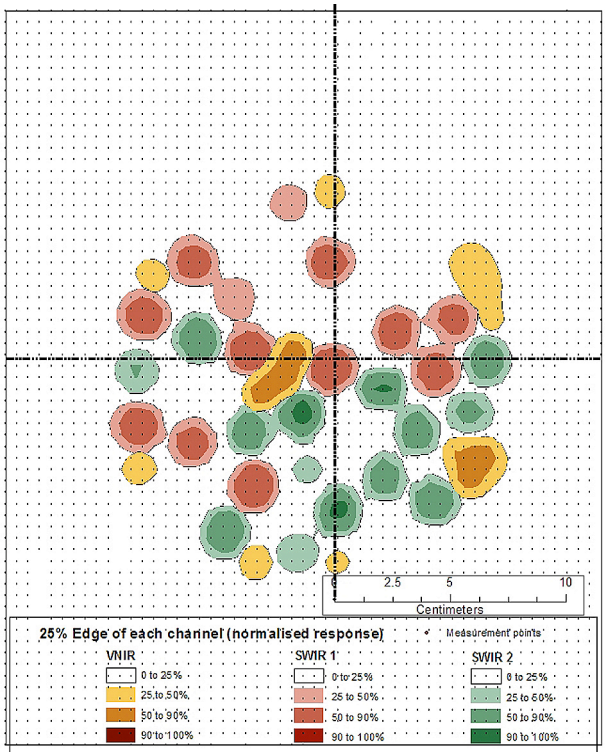

Figure 4: Normalized response contours for ASD FieldSpec Pro FR with 10° FOV (VNIR at 700nm, SWIR-1 at 1500nm, SWIR-2 at 2200nm) for an observation distance of 1m. The data points represent a 5mm grid. The figure is shown by courtesy of MacArthur et al. (2007).

2.2.2 Measurement environment – field versus laboratory

Only few systematic comparisons of field and laboratory measurements have been performed so far (Dangel et al., 2005; Schopfer et al., 2004). Even if the same goniometer system and the same target are used for field and laboratory measurements, the experiments considerably differ due to following reasons:

a) In field experiments the target is left in its natural environment and is exposed to the natural direct and diffuse illumination. Even under clear sky conditions the diffuse fraction can reach up to 10% to 30% depending on wavelength.

b) The direct illumination by the sun can be treated as being parallel (within 0.5°) and homogeneous over the area and height profile of the target, while laboratory illumination is usually non-parallel, non-homogeneous and not constant as a function of the target height.

c) The illuminated area in the laboratory is limited; adjacency and multiple scattering effects can therefore be very different to field experiments.

d) The spectrum of artificial light sources differs from that of the sun, which is additionally attenuated by the atmosphere. This is usually neglected since reflectance measurements are normalized using a reference target.

e) The polarization of the natural and artificial light sources can be different.

f) Living plants may behave differently under field and laboratory conditions due to large differences in environmental conditions, especially light intensity but also temperature, wind, etc.

Under field conditions the total illumination involves all directions within the hemisphere and consists of a diffuse and a direct part. By contrast, observation sensors usually collect the reflected radiation within a certain solid angle and of a small finite area. The atmospheric conditions, the presence of gases, clouds, and aerosols affect the amount and spectral distribution of the incoming direct and diffuse light and cannot assumed to be constant. Furthermore, the changing position of the sun during the measurement period leads to different illumination conditions associated with different scattering processes within the ray path. In order to keep track of such changing atmospheric conditions, reference measurements, e.g. using a Spectralon reference surface, have to be performed at regular time intervals. Alternatively, direct measurements of the total, direct and diffuse illumination provide the potential for a later BRF retrieval (atmospheric correction of the field HCRF). The atmospheric monitoring can either be performed using a sunphotometer instrument or by angular measurements of the incident radiation. Sunphotometer instruments usually provide an integrated value of the total and diffuse illumination whereas the direct illumination is either calculated (Yankee Environmental Systems, 2000) or directly measured using e.g. a Reagan sunphotometer (Ehsani et al., 1992). Angular measurements of the incident radiation can only be obtained from goniometer systems which are equipped with an upward "looking" sensor.
Laboratory measurements on the other hand provide a better control of the illumination conditions and the presence of diffuse light can be neglected if the experiment is conducted in a darkroom (Dangel et al., 2003). However, they suffer from other constraints since the artificial illumination shows a conical rather than directional geometry. Additionally, depending on the sensor FOV / GIFOV, measurements at large observation angles might not be possible since the illuminated area in the laboratory is spatially limited.

2.2.3 Goniometer characteristics

There are various differences between existing goniometer systems used in Remote Sensing and consequently, measurement results are not directly comparable. Such differences are related to the basic design of the system but also to the sensor, which is used and are directly determining the spectral and angular dimensions as well as the quality of the acquired spectrodirectional datasets. In the following the different types of goniometer systems as well as the angular dimension of the data are discussed. Furthermore, a special section is dedicated to the so-called dual-view goniometers, which are measuring both reflected and incident radiances.

2.2.3.1 Types of goniometers

Current goniometer systems used in Remote Sensing considerably differ by means of their measurement principle and their intended usage (field or laboratory system). Basically, two types of systems can be distinguished by referring to the observed target area. Some work with a constant observation centre whereas others keep the sensor position constant. Figure 5 schematically depicts the two measurement principles.

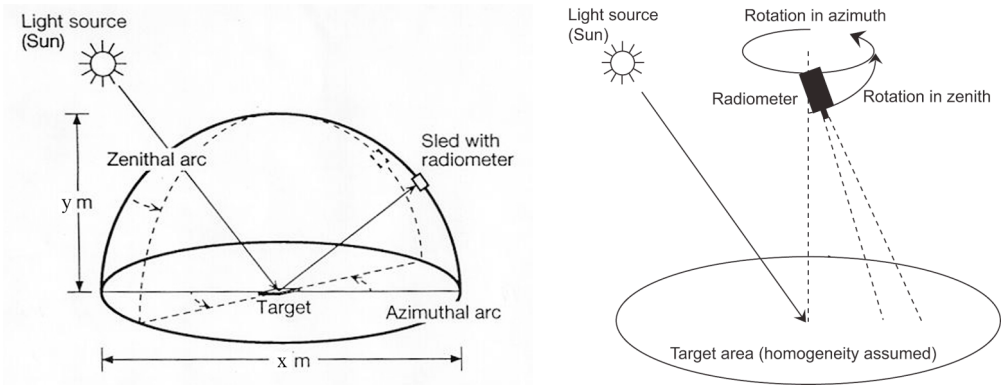

Figure 5: Two basic types of goniometers. Goniometer with a constant observation centre (left) and goniometer with a constant sensor position (right).

a) Goniometer systems with a constant observation centre

This type of system observes the target from various observation directions. The target is located in the centre of the observation hemisphere while the spectroradiometer is moved in the zenith and azimuth direction around the target. Most of these goniometers can be used either in the laboratory or in a natural environment. For many of them the design bases on some type of azimuth arc and zenith arc, on which the spectroradiometer is moved (Koechler et al., 1994; Painter et al., 2003; Sandmeier et al., 1999; Serrot et al., 1998). Other types use an extension arm with the optics attached at the front end of the arm to scan the hemisphere above the target in a coordinated manner (Bourgeois et al., 2006; Peltoniemi et al., 2005). Common for all ground-based systems of this group is that they are only able to observe targets up to a certain height.

An advantage of a) is that the observation distance remains the same for all viewing directions and that roughly the same target area within the integrated GIFOV is observed. With regard to vegetation targets this is of importance since plant biochemical and biophysical properties may spatially vary due to e.g. the underlying soil composition. Furthermore, the homogeneity assumption within the GIFOV is rather true since the target area needs to be of limited extent only. However, the obtained reflectance anisotropy is not necessarily representative for a larger area and comparison studies with airborne or spaceborne data, which are based on a larger pixel dimension, cannot easily be performed. A possible way of averaging the respective reflectance anisotropy over a larger area consists of conducting several goniometric measurements at different locations within the area. But in this case either the illumination conditions (especially the direct irradiance of the sun) is different for each dataset

acquisition or, if measurements are performed at the same time of day but on consecutive days, phenological changes in the vegetation play a role.

A sub-type of a) was developed by the Technical University of Munich (TUM) (Schneider et al., 2004). Its spectroradiometer is mounted to a large extendable boom, which is attached to a rover vehicle. The target is also observed by following the constant target position principle of a). However, the sensor is moved rather along a semi-ellipsoid in the observation hemisphere than along a semi-circle. This is obtained by altering the observation distance for every observation zenith angle. A big advantage thereof is that spatial changes of the GIFOV are kept minimal and the recorded signal of the spectroradiometer is integrated over roughly the same target area for all observation directions. A speciality of the system's spectroradiometer is that it uses a bifurcated fibre optic cable, one fibre optic observes the reference panel from a nadir view while the other fibre optic is attached to the moving extension arm and observes the target area from different observation directions. The respective entrance optic can be chosen by a shutter, which alternatively closes the object optic or the reference optic. The potential here is that reference measurements can be performed at any time, e.g. before each target measurement or at desired time intervals (e.g. corresponding to atmospheric changes), without significantly prolonging the overall measurement time. However, the compromise for this system is that very long fibre optic cables are used which coincides with a reduction of transmission by about 50% and a complete loss of signal at wavelengths above 2200nm (Schneider et al., 2004).

For comparison purposes the performance of various lengths of fibre optics is shown based on reports by ASD (Analytical Spectral Devices Inc.). Standard ASD FieldSpec 3 instruments are equipped with a 1.5m permanent fibre optic. For increased lengths of permanent fibre optics the expected attenuation is presented in Figure 6. If jumpers are used even a further attenuation occurs due to the junction of the two fibre optics.

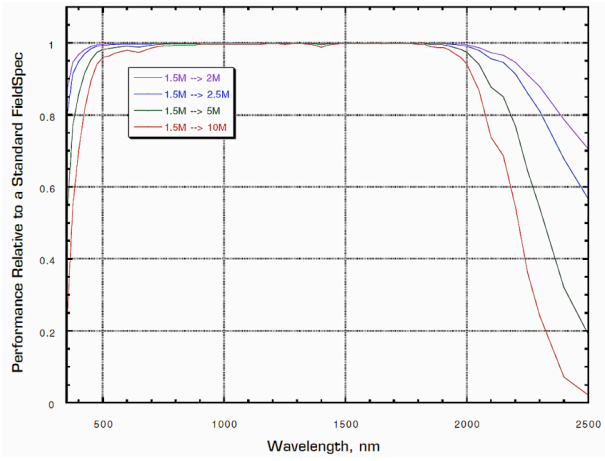

Figure 6: Performance of various fibre optic lengths compared to a standard fibre optic of 1.5m (by courtesy of Brian Curtiss (personal communication, December 2007)

b) Goniometer systems with a constant sensor position

Using this measurement principle the sensor position remains constant but the sensor is turned around its lateral axis to point in the desired observation directions.

Constant sensor position goniometers (Bruegge et al., 2000; Deering et al., 1986; Demircan et al., 2000a, Schneider et al., 2004) mostly consist of boom-mounted radiometers. Such systems acquire data samples at different spatial locations associated with different observation distances. This may lead to different target scale effects as well as to different multiple scattering effects within the reflected beams for every observation direction. Additionally, a surface homogeneity over a large spatial extent has to be assumed since the sensor does not observe radiation from a fixed target location. For these reasons such instruments can only be used in field experiments and are not able to observe targets and materials with a limited spatial extent such as artificial targets or single plants. However, in contrast to a) this type of goniometers show a considerable advantage for measuring the reflectance anisotropy of vertically extended vegetation types such as bush lands.

2.2.3.2 Angular dimension

A goniometer datasets consists of several single measurements obtained at different observation directions. The number of single measurements depends on the angular resolution with which measurements are performed in the azimuth and zenith plane. Most spectrodirectional measurements are performed using a spectroradiometer, which is mounted onto the goniometer and moved step by step in order to obtain the single measurements. This leads to one measured value per direction. In order to define the sampling positions with regard to the interpolation required at later processing steps various approaches can be discussed. The single measurements can either be a) regularly distributed over the observation angles, b) regularly distributed over the area of the observation hemisphere or c) be performed at the specific Gaussian quadrature positions. One could also argue to use a target specific measurement grid with especially dense sampling steps close to highly anisotropic reflectance directions such as e.g. the hotspot direction in vegetation BRF.

However, currently most goniometer systems sample the data over a regular angular grid. Depending on the system, an angular resolution ranging from 15° to 1° in zenith and 45° to 5° in azimuth direction is used, respectively. Some goniometer systems provide the possibility to choose the angular resolution within a certain range. However, the disadvantage of higher angular resolution is a longer measurement time per goniometer dataset, which is critical with regard to atmospheric and illumination changes in field experiments.

Other goniometer systems use a wide angle imaging sensor, e.g. a CCD line camera to scan the observation hemisphere and consequently obtain a much higher angular resolution in the order of 0.015° in azimuth and zenith direction, usually reduced to 0.5° for ease of data handling (Demircan et al., 2000b). This principle of measurement, which is registered as a patent by DLR (Röser et al., 1999), is performed at the Institute of Space Sensor Technology and Planetary Exploration of the German Aerospace Center (DLR).

2.2.3.3 Dual-view goniometer systems

Most goniometer systems are only capable of measuring radiances evolving from the target area into the lower hemisphere (with respect to the sensor position). Only few goniometer systems observe both the lower hemisphere (reflected radiances from the target area) as well as the upper hemisphere (incoming diffuse radiances). A dual-view capability is obtained by having two optics, one looking

upward to the sky and one looking downward at the target area. Depending on the used sensor the radiation is either collected in specific channels (multispectral) or continuously over the whole spectral range from 350nm – 2500nm (hyperspectral). The angular resolution and the optic FOV are normally kept the same for both observation directions. Such dual-view spectrodirectional measurements provide valuable knowledge about the distribution of the diffuse incoming radiation, which is necessary to correct field measurements for the atmospheric influence (BRF retrieval). Currently, such a capability is only provided by the PARABOLA instruments (Bruegge et al., 2000), the dual-view FIGOS (Schopfer et al., 2007a) and the Gonio Radiometer Spectrometer System (GRASS) (Pegrum et al., 2006).

The first version of the PARABOLA instrument evolved from a program to utilize in situ, multiangle datasets in the investigation of land cover/radiation interactions and was begun almost two decades ago (Deering et al., 1986). It consisted of three spectral bands (650-670, 810-840 and 1620-1690nm) and observations were performed using a FOV of 15°. Later versions, such as PARABOLA III, were designed in order to extend the wavelength range to eight spectral bands and to decrease the FOV. Currently, two of these instruments exist: one owned by the NASA/Goddard Space Flight Center (GSFC), and the other one owned by the Jet Propulsion Laboratory (Bruegge, 2004; Bruegge et al., 2000). PARABOLA III is predominantly used for MISR data validation purposes (Abdou et al., 2000; Bruegge et al., 2000) and is collecting the reflected and incident radiances on a spherical grid of 5° and in 8 spectral channels whereas four of these channels correspond to MISR spectral bands.
As of today the dual-view FIGOS (Schopfer et al., 2007a) is the most advanced dual-view goniometer system. It is based on the well known field goniometer systems FIGOS (Sandmeier et al., 1999) and LAGOS (Dangel et al., 2005) and will be discussed in detail in Chapter 3.2.
The third dual-view goniometer system, GRASS (Pegrum et al., 2006), is currently being developed at the National Physical Laboratory (NPL), Teddington, UK. It shows a promising dual-view design, which consists of an azimuth arc and 7 semi zenith arcs carrying a total number of 36 optic holders. Near simultaneous spectral reflectance measurements of a $1m^2$ target area are performed at up to 36 observation angles over half a hemisphere and for irradiance measurements all optic holders can be turned to an upward looking orientation. In total 36 fibres lead from the optic holders to a switching unit in such a way that the number of fibres can be reduced to one optical fibre output, which is then coupled to a spectroradiometer. As of today, no measurement experiences have been made since this system has not yet reached operational status. Possible drawbacks might be related to cast shadowing of the target area by the 7 semi zenith arcs and to some reduction in the transmitted signal, especially at wavelengths greater than 2200nm, since long fibre optic cables are used.

2.3 Review of current goniometer systems

The number of existing goniometer systems ranges from older systems dating back to the advent of bidirectional RS research to modern systems still being constructed today. Table 1 presents an overview of those systems, which are still actively used or mark milestones in the evolution of spectrodirectional research. The last column gives the respective references, which describe the corresponding goniometer system.

Note that at time only 4 dual-view goniometer systems exist and only two of them are capable of hyperspectral data collection whereas GRASS is not yet operational. Consequently, the dual-view FIGOS is currently the only operational hyperspectral dual-view goniometer system.

Meas. System	Institution	Characteristics	Reference
ABRAMS	Wave Scattering Research Centre, Electrical Engineering Department, University of Texas, USA	Field Coverage: Ground sphere Spectral: 632.8nm (1 band)	(Gibbs et al., 1993)
ASG	National Snow and Ice Data Centre, University of Boulder, USA	Field Coverage: Ground sphere Spectral: 350-2500nm (hyperspectral)	(Painter et al., 2003)
Automatic Multi-Angle Measuring Platform	Institute of Geography Sciences and Nature Resource Research, Beijing, China	Field Spectral: 8-13µm (thermal), broadband	(Li et al., 2004)
Goniometer	Department Geography and Geosciences, Bloomsburg University, Bloomsburg, USA	Laboratory Coverage: Ground sphere Spectral: 450, 550, 700, 930nm	(Johnson et al., 2004)
CCD Line Camera WAAC	Institute of Space Sensor Technology and Planetary Exploration at the German Aerospace Center (DLR)	Field Coverage: Ground sphere Spectral: 350-900nm (variable using filters)	(Demircan et al., 2000b)
CHARISMA	Laser Laboratorium Goettingen, Germany	Laboratory Based on coblentz-hemisphere with UV sensitive CCD camera Spectral: 157, 193, 633nm	(Apel et al., 2000)
CLabSpeG	Department of Land Management, Katholieke Universiteit Leuven	Laboratory Coverage: Ground sphere Spectral: 350-2500nm (hyperspectral)	(Biliouris et al., 2003)
EGO	Joint Research Center, Ispra, Italy	Laboratory Coverage: Ground sphere Spectral: radiometer dependant	(Koechler et al., 1994)
Finish Goniometer (Model 3)	Finnish Geodetic Institute, Masala, Finland	Field and Laboratory Coverage: Ground sphere Spectral: 350-2500nm (hyperspectral)	(Peltoniemi et al., 2005)
FiGIFiGo (Model 4)	Finnish Geodetic Institute, Masala, Finland	Field and Laboratory Coverage: Ground sphere Spectral: 350-2500nm (hyperspectral)	(Suomalainen, 2006)
Dual-view FIGOS / LAGOS	Remote Sensing Laboratories RSL, Institute of Geography, University of Zurich, Switzerland	Field and Laboratory Coverage: Ground and sky sphere Spectral: 350-2500nm (hyperspectral)	(Sandmeier et al., 1999), (Dangel et al., 2005), (Schopfer et al., 2007a)

Meas. System	Institution	Characteristics	Reference
GRASS	National Physical Laboratory, Teddington, UK / NERC	Field and Laboratory Coverage: Ground and sky sphere Spectral: 350-2500nm (hyperspectral)	(Pegrum et al., 2006)
PARABOLA	NASA/Goddard Space Flight Center (GSFC), USA	Field Coverage: Ground and sky sphere Spectral: 630-690, 760-900, 1550-1750nm (3 bands)	(Deering et al., 1986)
PARABOLA II	NASA/Goddard Space Flight Center (GSFC), Maryland, USA	Field Coverage: Ground and sky sphere Spectral: 430-455, 540-565, 665-680, 845-875, 1620-1690nm, PAN, 10-12µm (7 bands)	(Stockton et al., 1994)
PARABOLA III	NASA/Goddard Space Flight Center (GSFC) and Jet Propulsion Laboratory, California Institute of Technology, Pasadena, USA	Field Coverage: Ground and sky sphere Spectral: 444, 551, 581, 650, 860, 944, 1028, 1650nm (8 bands)	(Bruegge et al., 2000)
MUFSPEM	Chair for landscape planning and nature conservation, Technical University of Munich TUM	Field Coverage: Ground sphere Spectral: 350-2500nm (hyperspectral)	(Manakos et al., 2001; Schneider et al., 2004)
MGS	Limnological Station Iffeldorf, Technical University of Munich TUM	Field Coverage: Ground sphere Spectral: 350-2500nm (hyperspectral)	(Manakos et al., 2004; Schneider et al., 2004)
Goniometer of ONERA / DOTA	Office National d'Études et de Recherches Aérospatiales, Toulouse (France)	Field and Laboratory Coverage: Ground sphere Spectral: 400-950nm (hyperspectral)	(Serrot et al., 1998)
SFG	Stennis Space Center, NASA	Field Coverage: Ground sphere Spectral: 400-2500nm (hyperspectral)	(Turner et al., 2000)
Goniometric Optical Scatter Instrument	National Institute of Standards and Technology (USA)	Laboratory Coverage: Ground sphere Spectral: 633nm	(Asmail et al., 1994)
Chopping	USDA-ARS Hydrology Laboratory, Beltsville Agricultural Research Center-West	Field Coverage: Ground sphere Spectral: 520-600, 630-690, 760-900, 1550-1750nm (4 bands)	(Chopping, 2000)
IAC ETH Goniospectro-meter	Institute for Atmospheric and Climate Science, ETH Zurich, Switzerland	Field Coverage: Ground sphere Spectral: 350-1050nm (hyperspectral)	(Bourgeois et al., 2006)

Meas. System	Institution	Characteristics	Reference
SIBRE	MODIS Land Surface Temperature Group, Institute for Computational Earth System Science, University of California, USA	Field Coverage: Ground sphere Spectral: 2.5-6 µm, 7-15µm	(Snyder et al., 1996)
Goniometer	Department of Geography and Human Environment, Tel-Aviv University (Israel)	Laboratory Coverage: Ground sphere Spectral: 350-2500nm (hyperspectral)	(Feingersh et al., 2005)
Goniometer for calibrating field reference panels	University of Nebraska (USA)	Laboratory Coverage: Ground sphere Spectral: 450-520, 520-600, 630-690, 760-900, 1150-1300, 1550-1750 and 2080-2350nm (7 bands)	(Walter-Shea et al., 1993)
Leaf Goniometer	Université de Nantes (France)	Laboratory Coverage: spherical transmittance Spectral: 450-900nm (hyperspectral)	(Despan et al., 2004)
Goniometer	Center for Environmental Remote Sensing (CEReS), University of Chiba, Japan	Field Coverage: Ground sphere Spectral: 350-1050nm (hyperspectral)	(Susaki et al., 2004)
Goniometer measurements by Bausch	USDA-ARS Irrigation and Drainage Research, Beltsville Agricultural Research Center-West	Field Coverage: Ground sphere Spectral: 420-520, 520-600, 630-690, 769-900nm (4 bands)	(Bausch et al., 1989)
Goniometer measurements by Hahlweg	Helmut Schmidt University, Germany	Laboratory Coverage: Ground sphere Spectral: 405, 460, 480, 505, 520, 562, 588, 611, 626, 644, 660nm	(Hahlweg et al., 2005)
Goniometer measurements by Leroux	Centre National de la Recherche Scientifique, Université Joseph Fourier, Saint Martin d' Hères, France	Field Coverage: Ground sphere Spectral: 450, 650, 850, 1650nm (4 bands, with polarization filters)	(Leroux et al., 1998)
Measurements by Tanikawa	Graduate School of Life and Environmental Sciences, University of Tsukuba, Tsukuba, Japan	Field Coverage: Ground sphere Spectral: 350-2500nm (hyperspectral)	(Tanikawa et al., 2006)
Measurements by RSG	Remote Sensing Group, Optical Sciences Center, University of Arizona, USA	Field Coverage: Ground sphere Spectral: 470, 575, 660, 835nm	(Czapla-Myers et al., 2002)
Measurements by Steffen	Cooperative Institute for Research in Environmental Sciences, University of Colorado, Boulder, USA	Field Coverage: Ground sphere Spectral range: 350-1200nm (500-600nm using filters)	(Steffen, 1987)
Various spectrodirectional measurements performed with not permanent goniometer setups.			

Table 1: Overview of goniometers. Note that the dual-view FIGOS is currently the only operational hyperspectral dual-view goniometer system.

3 The Goniometer Systems FIGOS and LAGOS

3.1 Introduction

The field goniometer system FIGOS and the laboratory goniometer system LAGOS is the same goniometer system by means of its construction, design and the used spectroradiometer. It can be used either in a field or in a laboratory configuration. By labeling the system FIGOS and LAGOS the respective measurement setups (field or laboratory) are addressed. The goniometer system has originally been constructed for field use by W. Sandmeier at Lehner & Co. AG, Gränichen, Switzerland, in joint operation with the Remote Sensing Laboratories (RSL) at the University of Zurich, Switzerland (Sandmeier et al., 1999). It is a transportable system and has extensively been used in various campaigns for the acquisition of hyperspectral directional reflectance data of vegetation (Beisl, 2001; Sandmeier, 2000; Strub et al., 2002; Strub et al., 2003), snow (Odermatt et al., 2005) and artificial (Schopfer et al., 2004) targets. Over the years the capabilities of RSL's goniometer system have constantly been extended in order to support the accurate characterization of the reflectance properties of specific targets in the laboratory as well as in the field.

For laboratory usage a darkroom and an artificial light source have been installed and spectrodirectional measurements of e.g. a phenological cycle of summer wheat as well as direct comparisons to the field setup have been performed using an artificial target (Schopfer et al., 2004). An accurate characterization of the illumination source and geometry as well as a novel BRF retrieval scheme for typical laboratory goniometers is described by Dangel et al. (2005).

For the field usage the main extension consists of a dual-view combination (Schopfer et al., 2007a). A first series of measurements using the "new" field goniometer system has been performed in July 2006, when FIGOS was selected as a reference instrument for a goniometric intercalibration campaign in collaboration with various research groups of the Technical University of Munich (TUM) and the German Aerospace Center (DLR).

Within this chapter the characteristics of the current dual-view field goniometer system FIGOS and laboratory goniometer system LAGOS are discussed with a special focus on recently made extensions.

3.2 Dual-view FIGOS

By having a dual-view capability the reflected and incoming radiances are collected simultaneously at high spectral and high angular resolution. Two wirelessly computer controlled ASD FieldSpec-3 spectroradiometers are used to cover the spectral range from 350nm to 2500nm and data is sampled at intervals of 1.4nm (350 – 1050nm) and 2nm (1000 – 2500nm) with a spectral resolution of 3nm at 700nm and 10nm at 1400/2100nm, respectively (Analytical Spectral Devices Inc., 1999). Both spectroradiometers are mounted onto the zenith arc of the goniometer and operated with a 3° FOV foreoptic which is connected to the sensor using a 1.4m fibre optic. The downward looking spectroradiometer observes the target from a constant distance of 2m for all observation directions. The idea of having both instruments being moved while taking directional measurements evolved from various considerations. The design of a U-base plate Figure 8 supports the attachment of both

spectroradiometers as closely as possible to the zenith arc. Therefore, and since the zenith arc is eccentrically positioned, no cast shadow is generated on the target area (except for the dual optic holder at the hotspot direction), even though a large volume is moved along the zenith arc. Additionally, fibre optics of standard length can be used and a sufficient signal to noise ratio (SNR) is obtained. In contrast, having only the optics moved (and the spectroradiometers placed outside the goniometer) would create the need of having very long fibre optics (> 4m) and consequently a lower SNR.

The goniometer itself consists of three major parts: a zenith arc and an azimuth rail, each of 2m radius, and a motorized sled, onto which the two sensors are mounted. All parts are made of black-coated aluminum in order to minimize adjacency effects. The zenith arc is tightly fixed to four wagons which allow a manual 360° rotation on the azimuth rail. The sled with the two spectroradiometers is driven by a braking motor at a velocity of 2.5°/s. Fully adjustable labels on the zenith arc allow for an automated positioning of the spectroradiometers at desired steps. The mechanical positioning sensors as well as the electrical control unit of the motor were renewed in order to resist humidity and guarantee a stable performance (cf. Figure 7 middle and right). Currently, measurements are taken at azimuth steps of 30° and zenith steps of 15° (-75° to 75°). A full dual-view goniometer dataset is completed in about 25 minutes. Figure 7 (left) shows the dual-view goniometer FIGOS being used for data collection over an artificial target.

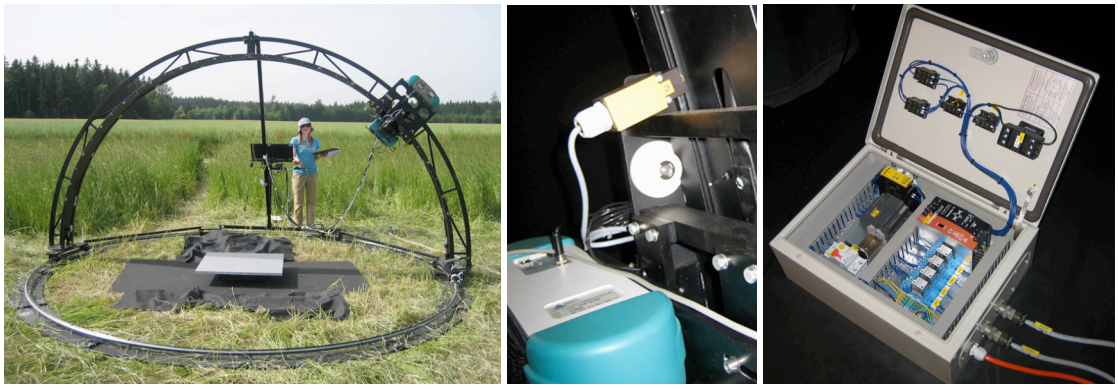

Figure 7: Left: Dual-view goniometer system FIGOS. Middle: Renewed mechanical positioning sensors. Right: Electrical control unit of the step motor. All mechanical and electrical parts are constructed for intensive outdoor use and well protected against humidity and other external influences.

By using a dual optic holder both optics are exactly aligned while pointing in opposite directions and the generated shadow at the hotspot direction is minimized to the optic's size, which is about 1cm in diameter. Consequently spectrodirectional measurements close to the hotspot are possible and may provide new insights into the reflectance characteristic of specific targets at this special observation direction. The optic rotating disk allows for easy and quick rotation of the dual optic holder, if necessary, for e.g. additional reference measurements in the beginning of each zenith arc cycle or instrument optimization purposes. Figure 8 shows the U-base plate carrying both spectroradiometers and the dual optic holder.

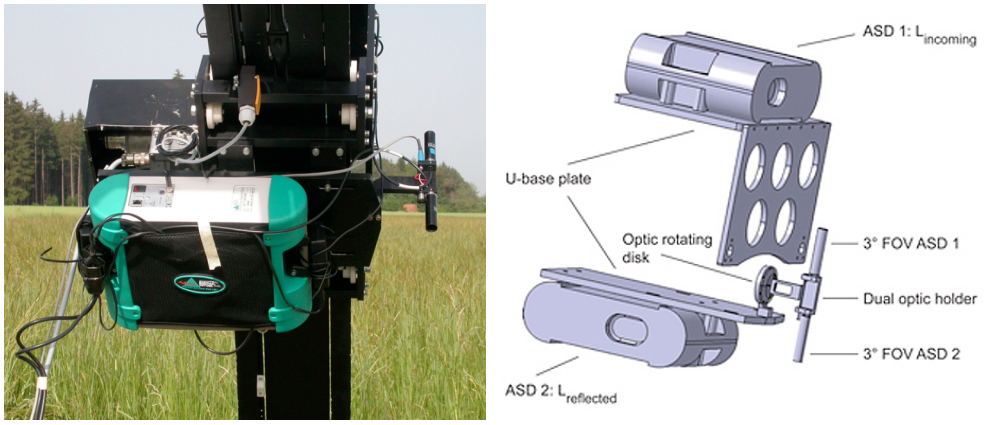

Figure 8: Dual-view combination as mounted onto the zenith arc (left) and corresponding technical sketch (right).

Since the instantaneous FOV is 3° and always pointing to the centre of the hemisphere (downward looking optic), the corresponding GIFOV is circular with 10.5cm (diameter) in nadir direction. However, for large off-nadir observation angles the sensor's footprint becomes elliptical with a maximum longitudinal extent of 41cm for an observation angle of 75°. It is therefore essential to consider the correct target reference height, especially when measuring a target with limited size e.g. under laboratory conditions. Table 2 and Figure 9 show the extent of the changing GIFOV for the current goniometer setup (3° FOV, 2m observation distance).

Observation angle [°]	**Major half axis forward [cm]**	**Major half axis backward [cm]**	**Total extent [cm]**
0	5.24	5.24	10.47
15	5.46	5.38	10.84
30	6.14	5.96	12.10
45	7.61	7.22	14.82
60	10.97	10.02	20.99
75	22.43	18.43	40.86

Table 2: Change of the ground instantaneous field of view GIFOV in dependence on the observation angle for the currently used angular resolution of FIGOS and LAGOS. Note that the major half axis is changing asymmetrically in the backward and forward direction from the centre point (backward = towards the sensor).

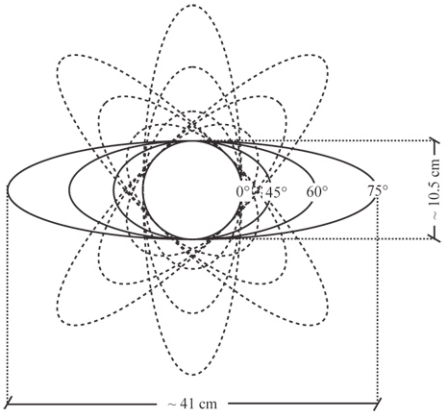

Figure 9: Graphical view of the changing GIFOV in dependence on the azimuth view direction.

In order to monitor the pointing accuracy of the downward looking optic, a small laser is integrated into the dual optic holder. The geometric precision of the zenith arc is then referenced while moving the sled over the zenith arc in the principal and in the orthogonal plane. Maximum deviation of the laser spot, representing the centre of the sensor GIFOV, is recorded at a view angle of -75° and is about 4cm (cf. Figure 10). A possible cause for this deviation might be a slight deformation of the respective part of the zenith arc due to extensive usage (assembly/disassembly) over time. However, this is not a limiting factor for field goniometer measurements since the target under observation is usually of satisfying spatial extent and assumed to be homogeneous.

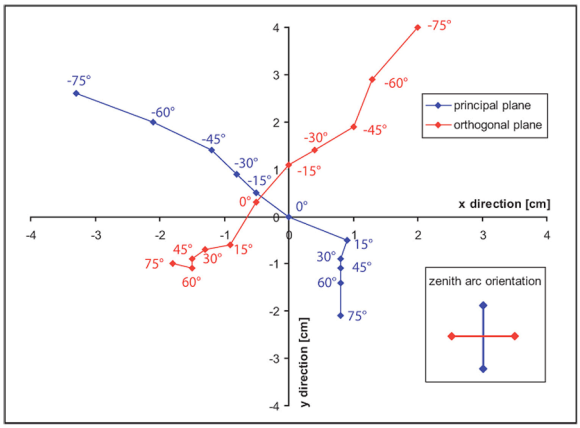

Figure 10: Pointing accuracy over the zenith arc. The convention –x/y and +x/y is used for the backward scattering and the forward scattering direction, respectively. The coordinate system is aligned to the centre of the azimuth arc. Note the different pointing accuracies in the principal and orthogonal plane due to small azimuth arc deformations.

3.2.1 Dual-view FIGOS measurement principle

The two spectroradiometers, which are used to simultaneously collect the reflected and incoming diffuse radiation, are usually operated in radiance mode. For further processing, the intercalibration coefficients have to be known for the two instruments. The last intercalibration experiment with the two FIGOS spectroradiometers has been performed in July 2006 at the intercalibration facility of the

German Aerospace Centre (DLR) offering an integrating sphere with the corresponding infrastructure for stable conditions (Suhr et al., 2005). Figure 11 shows a comparison of the absolute radiance values as measured with the two ASD FieldSpec 3, as well as the current intercalibration coefficient. The agreement for the VNIR detector lays within 1% whereas for the SWIR1 and SWIR2 detectors it consists of about 2%. Extreme values at both ends of the spectral range reach up to 4%.

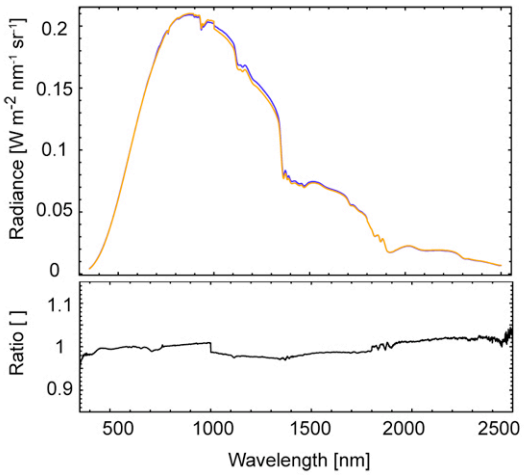

Figure 11: Upper part: Comparison of absolute radiance values for the upward looking sensor (dashed blue line) and the downward looking sensor (solid orange line). Lower part: Intercalibration coefficient.

Spectrodirectional measurements with the dual-view FIGOS usually start in the principal plane at a forward scattering direction of 75°. Following a predefined sequence the whole hemisphere is scanned at zenith steps of 15° and azimuth steps of 30°. Spectralon references are collected in the beginning and in the end of each goniometer dataset as well as at every nadir bypass with the downward looking sensor. This provides a) the potential of calculating reflectances, if wished at a later time, and b) of monitoring atmospheric changes or instrument drifts. In total 140 measurements are taken for one dual-view goniometer dataset (8 reference measurements plus 66 directional measurements of the reflected and incoming radiances, respectively). Figure 12 shows the measurement sequence for goniometric measurements with the dual-view FIGOS.

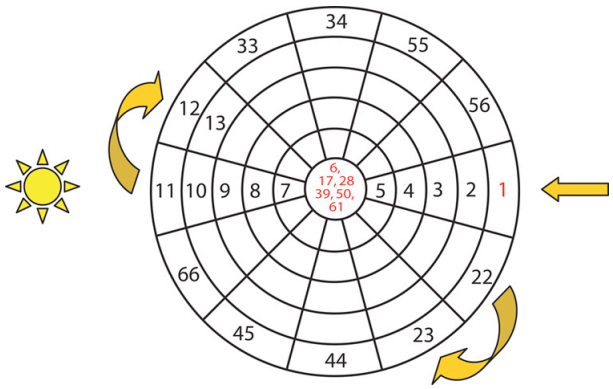

Figure 12: Measurement procedure for the dual-view FIGOS. Red coloured numbers represent reference measurement positions.

Even though shadowing is minimized it might occur anyway when the sun zenith angle equals one of the (downward looking) sensor view angle steps (e.g. at 15°, 30°, 45°, 60° or 75°). If this is the case, the corresponding measurements are either omitted, interpolated, or modelled by fitting to a BRF model.
Simultaneous sunphotometer measurements are necessary for two reasons: 1) monitoring the state of the atmosphere during the whole measurement time and 2) the direct sun irradiance is required as an input parameter to the field BRF retrieval algorithm. Currently, the dual-view FIGOS is not yet able to directly measure this quantity, mainly due to:

a) The upward looking sensor is saturating when directly aligned in the sun view direction. However, this problem might be solved by reducing the integration time of the upward looking spectroradiometer.

b) Using a 3° FOV accurate pointing at the sun disk is challenging and time consuming. The time for measuring one goniometer dataset is a critical factor and desired to be as short as possible.

Within the current measurement setup an MFR-7 shadowband sunphotometer (Yankee Environmental Systems, Inc) is used which directly records the total and diffuse irradiance in 7 bands (broadband, 415, 500, 615, 673, 870 and 940nm). The direct sun irradiance is then calculated as a difference of the two, taking the respective sun zenith angle into account.

3.3 LAGOS setup

The laboratory goniometer system LAGOS is operated in a single view (downward looking) configuration only. The downward looking observation geometry is exactly the same as for FIGOS. In order to minimize scattering and adjacency effects a special darkroom with black painted walls, well separated from the rest of the laboratory by a black curtain, has been prepared and all devices are covered with a black textile (Oscuratino, type Colorit 211). The ratio of the diffuse to total illumination has been measured using a Coherent LM-2 powermeter and was found to be below 0.5% for the spectral range 400nm – 1000nm (Dangel et al., 2005).
Figure 13 shows the LAGOS, which is currently positioned at a height of 80cm from the ground. The respective target under observation is placed on a height adjustable table in order to measure targets of variable vertical extents. However, the LAGOS can also be used directly on the ground.

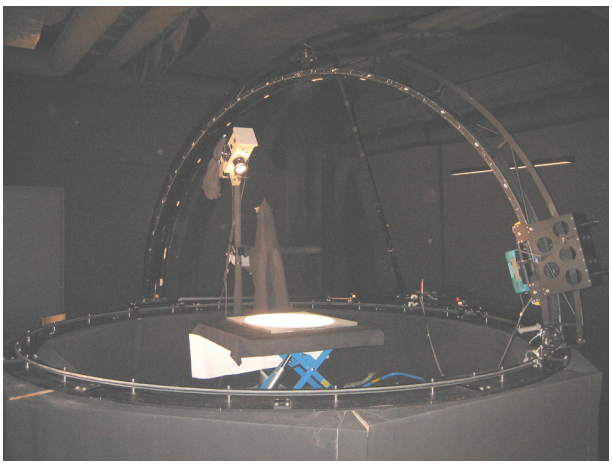

Figure 13: LAGOS measurement setup in the darkroom. All reflective parts are covered with a black textile. Eight wooden boxes and a height movable table allow for the necessary setup in order to measure targets of different vertical extent.

3.3.1 Artificial light source

As artificial illumination source a 1000W quartz tungsten halogen lamp (Oriel, type 6317) is used. The lamp intensity can be controlled via an external control unit and is stable within 0.05% rms according to the manufacturers' quality protocol. Although, and for experiment traceability reasons, the corresponding intensity values are written on the protocol for the respective laboratory measurements. Over the years, the total operational time has now reached 148.5 hours. By default, the lamp is equipped with an internal collimator F/0.7. However, when only the internal collimator of the lamp is used the illuminated area on the target level is very inhomogeneous. Therefore, a secondary lens system which images the condenser onto the target area according to Köhler's principle (Schröder, 1998) is placed outside the lamp, drastically ameliorating the homogeneity of the illuminated area (Dangel et al., 2003). Figure 14 shows the artificial illumination source and the corresponding control units.

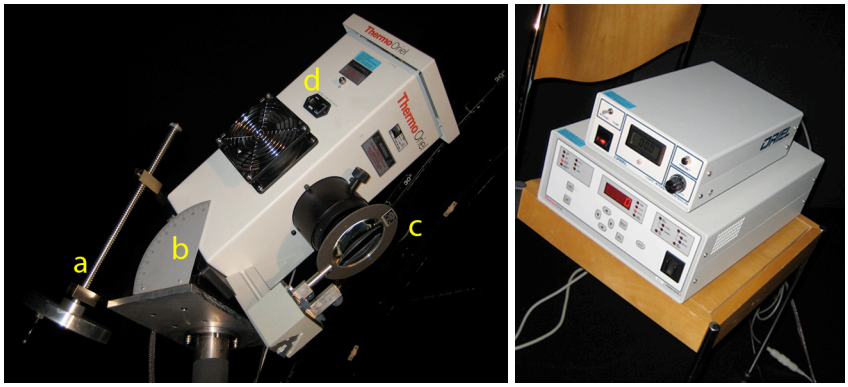

Figure 14: Left: Lamp with a) tilting mechanism, b) clinometer for illumination angle, c) secondary lens and d) operational timekeeper. Right: External intensity control unit (top) and lamp control unit (bottom).

The current illumination distance is usually set to 1.53m which leads to a semi angle of the light cone of about 11° and a minor axis of the illumination ellipse of about 60cm. This conicality of the illumination geometry leads to an inhomogeneity of the illuminated area as shown in Figure 15 for a typical illumination angle of 30°. The underlying measurements have been performed using a Spectralon panel and an ASD FieldSpec 3, which are both moved on a 5cm grid over the illumination ellipse. Within the sensor GIFOV the inhomogeneity is below 10% of the mean value for nadir illumination (for homogeneous and flat targets). With increasing illumination zenith angles, an approximately linear gradient has to be added resulting in a factor of about 2 for 40° zenith. Similar results have been found in an earlier study performed with the same illumination source using direct irradiance measurements from a Coherent LM-2 powermeter (Dangel et al., 2003).

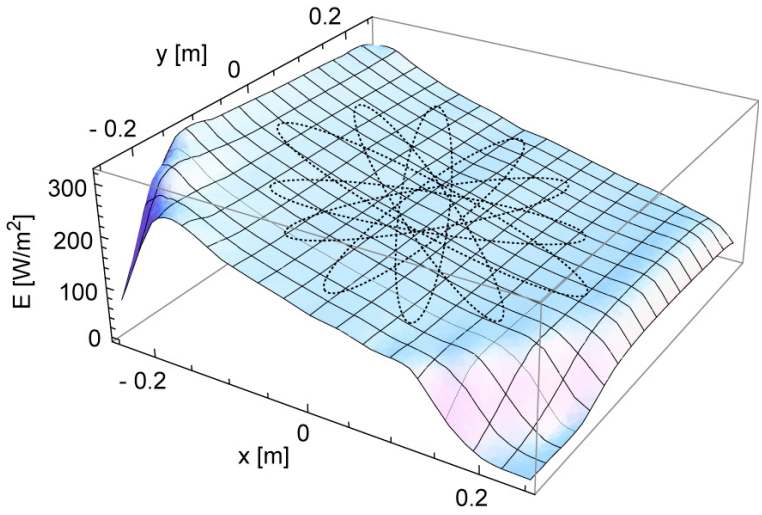

Figure 15: Measured inhomogeneity over the illuminated area for an illumination zenith angle of 30°, integrated from 400nm – 1000nm. The dashed ellipsoids represent the LAGOS GIFOV for an observation zenith angle of 75°.

For LAGOS measurements the lamp is mounted on a movable, height adjustable stand, which is currently positioned within the azimuth circle of the LAGOS. It consists of three major parts: a primary vertical pillar, a horizontal arm and a secondary pillar, which is attached to the latter. Both pillars as well as the horizontal arm can be moved along their central axis, which allows for the positioning of the lamp according to the desired illumination angle. The lamp itself is mounted about 10cm off the central axis of the secondary pillar in order to avoid masking of the target area by the secondary pillar for observation angles greater than the actual illumination angle. The illumination angle itself can be set by tilting the lamp to the requested inclination angle. Figure 16 shows the illumination setup with the lamp stand.

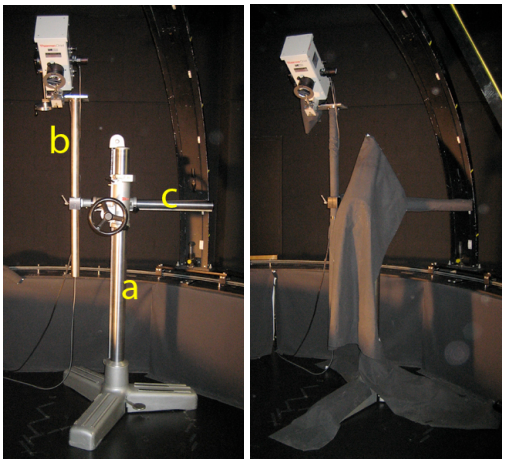

Figure 16: Left: Lamp stand in clean condition with a) the primary pillar which allows for height adjustments, b) the secondary pillar and c) the horizontal arm which allows for horizontal displacements, if needed. Right: Lamp stand in operational mode covered with black textile in order to minimize stray light.

Although the lamp can theoretically be tilted over the angular range from 0° (nadir) to 90° the set of illumination angles θ_i is limited to ($17° < \theta_i < 60°$) by the available horizontal space between the target and the azimuth rail of the goniometer. Regarding simulations of illumination directions as present during field campaigns e.g. for FIGOS – LAGOS comparison, this is sufficient for most cases. A larger range of nominal illumination angles can still be obtained by rearranging the single arms of the lamp stand or by positioning the lamp outside the goniometer. However, the outside positioning of the lamp is critical due to the size of the darkroom and, furthermore, it requires new analysis of the lens system and corresponding illumination homogeneity since the observation distance would differ from the actual one.

3.3.2 LAGOS measurement procedure

The sequence for spectrodirectional measurements performed with the LAGOS is similar to the FIGOS procedures. Data can either be stored as radiance or as reflectance values. However, if data with the ASD FieldSpec 3 is sampled in the reflectance mode, only reflectance values are stored and it is not easily possible to access the single radiance values for e.g. the Spectralon reference measurements, if needed. Therefore, it is proposed to work in a radiance mode and calculate reflectances afterwards.
Prior to actual target measurements a Spectralon reference measurement is performed from nadir. Since no changing atmospheric effects are present no further reference measurement are needed. However, after data acquisition is completed a reference measurement can be performed at nadir in order to check for illumination specific or sensor specific changes during the whole measurement sequence. The LAGOS measurement time of 20min is only critical if natural targets such as plants are measured which may suffer from drought stress due to the high illumination intensity of the lamp.

As for FIGOS, the actual target measurements are started at a forward scattering observation direction of 75° (towards the illumination source) and continued as sketched in Figure 12. Depending on the

adjusted illumination angle, between one and two view directions per dataset interfere with the lamp stand. One of them is usually masked at the corresponding illumination angle by the lamp housing itself. A further one might be masked in the backward scattering half of the adjacent observation plane by the horizontal arm of the lamp stand, but this is only the case for large illumination angles. A possible workaround for these situations, rather than not sample the data, can be found by slightly moving either the zenith arc or the sensor in order to get a free view on the target area. However, data collection close to the hotspot direction, as possible with the dual-view FIGOS, cannot be exploited with LAGOS due to the rather big lamp housing. In total 68 measurements are taken for one laboratory goniometer dataset (2 reference measurements plus 66 target measurements).

3.4 Discussion

The goniometer systems FIGOS and LAGOS face a long tradition of spectrodirectional data collection and their capabilities have substantially been extended over the years. The dual-view FIGOS is currently the only goniometer systems which is able to simultaneously collect radiance data at the same angular resolution from the upper as well as from the lower hemisphere over the spectral range from 400nm – 2500nm. This capability strongly supports the accurate characterization of surface reflectance anisotropy and, furthermore, provides the potential of acquiring the necessary datasets to perform a full field BRF retrieval. The combined use of the same system in the laboratory supports the generation of validation data on the one hand, and on the other hand the comparability can be ensured by permitting the cross-calibration of both experimental devices. In this sense, it can also be used to establish procedures or field-laboratory 'transfer-functions' that permit converting one type of measurement into the other.
The LAGOS itself strongly profits from its independence on weather conditions, time of day and season. The illumination angles can be freely chosen and held constant over time, which supports the repeatability of goniometric measurements. Various experimental setups can be tested in the laboratory in order to improve field goniometry measurement procedures e.g. by analyzing the potential benefit of different angular resolution (cf. Chapter 2.2.3.2). In addition, illumination characteristics could be altered by e.g. using polarization filters or generating artificial diffuse illumination. An experimental way of doing so might consist of spanning several 'Christmas-tree-like' cables in a regular manner over the goniometer. The single light bulbs could then be turned on all together or individually in order to simulate hemispherical diffuse irradiance or diffuse radiation incident from a certain solid angle of the hemisphere, respectively. Such experiments might support studies about adjacency effects of e.g. a nearby building or forest, or could help simulating the influence of a specific cloud distribution in field measurements.

However, improvements can still be made for both the dual-view FIGOS and the LAGOS setup. A critical issue for FIGOS is the time period needed to collect a goniometer dataset. This time period does neither depend on the dual-view combination (measurements for both spectroradiometers are triggered simultaneously) nor on the integration time of the sensors, but mainly on the automated displacement velocity of the sensor. Solutions to shorten the measurement time may consist of replacing the electric motor, changing the angular resolution or altering the sampling sequence. The

current sequence requires 62 automated sensor displacements (zenith plane) but only 5 manual displacements (azimuth plane). The manual displacements can usually be done faster than the motorized sensor movements are. Consequently, scanning the total azimuth plane for a respective observation zenith angle prior to moving the sensor to the next observation zenith angle substantially reduces the number of automated sensor displacements. A respective laboratory experiment revealed that the total measurement period for a goniometer dataset can be reduced by more than 50% to 10 – 13 minutes (original sequence lasts 25 – 30 minutes). However, such a measurement procedure requires careful positioning of the electric cables. Alternatively, for artificial or small targets, a turntable could be used to rotate the target instead of the goniometer zenith arc.

Another improvement would consist of assessing the changing GIFOV. Technically this could be achieved by choosing an adjustable lens system. However, such a lens system might be quite expensive. Alternatively, a constant GIFOV might be experimentally obtained by covering the targets under observation with a low reflecting surface having a hole corresponding to the GIFOV of the spectroradiometer at nadir. This would lead to the same observed target area for all view angles. The target reflectance could then be retrieved from subsequent principal component analysis given the endmember reflectance of the coverage material. However, for LAGOS the worsened SNR might have to be compensated by a strongly improved brightness of the illuminated area, since it is much smaller than in the standard case.

It has been seen in Figure 4 that the ASD spectroradiometer's FOV non-uniformity is also a critical factor, especially when heterogeneous targets are measured. So far, this fact has rarely been considered in detail. As Mac Arthur (Mac Arthur et al., 2007) reported, options for improving the uniformity of the ASD foreoptics could lie in the use of a field stop aperture in place of the lens, re-positioning the lens with respect to the fibre, optical mixers, holographic diffusers but it is expected that these improvements will be tied to reductions in system sensitivity.

4 Methods

4.1 Introduction

As discussed in Chapter 1.4 laboratory and field goniometer measurement results do not represent the true surface BRF and need to be corrected for the respective illumination and observation geometries. This procedure is called BRF retrieval and has to be performed separately for each case. A laboratory BRF retrieval, optimized for LAGOS results but also applicable to measurement results from other goniometer systems, is presented by Dangel et al. (2005) and is not further discussed here. This chapter focuses on the methodology used to assess the diffuse influence present in field spectrodirectional measurements. In addition, necessary pre-processing steps which evolve from measurement specific limitations of the dual-view FIGOS and associated sunphotometer measurements are discussed. Although these steps are valid in general, they are of course adapted to the specific instrumentation used here and may slightly differ for other spectrodirectional field experiments. Since the retrieval results are compared to traditionally obtained reflectance values of the same target using Equation 2 (Chapter 1.4), a special part of this chapter is dedicated to the determination of the Spectralon reflectance behaviour and respective correction factors R_{ref} for both the field and laboratory Spectralon panel.

4.2 Artificial target

In order to test the field BRF retrieval and quantify the diffuse influence, dual-view FIGOS and LAGOS measurements are performed using an artificial target for both cases. The reasons are to minimize differences other than such related to the illumination conditions and to maximize the reflectance anisotropy by choosing an appropriate target.

The artificial target used for this work has first been described by Govaerts et al. (1997) who evaluated a 3D radiative transfer (RT) model against goniometer measurements. The same artificial target has also been tested for its usefulness with FIGOS/LAGOS measurements in earlier studies (Schopfer et al., 2004). The target itself is made of sanded duralumin and consists of a regular matrix of cubes with known geometrical characteristics. It is well qualified for BRF investigations, since it exhibits a high angular anisotropy and is inert over time. However, for FIGOS/LAGOS measurements it was found to be too small since the sensor GIFOV for large observation angles outreached the spatial extent of the target area. Consequently a larger artificial target with similar characteristics has been constructed with the help of the Physics Workshop of the University of Zurich, Switzerland. Its suitability has subsequently been tested in various extensive field and laboratory measurement campaigns (Schopfer et al., 2006; Schopfer et al., 2007a). Figure 17 shows the artificial target and its reflectance anisotropy. The size of the cuboids is 3.3 x 3.3 x 3mm with a regular spacing of 2mm between the single cubes.

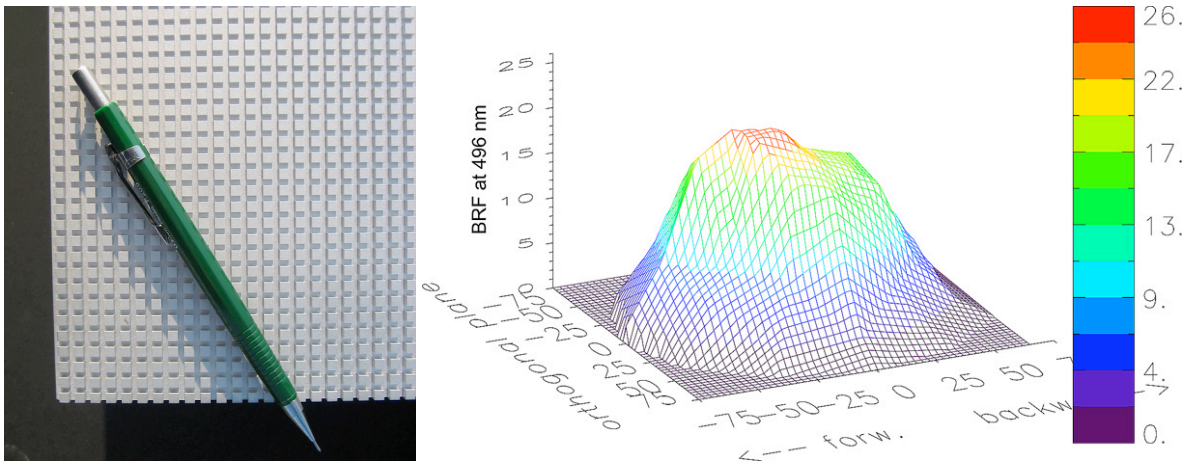

Figure 17: Artificial target, which is used for the BRF retrieval and field – laboratory comparison. Left: Close up of the artificial target. Right: Reflectance anisotropy at a wavelength of 496nm as measured in the laboratory (30° illumination direction from the right side). Note the forward scattering peak, which drastically increases for larger illumination zenith angles.

4.3 Field BRF retrieval

Typically, field measurements are affected by atmospheric conditions and underlie a direct and a diffuse illumination component. The distribution of the latter is not necessarily isotropic. Influencing factors are related to the cloud cover, aerosol content and the surrounding area (i.e. forest, hillsides, buildings etc.) which all lead to multiple scattering and a varying amount of incoming diffuse light for each incident direction. However, the observed (reflected) radiance L_r at the sensor is the result of the total incoming radiance L^{inc} (both the direct and the diffuse component) interacting with the target specific BRF. In other words, the BRF "tells" the incoming single radiation beams how, meaning how much and in which directions, they are reflected. Physically this is expressed in (3) as follows

$$L_r(-\mu,\mu_0,\varphi-\varphi_0)=\pi^{-1}\int_0^1\int_0^{2\pi} R(-\mu,\mu',\varphi-\varphi')*L^{inc}(\mu',\mu_0,\varphi-\varphi_0)\mu' d\mu' d\varphi' \qquad (3)$$

where $-\mu$, μ_0 = cosines of the view and solar zenith angles,
$\varphi-\varphi_0$ = is the view azimuth angle with respect to the solar principal plane and
R = the BRF of the target.

The notation $-\mu$ and μ is used here for upwelling and downwelling radiation, respectively (Martonchik, 1994). In order to accurately retrieve the BRF the reflected radiance as well as the single contributors to the incoming radiance field (direct and diffuse radiances) have to be known, preferably with high angular resolution. This can be achieved either by measurements or by modeling. The most accurate BRF retrieval for field measurements is currently performed by following the procedure proposed by Martonchik et al. (1994). It is based on the idea of splitting up the radiation into a direct and diffuse part E_{dir} and L_{diff}, respectively, and considering their respective reflection processes (the interaction with the surface) separately. The reflected radiance L_r is then calculated as

$$L_r(-\mu,\mu_0,\varphi-\varphi_0) = \pi^{-1}R(-\mu,\mu_0,\varphi-\varphi_0) * E_{dir}(\mu_0) + L_{diff}(-\mu,\mu_0,\varphi-\varphi_0) \quad (4)$$

E_{dir} is obtained from sunphotometer measurements and the dual-view FIGOS directly provides spectrodirectional measurements of L_r. The upward diffuse radiance L_{diff} is also dependant on the surface BRDF ($\pi^{-1}R$) and is calculated using (5) where the incident diffuse radiance L_{diff}^{inc} is directly obtained from dual-view FIGOS measurements.

$$L_{diff}(-\mu,\mu_0,\varphi-\varphi_0) = \pi^{-1}\int_0^1\int_0^{2\pi} R(-\mu,\mu',\varphi-\varphi') * L_{diff}^{inc}(\mu',\mu_0,\varphi'-\varphi_0)\mu' d\mu' d\varphi' \quad (5)$$

The bidirectional reflectance factor R can then be iteratively solved using (4) and the $(n-1)^{th}$ iteration of (5), and is formulated as

$$R^{(n)}(-\mu,\mu_0,\varphi-\varphi_0) = \frac{L_r(-\mu,\mu_0,\varphi-\varphi_0) - L_{diff}^{(n-1)}(-\mu,\mu_0,\varphi-\varphi_0)}{\pi^{-1}E_{dir}(\mu_0)} \quad (6)$$

As an initial estimate of the BRF, $R^{(0)}$ is used where L_{diff}^{inc} is neglected and atmosphere-surface reflections are ignored ($R^{(0)} = L_r/(\pi^{-1} * E_{dir})$). For each iteration, the reflected radiance L_r is calculated using the current iteration estimate of R. The iteration is ended when the difference between the calculated and measured reflected radiances, $L_r^{calculated}$ and $L_r^{measured}$, respectively, becomes smaller than a previously defined threshold. Figure 18 shows an overview of the field BRF retrieval concept. Highlighted boxes represent measured quantities obtained by the sunphotometer and the dual-view FIGOS.

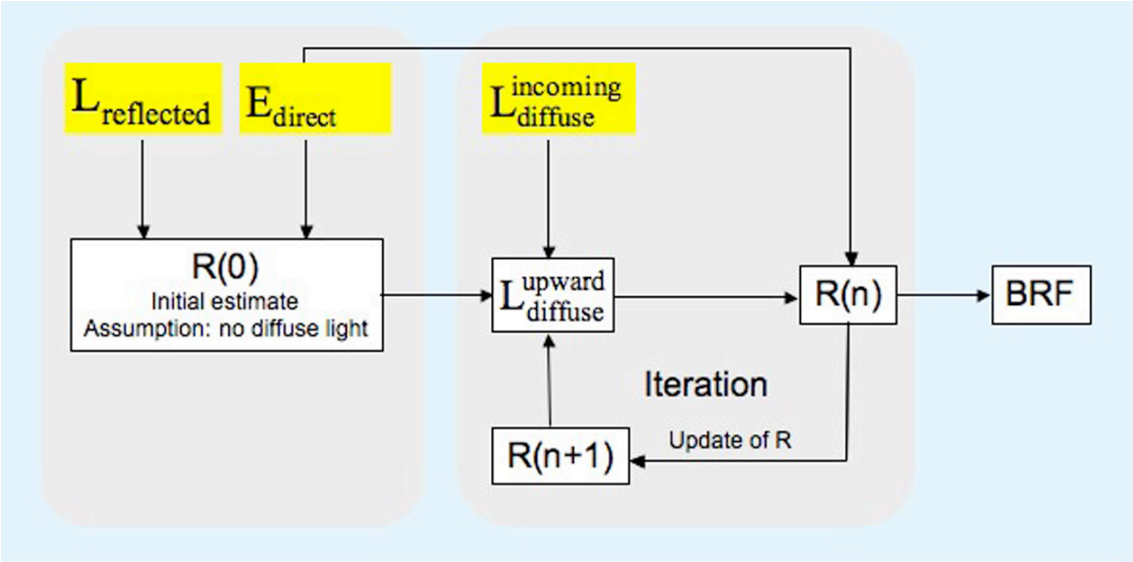

Figure 18: BRF retrieval concept following the approach proposed by Martonchik et al. (1994). The yellow highlighted boxes represent directly measured quantities with the dual-view FIGOS and the MFR-7 sunphotometer, respectively.

4.4 Assessment of measurement specific limitations

In an ideal case all necessary input data for the abovementioned BRF retrieval algorithm are measured with the same instrument and at the same point of time. However, practically this is not feasible and certain limitations affecting the retrieval results emerge due to the specific measurement setup, which is only an approximation to the ideal case. The limitations are predominantly related to instrument specific characteristics such as the spectral range and spectral resolution and to the time period needed to acquire a complete goniometer dataset. In the following, these issues are addressed and their assessment is described.

4.4.1 Determination of intercalibration coefficients

The need for intercalibration coefficients evolves from the fact that currently three spectroradiometers are used to obtain the necessary input data to the retrieval algorithm. The angularly resolved reflected and incoming diffuse radiation is obtained with the same type of instrument (ASD FieldSpec 3). The corresponding intercalibration coefficient has been determined during a different study and is presented in Figure 11. Here, the intercalibration between the ASD FieldSpec 3 and the MFR-7 sunphotometer is addressed. It is obtained by comparing the total irradiance values from sunphotometer measurements $E_{tot,mfr}(\theta_i)$ and the total irradiance values $E_{tot,asd}(\theta_i)$ retrieved from Spectralon reference measurements performed with the ASD FieldSpec 3. For deriving $E_{tot,asd}(\theta_i)$, the Spectralon panel is either assumed to be Lambertian or, more accurately, a BRF correction factor has to be taken into account. The latter has been assessed for this study as explained, along with the determination of $E_{tot,asd}(\theta_i)$ in Chapter 4.5. Provided the knowledge of $E_{tot,mfr}(\theta_i)$ and $E_{tot,asd}(\theta_i)$ the respective intercalibration coefficient can be written as

$$c_{mfr}(\theta_i) = \frac{E_{tot,mfr}(\theta_i)}{E_{tot,asd}(\theta_i)}. \quad (7)$$

Within a standard goniometer data take the Spectralon panel is measured in the beginning and at each nadir bypass (seven times in total) and the sunphotometer provides a record of the irradiance in 30s intervals. Consequently, a mean value of $c_{mfr}(\theta_i)$ can be calculated for each goniometer dataset. Since the cosine response function of the sunphotometer's receiver depends on the solar zenith angle and deviates by up to 7% of that of a perfect Lambertian receiver (Yankee Environmental Systems, 2000) the coefficients $c_{mfr}(\theta_i)$ are again averaged over six goniometer datasets for solar zenith angles ranging from 24.7° to 52.9°. Figure 19 shows a comparison of $E_{tot,mfr}(\theta_i)$ and $E_{tot,asd}(\theta_i)$ for 496nm and the obtained intercalibration coefficients for the sunphotometer bands

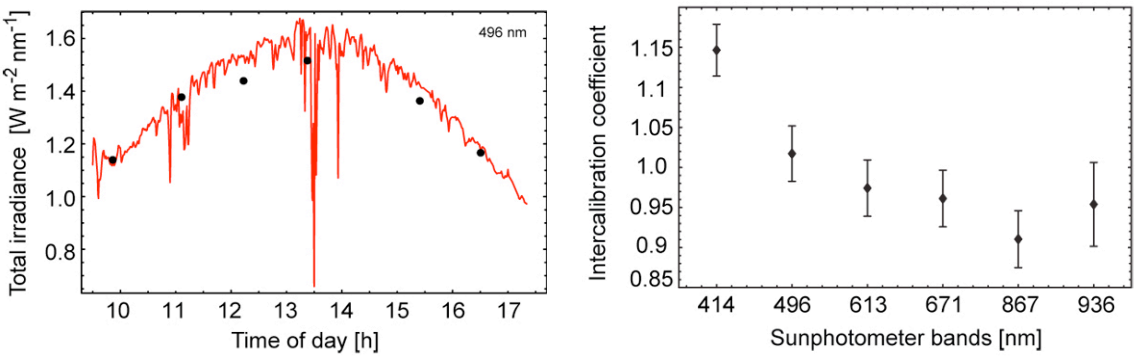

Figure 19: Left: Comparison of the total irradiance obtained from sunphotometer measurements (red line) and the total irradiance values calculated using the Spectralon reference panel for a wavelength of 496nm (black points). Right: ASD FieldSpec 3 – sunphotometer intercalibration coefficients for the respective sunphotometer bands. The plotted data represent the averaged value for a solar zenith angle range from 24.7° to 52.9° and the respective standard deviations.

4.4.2 Spectral resolution and spectral range

For this study both the reflected and the incoming diffuse radiation are measured with an ASD FieldSpec 3 providing continuous spectral information from 400nm to 2500nm. However, the direct irradiance from the sun is obtained from sunphotometer measurements and is available in six spectral bands from 414nm to 936nm only. Principally, this limits accurate retrieval results to the sunphotometer spectral bands. One might try to obtain a continuous spectral coverage by linear interpolation between the sunphotometer bands, but due to the highly variable atmospheric absorption features this is only a coarse approximation as Figure 20 shows.

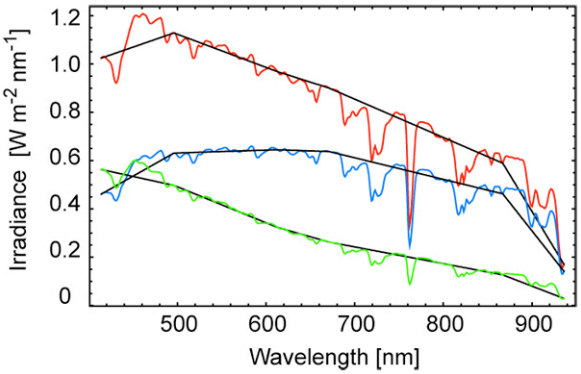

Figure 20: Total (red) and direct (blue) and diffuse (green) irradiance at high spectral resolution versus interpolated sunphotometer measurements (black lines)..

A more accurate assessment of the atmospheric absorption features is obtained by weighing the interpolated values for each spectral section between the sunphotometer bands. The respective weight factors are calculated by rationing the interpolated values to $E_{tot,asd}$ (continuous spectral coverage) for the respective solar zenith angles θ_i. However, in doing so the total irradiance is estimated and not the direct irradiance of the sun. Thus, the ratio of direct to total irradiance from respective sunphotometer measurements needs to be applied to the estimated irradiance values prior to calculating the weight

factors. This method is applied to each set of direct irradiance measurements, which are used for the retrieval algorithm (66 measurements per goniometer dataset). Figure 21 shows the effect of such an assessment on the reflectance calculated for a vegetation target.

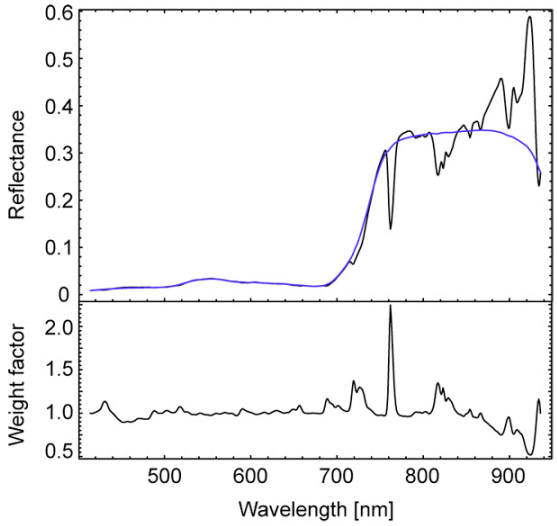

Figure 21: Nadir reflectance calculated with spectrally weighted interpolation of total irradiance (blue line) versus nadir reflectance calculated with linear interpolation of total irradiance (black line). The largest deviation occurs for the oxygen absorption feature at 760nm.

4.4.3 Time period of goniometer measurements

One goniometer dataset typically consists of 66 measurements for the upward looking as well as for the downward looking sensor. Since the sensors have to be moved between each measurement, these 66 measurements cannot be performed at the same time; the total time period needed consists of about 20 to 25 minutes. Within that time span the illumination conditions do change. This is due to the movement of the sun and the changing atmospheric properties (e.g. clouds), which affect the amount and the distribution of the incoming diffuse light. Therefore, it is tried to account for these effects by weighing a) the measured incoming diffuse radiance L_{diff}^{inc} and b) the measured reflected radiance L_r. The weight factors f_{diff} and f_{tot} are obtained using the continuous diffuse and total irradiance readings of the sunphotometer, respectively. Thereby, certain assumptions have to be made which consist of:

a) Weighted incoming diffuse radiation

Here it is assumed that changes of the diffuse irradiance $E_{diff,mfr}$ within the time period $T(t_1, t_2, \ldots, t_{66})$ of a goniometer dataset affect the 66 single incoming diffuse radiation measurements L_{diff}^{inc} to a similar degree. The weight factor $f_{diff}(t_x)$ can then be obtained from the ratio $E_{diff,mfr}(t_x)$ / $E_{diff,mfr}(t_1)$ and the incoming diffuse radiation is written as

$$L_{diff}^{inc}(t_x) = L_{diff}^{inc}(t_x) * f_{diff}(t_x). \quad (8)$$

b) Weighted reflected radiation

A similar assumption as for a) is made for the total irradiance $E_{tot,mfr}$ which affects the angularly resolved reflected radiation L_r from the target. The respective weight factor $f_{tot}(t_x)$ is then obtained from $E_{total,mfr}(t_x)$ / $E_{total,mfr}(t_1)$ and the reflected radiation from the target is written as

$$L_r(t_x) = L_r(t_x) * f_{tot}(t_x). \quad (9)$$

4.5 Spectralon correction factor

Spectralon panels (Labsphere Inc.) are widely used as a Lambertian reference standard in order to deduce reflectance quantities from field and laboratory measurements. However, as other studies (Kimes et al., 1982) have shown, a perfectly Lambertian panel cannot be achieved in practice and also Spectralon does not follow the Lambertian assumption (Sandmeier et al., 1998b). In this study two different Spectralon panels are used, one for field measurements and the other one for laboratory measurements. The reason behind this is to keep the laboratory Spectralon always as clean as possible. For the field Spectralon panel this is not feasible since extensive usage and exposure to the natural illumination lead to a certain degradation over time (Möller et al., 2003). Such ageing effects can be assessed by direct comparison to the laboratory Spectralon panel. Therefore, the deviation of the laboratory Spectralon panel from a lossless Lambertian reflector is determined along with its bidirectional reflectance factor following the method described by Sandmeier et al. (1997).

An absolute calibration of the light source, the sensor and the reference panel is often not feasible. However, the irradiance E for a certain illumination zenith angle θ_i can still be derived by hemispherical integration of the reflected radiances L_r of the Spectralon panel. For this study, L_r is obtained from LAGOS spectrodirectional measurements at zenith and azimuth angle steps of 5° and 30°, respectively. Effects of the non-parallelism of the irradiance are minimized by illuminating the Spectralon panel from nadir. E(0°) is then written as

$$E(0°) = \frac{1}{\rho_{ls}} \int_0^{2\pi} \int_0^{\frac{\pi}{2}} L_r(\theta_r, \varphi_r) * \cos(\theta_r) \sin(\theta_r) d\theta_r d\varphi_r. \quad (10)$$

The albedo ρ_{ls} is provided by Labsphere's calibration protocol. However, Labsphere obtains ρ_{ls} from one specific measurement performed at an illumination zenith angle of 8° (Labsphere, 2004) which causes a little error in estimating E(0°). Since the diffuse irradiance is negligible in the laboratory (cf. Chapter 3.3) the hemispherical irradiance for specific illumination zenith angles can be derived by $E(\theta_i) = E(0°)*\cos(\theta_i)$ for the centre point of the lamp beam.

Assuming a Lambertian behaviour of the Spectralon panel the hemispherical irradiance $E(\theta_i)$ is often derived from a single measurement of the reflected radiation L_r taking the albedo ρ_{ls} of the calibration protocol into account and is written as

$$E(\theta_i) = \frac{L_r(\theta_r, \varphi_r) * \pi}{\rho_{ls}}. \quad (11)$$

Based on a spectrodirectional dataset obtained at high angular resolution, the deviation Δ of the Spectralon panel from Lambertian behaviour is then determined by

$$\Delta(0°, \theta_r, \varphi_r) = \frac{L_r(\theta_r, \varphi_r) * \pi}{E(0°) * \rho_{ls}}. \quad (12)$$

For a new Spectralon panel, Sandmeier et al. (1998b) found that the Spectralon obeys Helmholtz's reciprocity law to a satisfying extent, allowing for the exchange of the source and the viewing directions. Since Spectralon reference measurements are usually performed from a nadir position the panel's nadir reflectance factor R_{ref} for an arbitrary source zenith angle is derived by applying reciprocity and written as

$$R_{ref}(\theta_i, \varphi_i, 0°, \lambda) = \frac{L_r(0°, \theta_r, \varphi_r, \lambda) * \pi}{E(0°, \lambda)}. \quad (13)$$

The hemispherical irradiance E(0°) is derived from the same spectrodirectional dataset using (10). Although the currently used foreoptic produces only little shadow on the target area, measurements at the exact hotspot position (nadir in this case) need to be interpolated.
In order to determine the bidirectional reflectance factor R_{ref} of the field Spectralon, L_r in (13) can be replaced by the corresponding reflected radiances of the field Spectralon $L_{r,\ field}$ obtained under the same laboratory conditions. R_{ref} then corrects the respective Spectralon panel's reflectance characteristics for its non-Lambertian behaviour and using Equation 2 (Chapter 1.4) it can be applied to correct any traditional target reflectance measurements.

5 Data Acquisition

In this study, two separate datasets have been analyzed. The first dataset was obtained using a preliminary setup in order to gather experiences with a combined use of an upward and downward looking sensor. Thereby, the artificial duralumin target as well as a natural grass surface were measured both in the field and in the laboratory.

The second dataset was obtained using the dual-view FIGOS in the framework of an extensive field campaign (GonioExp06) performed in summer 2006 in Germany (Schneider et al., 2007; Schopfer et al., 2007b). During the GonioExp06 campaign dual-view spectrodirectional measurements were performed using the artificial target as well as a natural target. Measurements of the artificial target were specifically performed to test the dual-view FIGOS setup and perform the field BRF retrieval. A corresponding dataset of the artificial target was also obtained in the laboratory. Within this chapter only the field and laboratory data collection of the artificial target is presented. A broader overview about the GonioExp06 campaign, also focusing on the BRF retrieval applied to a natural target, will be given in the application section in Chapter 7.

Table 3 presents an overview of all available goniometer datasets along with the respective acquisitions characteristics.

	Preliminary experiment		**Final experiment**		**Spectralon experiment**
Character	**PA**	**PV**	**FA**	**FV**	**S**
Purpose	Test of dual-view capability. Comparison of field and laboratory measurements.		Evaluation of dual-view FIGOS. Data take for field BRF retrieval.	Comparison of ground based and spaceborne surface reflectance.	Deviation from Lambert. Determination of Spectralon BRF.
Target	Artificial	Grass	Artificial	Triticale	a) Field Spectralon b) Laboratory Spectralon
System	Field: FIGOS + ASD FSFR Lab: LAGOS		Field: Dual-view FIGOS. Lab: LAGOS	Dual-view FIGOS	Protractor setup
Instrument	GER 3700 (FIGOS) ASD FSFR on tripod		2 x ASD F3	2 x ASD F3	ASD F3
Spectral range	GER: 250-2500nm ASD: 350-2500nm		350-2500nm		ASD: 350-2500nm
FOV / observation distance	GER: 3°, ASD: 8° / 2m		3° / 2m	3° / 2m	3° / 0.4m
Illumination angles θ_i	Field: 38.7° - 73° Lab: 38.7° - 48.5°	Field: 38.7° - 67.3° Lab: 38.7° - 55.4°	24.8° - 52.9°	24.7° - 49.2°	a) 0° - 60° (steps 10°) b) 10° - 60° (steps 10°)
Sampling (zn/az)	15° (-75° to 75°) / 30°				θ_i = 0°: 5° / 30° 10°≤ θ_i ≤ 60°= 0°5° / 30°
ID of available datasets	PA1 – PA6	PV1 – PV5	FA1 – FA11	FV1 – FV4	S
Reflectance type	Field HCRF, BCRF		Field HCRF, BCRF	Field HCRF	BCRF

	Preliminary experiment		Final experiment		Spectralon experiment
Character	**PA**	**PV**	**FA**	**FV**	**S**
Additional data	Sunphotometry				-
Acquisition date / location	August 2005, Dübendorf (CH)		June 2006, Gilching (D)		July 2007, Zurich (CH)

Table 3: Overview of the measured datasets. The letter codes P and F are used for datasets obtained with the preliminary and the final experiment, respectively, whereas A and V abbreviate the target type (A = artificial, V = vegetation). S is used for the Spectralon experiment.

5.1 Data acquisition – preliminary setup

In August 2005 a preliminary setup for the dual-view FIGOS was tested at the airport of Dübendorf (DUB), Switzerland. The test site DUB (47°24' N; 8°38' E) is located in the canton Zurich about 10km northeast of the city of Zurich. It is a flat area at a height of 590m above mean sea level with no major buildings in the surroundings and, hence, well suited for spectrodirectional measurements. Spectrodirectional measurements at similar illumination zenith angles were accomplished in the field and in the laboratory.

5.1.1 Target

For both cases (field and laboratory) the previously described artificial duralumin target (cf. Chapter 4.2) was used as well as a natural grass surface obtained from a gardening enterprise. The grass was put in a box of 1m^2 and bedded on a mixed layer of sand and mould in order to keep it on its best natural environment (Figure 22). Regular watering was assured over the whole day in order to minimize spectral changes due to water stress. The grass itself consists of a homogenous surface at a height of 3cm.

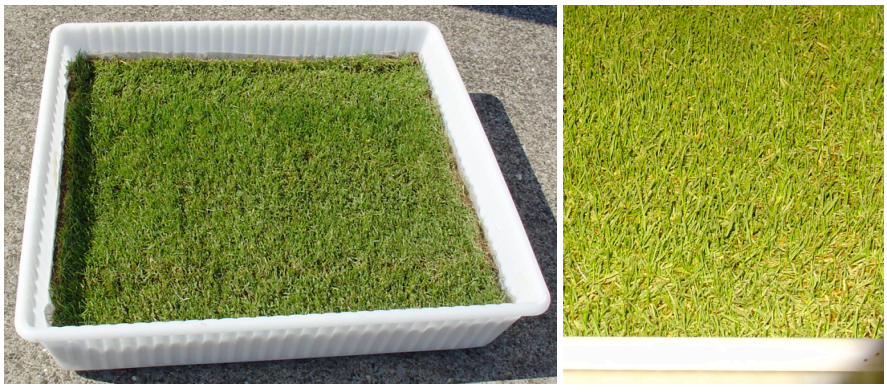

Figure 22: Left: Natural grass surface as measured with the FIGOS and LAGOS setups. Right: Close up of the grass surface. Note the white margins of the box, which may lead to adjacency effects in the reflectance data.

By keeping the grass in a box a trade-off had to be agreed. On one hand the box allows for a comfortable transportation for subsequent laboratory measurements, on the other hand potential

adjacency effects, especially for large illumination and observation directions, had to be accepted. Furthermore, for large illumination zenith angles, cast shadow is produced by the rim of the box leading to a decreased illuminated area. With regard to the changing GIFOV of the sensor this effect was critical and therefore, only observation angles up to 60 ° could be used. In order to assess such limitations in future studies, a black box with significantly lower rims should be considered.

5.1.2 Spectrodirectional measurements

Laboratory measurements were performed using the LAGOS setup as described by Dangel et al. (2005) and in Chapter 3.3. For field measurements the traditional FIGOS setup was used (Sandmeier et al., 1999). It consists of a GER3700 spectroradiometer (Spectra Vista Corporation) which was mounted onto the zenith arc of the field goniometer system FIGOS. The GER3700 sensor was operated with a 3° FOV and data were sampled in a spectral range from 300nm to 2500nm at intervals of 1.5nm (300 – 1050nm), 6.5nm (1050 – 1900nm) and 9.5nm (1900 – 2500nm), respectively (Schaepman et al., 2000). The sampling strategy corresponds to the standard measurement procedure as described in Chapter 3.2.1. Figure 23 shows the traditional FIGOS setup with the GER3700 sensor.

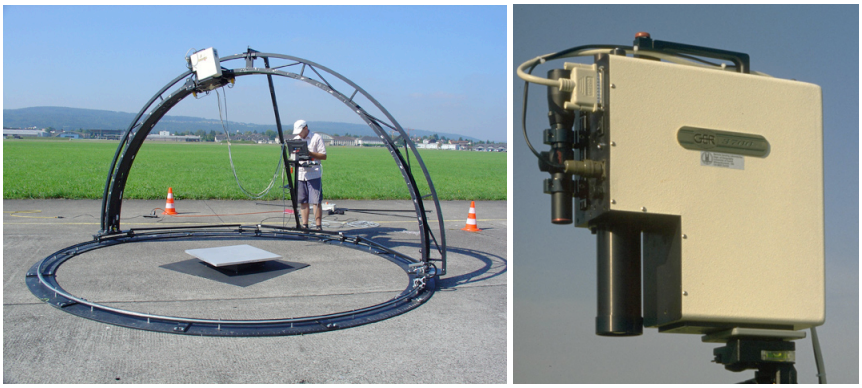

Figure 23: Left: Well known FIGOS setup as used in the preliminary setup. Measurements are performed of an artificial target. Right: Close-up of the GER3700 spectroradiometer.

Simultaneously, the incoming diffuse radiances were measured using a FieldSpec Pro FR spectroradiometer (Analytical Spectral Devices Inc., 1999) which was mounted on a camera tripod and pointing upward using a 3° FOV. The incoming diffuse radiances were sampled over a spectral range of 350nm to 2500nm at intervals of 1.4nm (350 – 1050nm) and 2nm (1050 – 2500nm) and a spectral resolution of 3nm at 700nm and 10nm at 1400/2100nm, respectively. The measurements were accomplished at the same angular resolution as the reflected radiances. However, the positioning of the upward looking sensor was performed manually by using the standard azimuth and zenith scales of the camera tripod. Figure 24 shows the preliminary setup for measuring the incoming diffuse radiances.

Figure 24: Test measurements of the incoming diffuse radiation. Left: A FieldSpec FR is positioned on a camera tripod and pointing upwards. The angular sampling is done manually using the angle scale of the tripod. Right: Close-up of the upward pointing 8° foreoptic.

In total 11 goniometer datasets were obtained for illumination zenith angles ranging from 38.7° to 73°. In the field, the artificial and natural target was measured for 6 illumination angles and 5 illumination angles, respectively. However, due to the target box and positioning limitations of the artificial light source, corresponding laboratory goniometer datasets could only be obtained for 4 illumination angles for both cases. Table 4 reports an overview of the goniometer datasets obtained using the preliminary setup for both target types.

ID	DOY	Target	Start LT [h:min]	Period [min]	Start zenith [°]	Delta zenith [°]	Delta azimuth [°]	MFR	FIGOS	LAGOS
PA1	242	Artificial	10:35	30	52.8	4.1	8.0	ok	ok	ok
PA2	242	Artificial	13:10	30	38.7	0.1	11.9	ok	ok	ok
PA3	242	Artificial	14:34	20	41.1	1.7	7.0	ok	ok	ok
PA4	242	Artificial	15:45	29	48.5	7.3	7.7	ok	ok	ok
PA5	242	Artificial	17:16	28	61.8	4.5	5.8	ok	ok	-
PA6	242	Artificial	18:24	32	73.0	5.4	6.0	ok	ok	-
PV1	242	Grass	11:32	25	46.5	3.6	10.8	ok	ok	ok
PV2	242	Grass	13:45	29	38.7	1.1	11.2	ok	ok	ok
PV3	242	Grass	15:01	29	43.5	3.1	9.1	ok	ok	ok
PV4	242	Grass	16:35	30	55.4	4.6	6.9	ok	ok	ok
PV5	242	Grass	17:50	28	67.3	4.7	5.4	ok	ok	-

Table 4: Characteristics of the goniometer datasets obtained with the preliminary setup for the artificial and the natural target named as PA and PV, respectively.

Additionally, an MFR-7 shadow-band sunphotometer (Yankee Environmental Systems, 2000) was used to permanently monitor the atmospheric conditions. Although the meteorological situation was very favorable with clear sky conditions during the whole day, the 11 goniometer datasets are affected by varying diffuse influence. In this case with almost no atmospheric disturbances due to clouds, the diffuse fraction (E_{diff}/E_{tot}) is strongly dependant on the sun zenith angle. However, its variability during a single goniometer dataset also depends on the time period needed for the 66

spectrodirectional measurements. A maximum sun elevation with a zenith angle of 38.5° was reached at 1330h LT (local time) for DOY 242 and the corresponding geographical position of DUB. A maximum diffuse influence and variability is seen for a sun zenith angle of 73° with a measurement time period of 32 minutes. Figure 25 depicts the total, direct and diffuse irradiance data obtained from sunphotometry (left) and the diffuse fraction of the total irradiance for each goniometer measurement period (right).

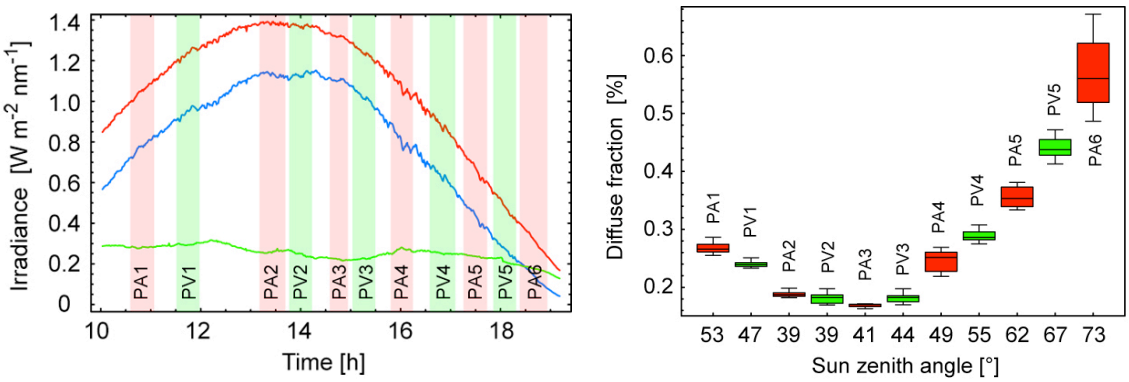

Figure 25: Left: Total (red), direct (blue) and diffuse (green) irradiance as measured with the sunphotometer. The vertical bars represent the FIGOS measurement times for the artificial target (red) and the lawn (green). Right: Box plot of the diffuse fraction of the total irradiance for the respective sun zenith angles for the artificial and natural target (red and green, respectively). The size of the boxes represents the interquartile variability (25% - 75% of the values) of the diffuse irradiance during the FIGOS measurement period. The median value is indicated by the horizontal black line and the whiskers show the total extent of the dataset. All data are shown for a wavelength of 496nm.

5.2 Data acquisition – final setup

The presented data in the following paragraphs were sampled using the actual dual-view FIGOS and the LAGOS setup. The corresponding measurement procedures are discussed in Chapter 3 and illustrated in Figure 7, 8, 13 and 14.

Spectrodirectional data of the artificial target were collected in June during the GonioExp06 field campaign (Schneider et al., 2007; Schopfer et al., 2007b). Measurements were performed at 3 different days (DOY 171, 172 and 175) in order to assure a representative range of illumination zenith angles for the field BRF retrieval. Permanent atmospheric monitoring was assured by using a MFR-7 sunphotometer. In total 11 goniometer datasets were measured with the dual-view FIGOS at solar illumination angles ranging from 24.7° to 52.9°. Table 5 lists all datasets obtained at the respective DOYs.

ID	DOY	Target	Start LT [h:min]	Period [min]	Start zenith [°]	Delta zenith [°]	Delta azimuth [°]	MFR	FIGOS	LAGOS
FA1	171	Artificial	11:55	32	29.5	3	14.3	ok	ok	ok
FA2	171	Artificial	13:32	33	24.8	1.7	17.2	ok (+/-)	ok	ok
FA3	171	Artificial	15:35	29	36.8	4.7	8.5	-	ok	ok

ID	DOY	Target	Start LT [h:min]	Period [min]	Start zenith [°]	Delta zenith [°]	Delta azimuth [°]	MFR	FIGOS	LAGOS
FA4	172	Artificial	09:24	23	51.7	3.8	4.8	-	ok	ok
FA5	172	Artificial	10:41	26	39.4	3.9	7.6	-	ok	ok
FA6	172	Artificial	12:05	22	28.4	1.9	10.1	-	ok	ok
FA7	172	Artificial	13:28	29	24.7	1.2	15.4	-	ok	ok
FA8	172	Artificial	15:37	23	37.1	3.4	6.3	ok	ok	ok
FA9	175	Artificial	15:15	23	33.9	3.3	7.1	ok	ok	ok
FA10	175	Artificial	16:11	51	42.2	8.2	11.5	ok	ok	ok
FA11	175	Artificial	17:17	27	52.9	4.5	5.2	ok	ok	ok

Table 5: Characteristics of the goniometer datasets obtained with the final setup (dual-view FIGOS) for the artificial named as FA1 to FA11.

Unfortunately, system malfunctioning of the sunphotometer led to missing or false direct irradiance data in 6 MFR datasets. However, using inter- and extrapolation, the missing values in dataset FA2 could be replaced to a satisfying extent. Because the direct sun irradiance is a prerequisite to perform the field BRF retrieval, only 6 FA datasets could be used for this purpose. The maximum sun zenith angles for the respective measurement days were[3]: 24.6° at 1320 LT (DOY 171), 24.6° at 1312 LT (DOY 172) and 24.07° at 1307 LT (DOY 175). Figure 26 shows the irradiance conditions for the 3 DOYs along with the respective goniometer datasets and corresponding measurement times.

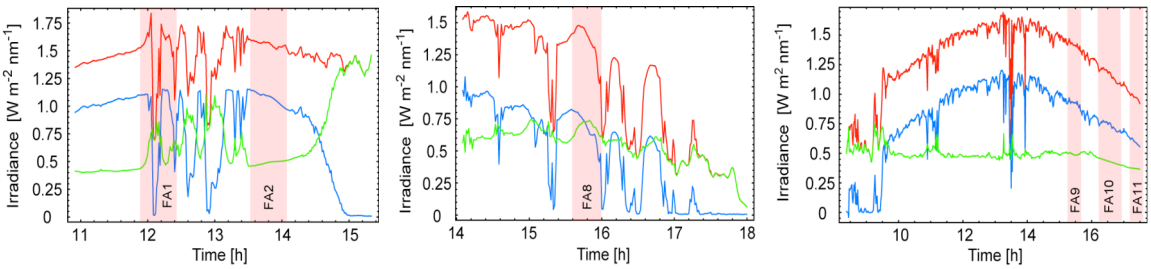

Figure 26: The goniometer datasets for DOY 171 (left), DOY 172 (middle) and DOY 175 (right) with the respective total (red), direct (blue) and diffuse (green) irradiance for 496nm as measured with the sunphotometer.

Since the intrinsic characteristics of the artificial target do not change over time and spectrodirectional measurements were always performed with the same system, the single measurement results depend only on the illumination conditions. The illumination contributions (direct sun irradiance and incoming diffuse radiance) are directly measured for each goniometer dataset and consequently the 6 dual-view goniometer datasets can be used for the field BRF retrieval. The diffuse fraction of the total irradiance significantly varies within the individual datasets. High diffuse variability as seen in datasets FA1 and FA3 is predominantly attributed to passing clouds, whereas the diffuse variability in other datasets is related to the respective sun zenith angle. Figure 27 depicts the diffuse fraction of the total irradiance for the 6 goniometer datasets used for the field BRF retrieval.

[3] Sun altitude and azimuth tables for worldwide locations provided by the Astronomical Applications Department of the U.S. Naval Observatory: http://aa.usno.navy.mil/data/docs/AltAz.php

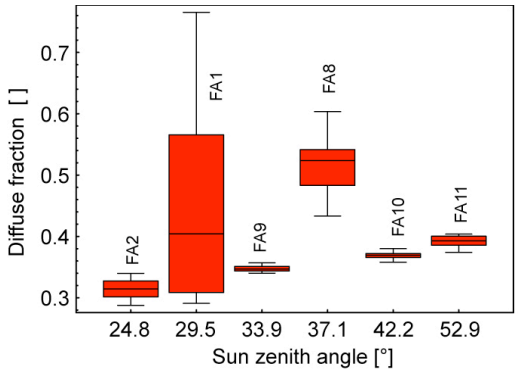

Figure 27: Box plot of the diffuse fraction of the total irradiance for investigated FA datasets. The size of the boxes represents the interquartile variability (25% - 75% of the values) of the diffuse irradiance during the FIGOS measurement period. The median value is indicated by the horizontal black line and the whiskers show the total extent of the dataset. All data are shown for a wavelength of 496nm.

5.3 Data acquisition – Spectralon reference panel

Currently, two Spectralon panels are used at RSL, one for field measurements and the other one for laboratory measurements. In order to account for the deviation from Lambertian behaviour spectrodirectional measurements of both panels have been performed using a specifically constructed protractor setup as shown in Figure 28. The special setup is necessary since the size of the Spectralon panel (25cm x 25cm) is too small for being observed with the LAGOS from large observation angles.

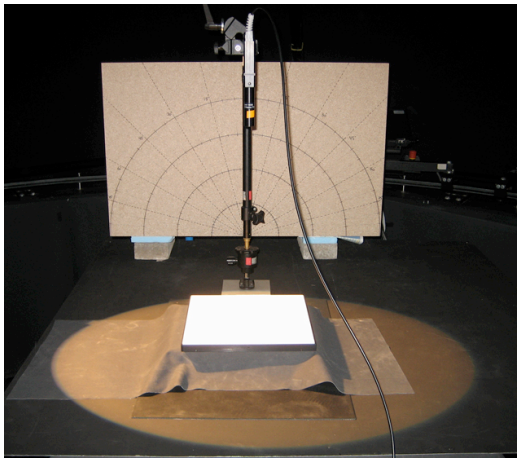

Figure 28: Protractor setup with angular positioning scale.

The protractor setup consists of a vertical telescope post, which is attached to a pivoting ball joint at the bottom, allowing the post to be positioned at any inclination angle. On top of the post a clamp is used to fasten a horizontal bar, which supports the downward looking sensor foreoptic at one end and a pointer device at the other end. The angular positioning in the zenith plane is then performed by setting the pointer to the respective tilt angle on the protractor scale and the desired azimuth observation angle is set by rotating the whole protractor setup around the target. Spectrodirectional data are collected using the same illumination source and spectroradiometer configuration as for LAGOS. The

observation distance is held constant at 0.4m for all observation angles. Consequently, a GIFOV with a diameter of 2cm and a maximal longitudinal extent of 8.16cm is obtained for nadir observation and 75° off-nadir observation, respectively.

In order to determine the deviation from Lambert and to derive the irradiance of the lamp source, the data is sampled using a fine zenith angle resolution of 5° and an azimuth resolution of 30° for nadir illumination ($\theta_i = 0°$). Additionally, spectrodirectional measurements in the principal plane (also at 5° zenith steps) were acquired for both Spectralon panels for illumination angles ranging from 10° to 60°. In total, 7 spectrodirectional datasets were obtained for the laboratory reference panel and 6 datasets for the field reference panel. An overview of the total Spectralon experiments is given in Table 3 in the beginning of Chapter 5.

6 Results

The results obtained from the preliminary experiments of the artificial and vegetation target (PA and PV), the final experiment of the artificial target (FA) and the Spectralon experiment (S) (cf. Table 3, Chapter 5) are presented in this section. They consist of a direct comparison of field and laboratory measurements, the characterization of the diffuse illumination distribution and the field BRF retrieval for the artificial target.

The last section of this chapter is dedicated to the Spectralon experiment. It presents the comparison of the reflectance characteristics of the two Spectralon panels as well as the deviation of the laboratory Spectralon reflectance from a Lambertian reflector.

6.1 Direct comparison of field and laboratory spectrodirectional measurements

6.1.1 Artificial target

Spectrodirectional reflectances are shown for the artificial target as measured in the field and in the laboratory for the same illumination and observation angles. Since the same goniometer systems and an artificial target were used, resulting reflectance differences are attributed to the irradiance conditions solely. Figure 29 shows the nadir reflectances for various illumination zenith angles.

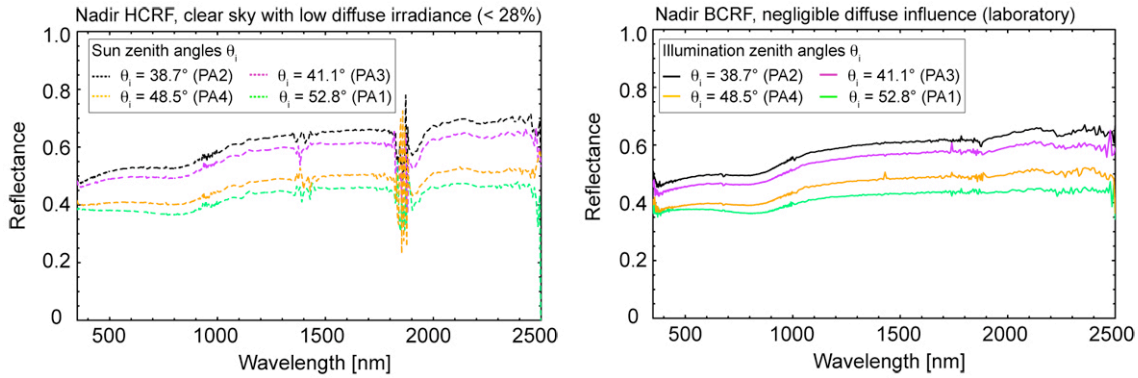

Figure 29: Field (left) and laboratory (right) nadir reflectances of the artificial target for various illumination zenith angles. The spectral variability around 1400nm and 1800nm in the field dataset is related to the atmospheric water absorption features. For the PA dataset description refer to Table 4 and Figure 25.

The artificial target does not exhibit distinct reflectance features in the spectral range from 400nm – 2500nm. Minimum reflectance values are generally obtained in the VIS and maximum values around 2400nm. The differences between maximum and minimum reflectance values are on the order of 15% for small and 5% for large illumination zenith angles. At 800nm a slight absorption feature can be identified. The spectral features around 1400nm and 1800nm in the field reflectances (Figure 29 left) occur due to water absorption in the atmosphere and are typically missing for the laboratory case. The percentual differences between the corresponding field and laboratory nadir reflectances were

computed using $(R_{nadir,field} - R_{nadir,lab})/R_{nadir,lab})*100$) and found to lie within 10% for all illumination zenith angles and over the whole spectral range.
For both the field and laboratory case, the highest reflectance values were observed for small illumination zenith angles and lowest values for large illumination zenith angles. This is related to the geometrical properties of the artificial target, namely to the amount of shadowed area which is observed from nadir. The respective area of cast shadow generated by a single cube strongly depends on the illumination zenith angle and increases for increasing zenith angles and vice versa. Theoretically, no cast shadow is expected for exact nadir illumination in a natural environment since the direct irradiance by the sun is parallel within 0.5°. However, in the laboratory this is not the case and the typically conical illumination geometry leads to minimal cast shadow even for nadir illumination conditions.

The regular geometrical structure of the artificial target leads to a high angular reflectance anisotropy, which strongly correlates with the distribution of the illuminated and shadowed areas for the respective illumination and observation directions. Additionally, due to the optical properties of the sanded duralumin, the artificial target exhibits a strong specular reflectance characteristic, as is shown in Figure 30. For the laboratory case a specular reflectance peak of almost 200% (with respect to the Spectralon) is obtained for an illumination zenith angle of 38.7° whereas in the field case the corresponding reflectance value is about 140%. In general, one can argue that directional effects in the laboratory case are more pronounced than in the field case since for the latter, the diffuse irradiance incident on the target is illuminating the shadowed areas and mitigating dominant reflectance structures. Consequently, dark (shadowed) areas are less dark in the field than in the laboratory where no (neglectable) diffuse irradiance is present.

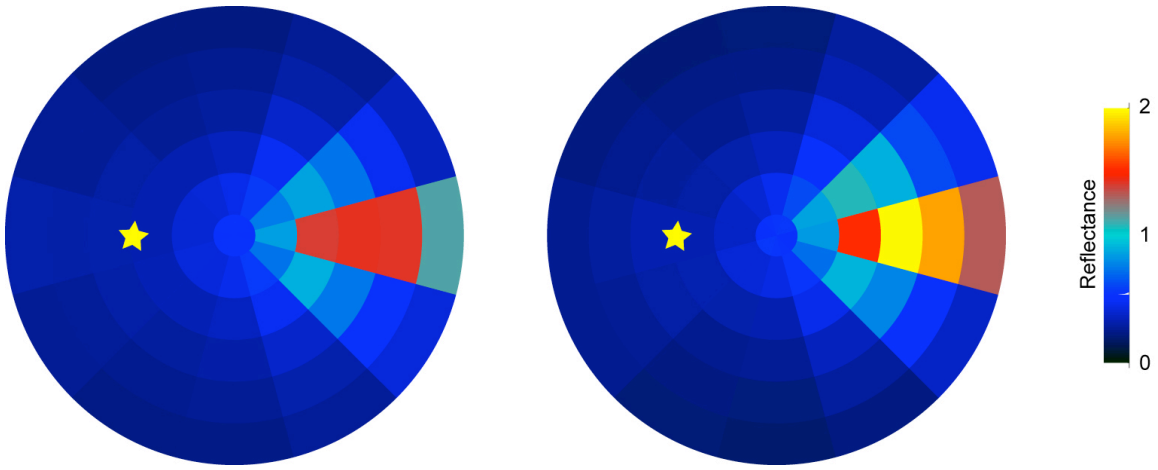

Figure 30: Field HCRF (left) and BCRF (right) of the artificial target for a wavelength of 496nm and an illumination zenith angle of 38.7° (from experiment PA). Note the strong forward scattering characteristics of the artificial target. The reflectances are shown using the respective goniometer sampling grid (refer to Figure 12). The position of the illumination source is marked by the sun symbol

6.1.2 Grass target

Figure 31 shows the spectrodirectional comparison of the field and laboratory measurements of the grass target, which are performed using the datasets PV2 (small illumination zenith angle of 38.7°) and PV4 (large illumination zenith angle of 55.4°). Due to experiment specific reasons (cf. Chapter 5.1.1) directional reflectances could only be obtained for observation zenith angles ranging from -60° (backscattering) to 60° (forward scattering).

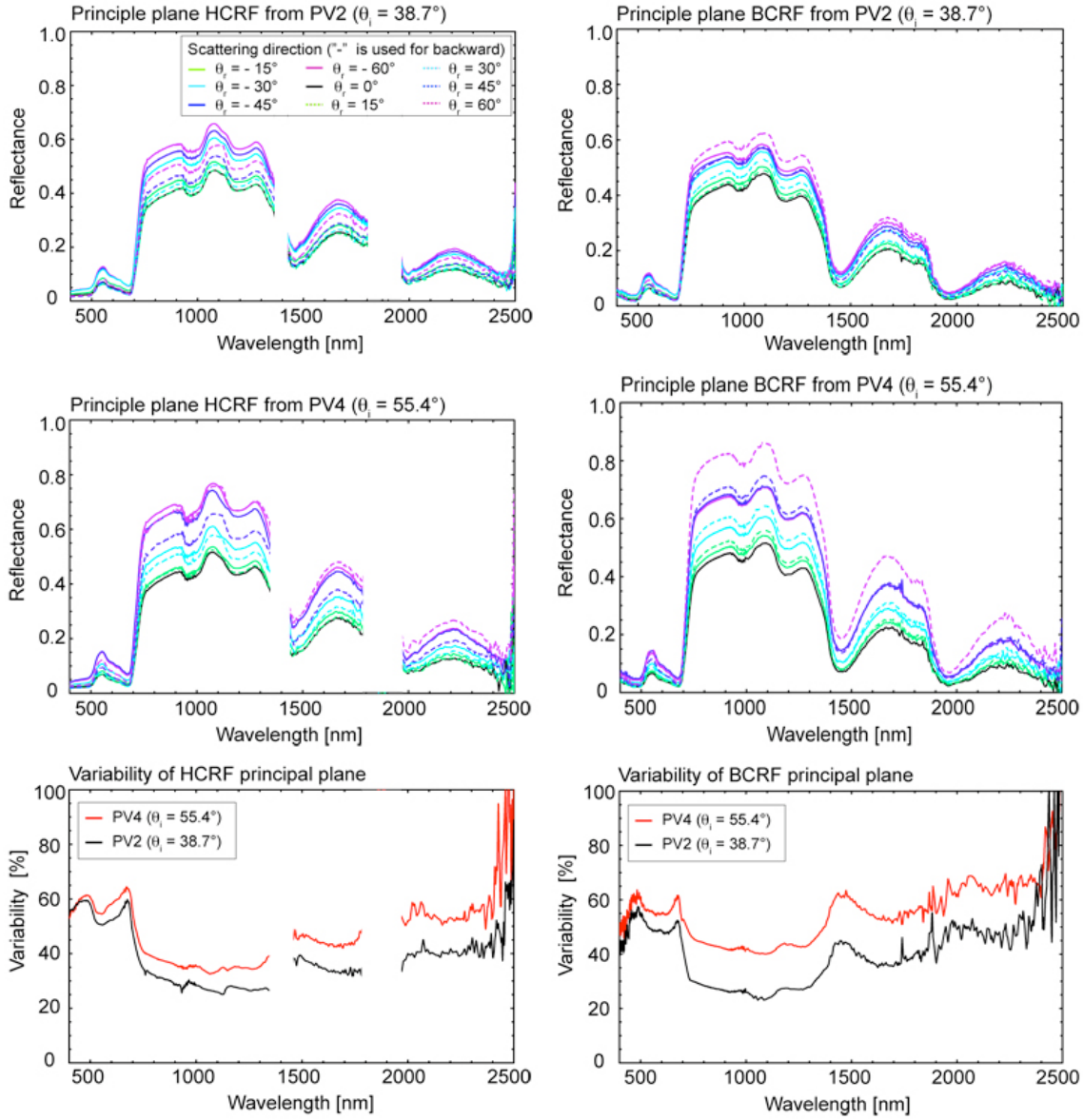

Figure 31: Spectrodirectional reflectance of grass and corresponding directional variability for the field case (left column) and the laboratory case (right column) for two illumination zenith angles (38.7° and 55.4°). Atmospheric water absorption bands are masked out in the left column. For the dataset descriptions of PV2 and PV4 refer to Table 4 and Figure 25.

Typically, higher reflectance values are obtained for backward scattering than for forward scattering directions. The influence of the underlying soil is predominantly visible for nadir observations and leads to lowest reflectance values for that sensor position. The directional reflectance variability within

the principal plane reaches up to 60% typically in the VIS where BRF effects are stronger than in the NIR and SWIR region. The reason for that is that directional effects in the VIS are predominantly driven by shadow casting whereas in the NIR more diffuse light is available through multiple scattering within the canopy and consequently higher reflectance values are obtained.
As can further be seen in Figure 31 the directional reflectance variability within the principal plane clearly depends on the illumination direction and increases for larger illumination zenith angles. For the laboratory case, the dependence on the illumination direction seems to be even stronger and leads to a high variability also in the NIR/SWIR range of the spectrum.

6.2 Directional characterization of the incoming diffuse light

The amount and the angular distribution of the incoming diffuse light substantially depend on the atmospheric constituents and on the solar zenith angle. Even on a clear day, the diffuse fraction of the total irradiance can range from 15% to 55% depending on the respective illumination zenith angle and wavelength (Figure 25). Typically, standard sunphotometer measurements are performed in order to characterize the hemispherical diffuse irradiance. For most cases this is sufficient. However, such measurements do not provide any information about the angular distribution of the diffuse radiation.
The distribution of the diffuse light has been measured with the upward looking sensor at a certain angular resolution and for various solar zenith angles. In order to obtain an estimate on how accurately such measurements reproduce the hemispherical diffuse irradiance, the respective directional results were integrated over all observation angles and compared to the mean values obtained from standard sunphotometer measurements during the FIGOS measurement time periods. This comparison has been performed for solar zenith angles ranging from 38.7° to 73° (experiments PA and PV). The respective correlation coefficients for the sunphotometer bands amount to: 0.97 (414nm), 0.95 (496nm), 0.89 (613nm), 0.81 (671nm), 0.66 (867nm) and 0.93 (936nm). Remaining differences may either be attributed to the angular coverage (oversampling / undersampling) at which incoming diffuse radiances are collected or to over or underestimation of the diffuse radiance close to the sun view direction. Furthermore, inter- and extrapolation was used for diffuse radiance values between the sampling steps and for observation angles larger than 75°, respectively. The significantly lower correlation coefficient of 0.66 at 867nm may be related to the higher atmospheric variability at that wavelength. Since a certain time period is needed for the completion of a whole goniometer measurement cycle, every single diffuse radiance measurement is affected differently by atmospheric changes. Consequently, also the integrated diffuse irradiance is influenced. Figure 32 depicts the correlation results for a wavelength of 496nm.

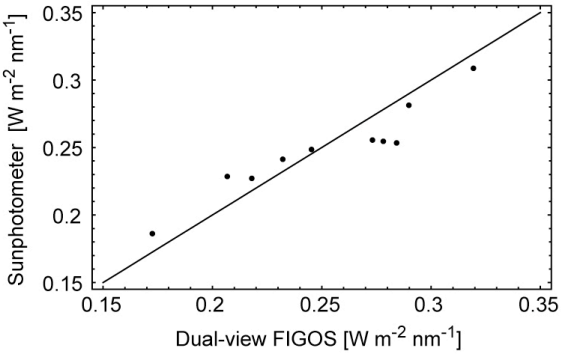

Figure 32: Scatterplot of diffuse irradiance obtained with sunphotometry vs. integrated diffuse radiance measurements obtained from dual-view FIGOS.

The distribution of the incoming diffuse radiation has been measured for different atmospheric conditions. Figure 33 shows the angular diffuse fractions (L_{diff}^{inc} / E_{tot}) of the total irradiance for each measured observation direction (upward looking). On a clear day situation the angular diffuse fractions are mainly determined by the solar zenith angle. A major amount of diffuse light is observed close to the sun view direction and minimum values are observed for opposite viewing directions (with the sun in the back). Typically, the angular diffuse fractions also tend to increase for large observation angles since the respective incident light paths are longer and more multiple scattering takes place. For a clear sky situation and a small illumination zenith angle, a change of the angular diffuse fractions of about 15% is obtained over the whole sky hemisphere. For a clear sky condition and a large illumination zenith angle the observed change of the angular diffuse fractions consists of up to 40%. A cloudy day situation looks even more complicated. Although a maximum value of the angular diffuse fraction is still observed close to the sun view direction, the distribution of the diffuse light is very much dominated by atmospheric disturbances such as moving clouds. Consequently, the angular diffuse fractions can substantially vary over time and for small changes of the observation direction, and the total angular variability can reach up to about 70%.

With regard to the BRF retrieval and associated atmospheric correction this highlights the importance of assessing the incoming diffuse radiance at angular resolution even for clear day situations. Figure 33 represents the angular diffuse fractions of the total irradiance for different illumination zenith angles and atmospheric conditions.

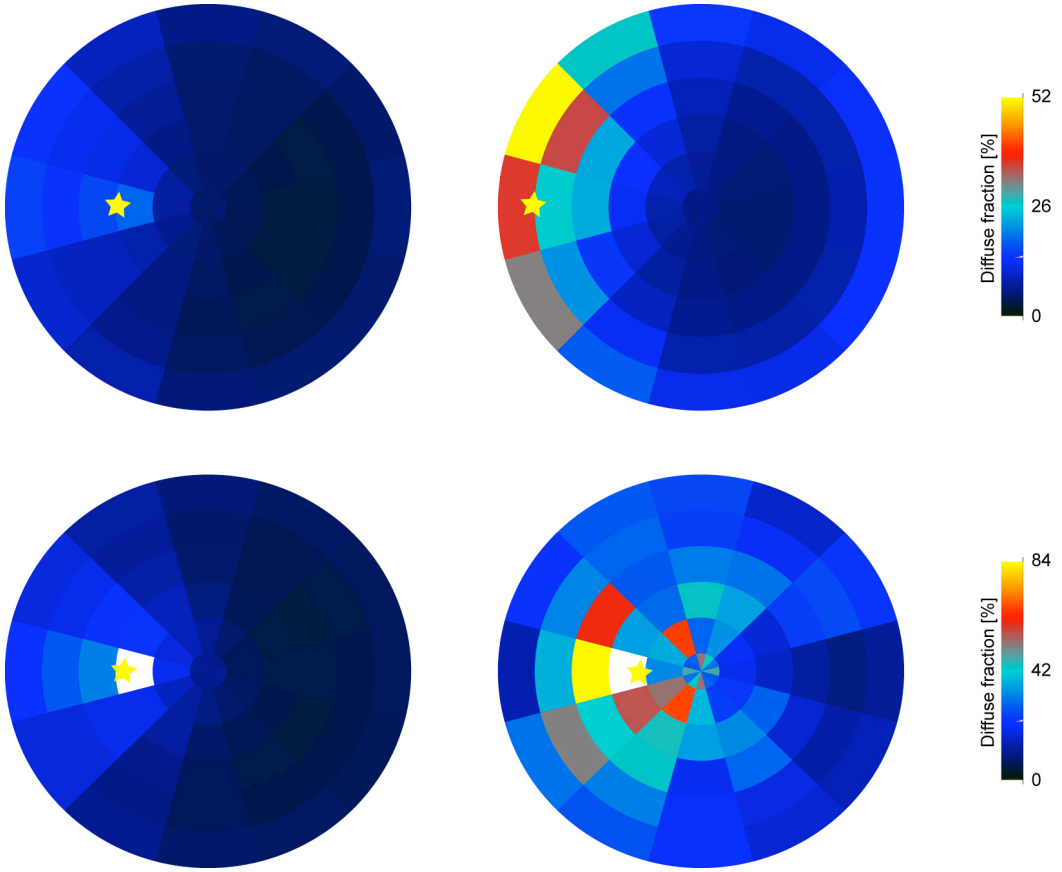

Figure 33: Diffuse fraction for different illumination conditions. Top (datasets PV2 and PV5): Clear day situation for an illumination zenith angle of 38.7° (left) and an illumination zenith angle of 67.3° (right). Bottom (datasets FA9 and FA1): Diffuse incident radiance distribution for a clear day (left) and a cloudy day (right) for illumination zenith angles of 33.9° and 29.5°, respectively. The position of the illumination source is marked by the sun symbol.

6.3 Field BRF retrieval

The field BRF retrieval of the artificial target has been performed for a combined dataset consisting of six complete goniometer measurement cycles obtained at sun zenith angles ranging from 24.8° to 52.9°. The change in the illumination conditions during the measurement of a single goniometer dataset (20 – 30 minutes) affects the retrieval accuracy. This was accounted for by applying different weight factors using Equations (8) and (9) to the reflected and the incoming diffuse radiance measurements prior to the retrieval. The BRF retrieval was then performed for three cases of pre-processed data which are identified as follows: "case 1" (not weighted), "case 2" (weighted using Equation (8)) and "case 3" (weighted using both Equations (8) and (9)).

In this part of the results section the accuracy of the retrieval is described for each case by directly comparing the retrieved BRF datasets to the corresponding laboratory BCRF datasets for a wavelength of 496nm. Results for other wavelengths look similar and are not specifically addressed here. BRF retrieval results over the whole spectral range will be shown in Chapter 7 with regard to a natural target (Triticale).

Firstly, the single measurements are compared one-by-one using a measure for the fractional deviation δ as described in Martonchik et al. (1994). Secondly, the directional hemispherical reflectances (DHR) of the respective datasets are used and thirdly, spectrodirectional reflectances in the principal plane are compared to each other. The fractional deviation δ for a given retrieved BRF R is defined by calculating its difference from a true BRF (in this study: laboratory BCRF) R_{lab} as follows:

$$\delta(\mu_0) = \frac{1}{N}\sum_{ij}\left|\frac{R(\mu_i,\mu_0,\varphi_j-\varphi_0) - R_{lab}(\mu_i,\mu_0,\varphi_j-\varphi_0)}{DHR_{lab}(\mu_0)}\right|. \quad (14)$$

The DHR_{lab} is the laboratory directional hemispherical reflectance and N is the number of single measurements per goniometer dataset (66 for the dual-view FIGOS and LAGOS) for the respective illumination zenith angles. In order not to overweigh small values of R_{lab} the normalization is performed using the DHR_{lab} instead of R_{lab}. Figure 34 displays the fractional deviation for a wavelength of 496nm and the abovementioned 3 retrieval cases for various illumination zenith angles. The fractional deviation of the field reflectance measurements (uncorrected field HCRF) is shown for comparison reasons. Both R_{lab} and the field HCRF are calculated with standard normalization techniques using the Spectralon reference panel.

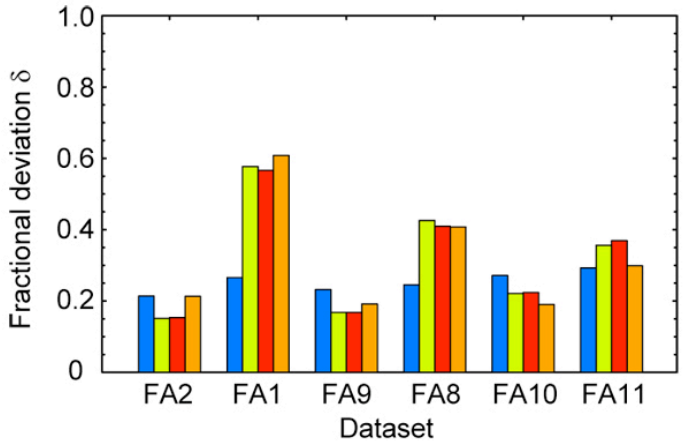

Figure 34: Fractional deviation for the uncorrected field case (blue), BRF case 1 (green; no weighing), BRF case 2 (red; weighted using Eq. 8) and BRF case 3 (orange; weighted using Eq. 8 and 9). For the FA dataset description refer to Table 5, Figure 26 and Figure 27.

The fractional deviation for the field HCRFs (field case) consists of 20% to 30% for all datasets whereas partly larger deviations are obtained for the retrieved BRFs. This is especially the case for those datasets being measured during varying atmospheric conditions within the goniometer observation window. One can therefore argue that rapidly changing atmospheric conditions are well accounted for by repetitive Spectralon reference measurements. With the current goniometer setup in total 7 reference measurements are performed, one in the beginning of the measurements cycle and afterwards one at each nadir bypass. However, it is also seen in Figure 34 that for some datasets (FA2, FA9 and FA10) corrections of 5% to 10% are obtained by the BRF retrieval. A reason for such small differences may be the fact that the fractional deviation consists of a sum of differences between single

directional reflectance pairs. Consequently, large differences, which e.g. are obtained for specific observation directions, contribute quite strongly to this sum. As will be seen later in the principal plane analysis, such large differences occur primarily for the specular reflectance configuration. Another source of error might be related to oversampling[4] or undersampling[5] of the angularly dependent diffuse radiation, especially for those datasets, which are affected by high angular and temporal atmospheric variability. Consequently, this would lead to an over- or underestimation of the total diffuse irradiance in the retrieval algorithm.

The hemispherical reflectance has been calculated for each dataset by integration over the observation angles. In order to avoid extrapolation errors the integration was performed up to observation angles of 75° only. Note that for the retrieved BRF datasets the hemispherical reflectance consists of a DHR whereas for the field case the corresponding integration result is rather a field hemispherical reflectance than a DHR since the incident light consists of both the direct and the diffuse component. The respective deviations from the laboratory DHR_{lab} are then calculated as percentage difference for each case, e.g. $100 * (DHR_{case}(\mu_i) - DHR_{lab}(\mu_i)) / DHR_{lab}(\mu_i)$. Figure 35 shows the hemispherical reflectance differences for the respective goniometer datasets.

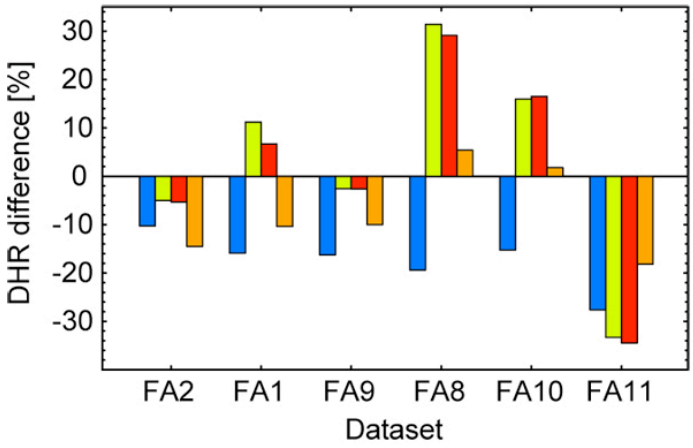

Figure 35: Percentage difference of the DHR for the field case (blue), BRF case 1 (green; no weighing), BRF case 2 (red; weighted using Eq. 8) and BRF case 3 (orange; weighted using Eq. 8 and 9). For the FA dataset description refer to Table 5, Figure 26 and Figure 27.

It can be seen that field hemispherical reflectance values are affected between 10% to 27% by the diffuse irradiance. Surprisingly, the largest differences are not obtained for the dataset measured under highly variable atmospheric conditions (dataset FA1) but for FA11 instead, which was obtained at a solar zenith angle of 52.9°. Consequently, this supports the abovementioned statement that short-term atmospheric changes can be addressed to a certain degree by regular Spectralon reference measurements. For the datasets FA1, FA2 and FA9 substantially better results are obtained with the BRF retrieval using cases 1 and 2. The respective percentage differences of the DHR consist of 5%, 11.2% and 2.5% for case 1 and 5.3%, 6.6% and 2.6% for case 2. For the highly influenced dataset FA1

[4] Oversampling: Too much incoming diffuse radiation may be sampled from adjacent view directions due to the 3° FOV or the rapidly changing atmospheric conditions.

[5] Undersampling: Too less incoming diffuse radiation may be sampled e.g. if the sampling grid is too coarse.

the assessment of the diffuse variability using case 2 leads to significantly better results than case 1. On the other hand cases 1 and 2 seem to fail for larger solar zenith angles where case 3 shows best results (5.3%, 1.7% and 18.1% for datasets FA8, FA10 and FA11, respectively). Unlike the case 2, the input data for the BRF retrieval using case 3 are obtained by additionally weighing the directionally reflected radiances as described in Chapter 4.4.3. In doing so, changes in the solar zenith angle are considered to a stronger extent than in case 2. For the respective datasets (FA8, FA10 and FA11) also bigger solar zenith changes were calculated (3.4°, 8.2° and 4.5°) than for the first three datasets. Note that an especially good correction is obtained for dataset FA10 for which the acquisition took over 50 minutes and the sun zenith substantially changed by 8.2°. In general, it is observed that with regard to the different retrieval cases (case 1, 2 and 3) accounting for the time period of the reflected radiance measurements results in a superior correction of the diffuse influence for larger solar zenith angles only.

Typically, for this target the largest directional effects are expected in the principal plane. Figure 36 shows the corresponding principal plane reflectance values for observation angles ranging from -75° (backward scattering) to 75° (forward scattering) for the field case, the laboratory case and the BRF retrieval case 2.

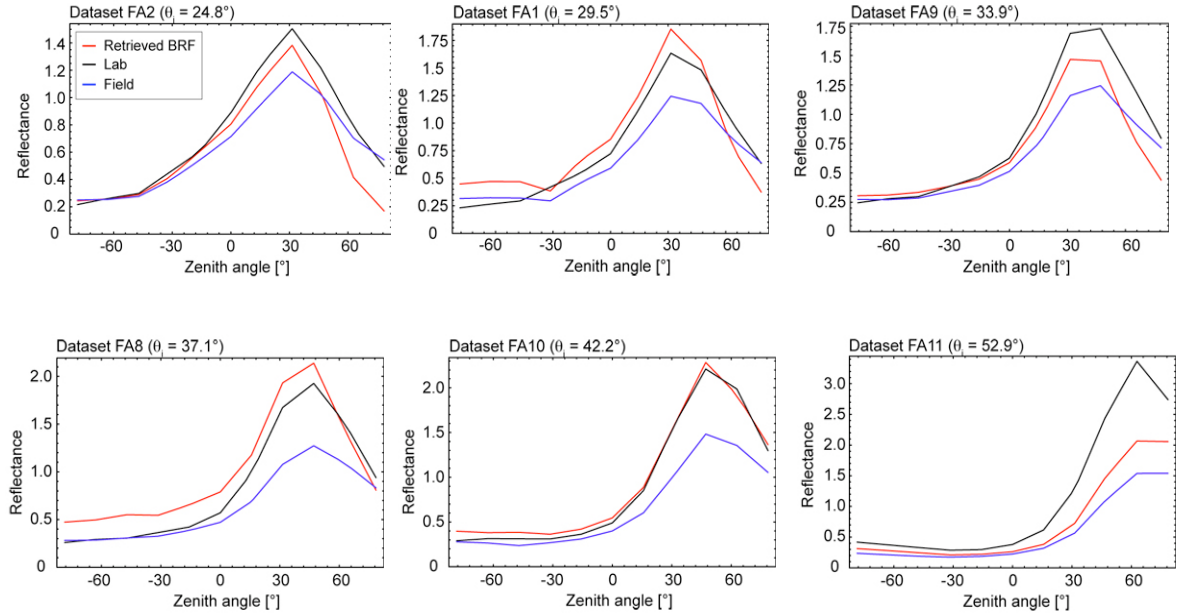

Figure 36: Comparison of BRF retrieval results and spectrodirectional field and laboratory measurements in the principal plane (-75° backward scattering to 75° forward scattering). The illumination is from the left. For the description of the datasets refer to Table 1 and Figure 26.

A specular reflectance characteristic of the artificial target is observed for all datasets. The maximum extent of the specular reflectance peak is obtained at the largest illumination zenith angle (52.9°) and consists of over 300% for the laboratory case of dataset FA11. It can be seen for all datasets that the directional reflectance characteristic for the laboratory case is more distinct than for the field case (refer to Chapter 6.1 and Figure 30). With regard to the retrieved BRF, it can be observed that in general a reasonable approximation to the laboratory reflectance is achieved and for most datasets the

specular peak is reproduced well. Best results were obtained for dataset FA10. The largest overall deviations occur for the two datasets, which were obtained at highly variable atmospheric conditions (FA1 and FA8). Furthermore, the retrieval results for large forward scattering directions tend to underestimate the laboratory reflectance. These differences might primarily be related to the needed time period and to the sampling (oversampling/undersampling) of the incoming diffuse radiances, especially for large observation angles.

6.4 Spectralon reflectance characteristics

The Spectralon analysis has been performed for two different Spectralon reference panels: a new Spectralon panel which is primarily used as laboratory standard and an old Spectralon panel which is extensively used in field campaigns. For both panels the deviation from Lambertian reflectance characteristics as well as the bidirectional reflectance factor are calculated and are shown in the following. Based on the spectrodirectional dataset obtained for nadir illumination in experiment S (see Table 3) the irradiance of the lamp has been derived for illumination zenith angles ranging from 0° to 60° using Equation (10) and the cosine law. Maximum irradiance values are observed at 750nm as can be seen in Figure 37. Compared to the solar irradiance maximum this consists of a displacement to longer wavelengths of about 200nm.

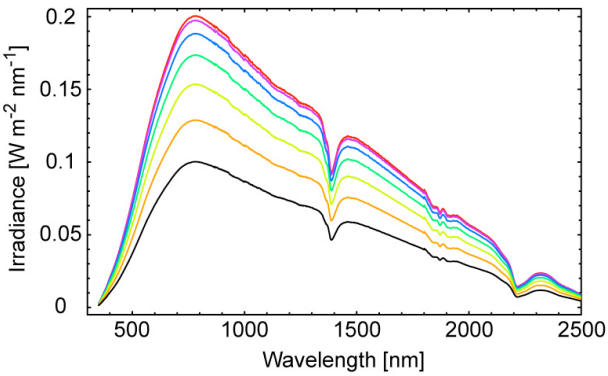

Figure 37: Irradiance of the laboratory illumination source for zenith angles of 0° (red), 10° (magenta), 20° (blue), 30° (green), 40° (yellow), 50° (orange) and 60° (black).

Spectralon reference panels are usually assumed to show a Lambertian reflectance behaviour. Using Equation (12) the deviation from Lambert has been calculated for the laboratory Spectralon panel. Figure 38 (left) displays the respective results for zenith angles ranging from 5° to 75° for a wavelength of 550nm. Since the Spectralon panel obeys Helmholtz's reciprocity law (Sandmeier et al., 1997), the zenith angles can be interpreted either as illumination angles (for nadir observation directions) or as observation angles (for nadir illumination). As can be seen the Lambertian assumption is only true for a scattering angle of 50°. For scattering angles of 5° and 75° deviations of 7% and almost 10% are obtained, respectively. Figure 38 (right) reports the deviation over a spectral range from 400nm to 2500nm. A potential wavelength dependency is found to lie within 1% for nadir illumination and the respective observation zenith angles. The results presented here deviate by less

than 2% from similar results obtained in another Spectralon study performed by Sandmeier et al. (1998).

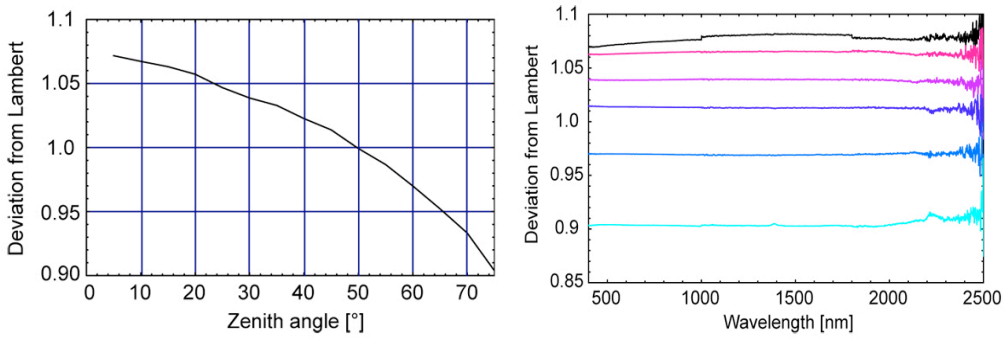

Figure 38: Deviation from Lambert of the laboratory Spectralon. Left: Directional deviation. Right: Spectral deviation for observation zenith angles of 5° (black), 15° (pink), 30° (purple), 45° (dark blue), 60° (blue) and 75° (bright blue).

Based on the above findings it can be argued that even a new Spectralon panel does not follow the Lambertian assumption. Assuming that in practical applications Spectralon reference measurements are taken from nadir this leads to an underestimation of target reflectances obtained at solar zenith angles smaller than 50° and to an overestimation for solar zenith angles larger than 50°. Consequently, a need evolves to correct for the non-Lambertian behaviour by incorporating the Spectralon BRF R_{ref} into the derivation of actual target reflectances. The Spectralon BRF R_{ref} for the usual nadir viewing is obtained using (13). Figure 39 shows R_{ref} of the laboratory Spectralon panel for various illumination angles over the spectral range from 400nm to 2500nm. Additionally, the directional reflectance characteristic at 550nm is displayed for nadir illumination and for a fine grid of observation angles. The observed inhomogeneity might not solely be attributed to the Spectralon itself, but also to slight pointing inaccuracies with the protractor setup and to minimal inhomogeneity of the illuminated area due to the lamp's bulb.

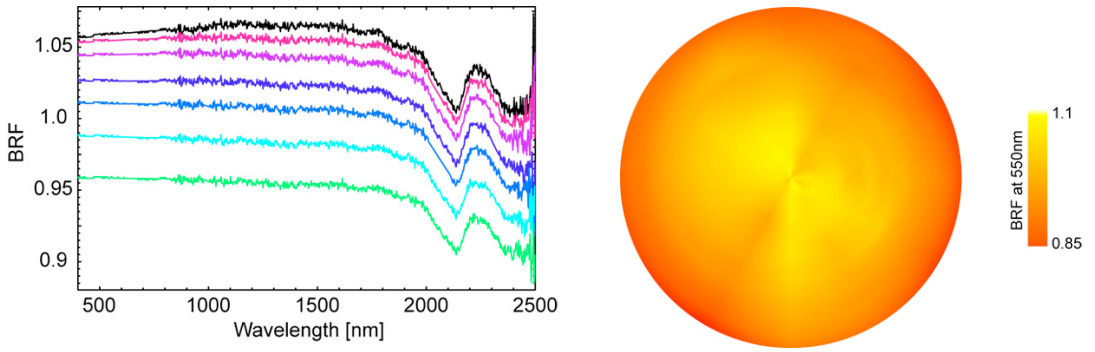

Figure 39: Left: Nadir BRF of laboratory Spectralon for illumination zenith angles of 5° (black), 10° (pink), 20° (purple), 30° (dark blue), 40° (blue), 50° (bright blue) and 60° (green). Right: BRF at 550nm for nadir illumination.

In order to keep the laboratory Spectralon panel clean and avoid unnecessary exposure to the natural illumination conditions, a different Spectralon reference is used for the field measurements presented

in this study. Over the years it has been extensively used in various field campaigns and has also been cleaned in 2006 following a well defined procedure (Anderson et al., 2002; Labsphere). Since earlier defined correction factors were not applicable anymore, the reflectance characteristics needed to be re-assessed. The calculated R_{ref} of the field Spectralon is compared to the laboratory Spectralon BRF and presented in Figure 40 for 4 different illumination zenith angles. In general, one can observe a substantial deviation from the laboratory Spectralon reference panel for all investigated cases. Surprisingly, R_{ref} of the laboratory Spectralon is even higher for an illumination zenith angle of 10°. This might be attributed to the cleaning process (e.g. polishing procedure), which may have led to a slightly specular behaviour. For small illumination angles (θ_i = 10°) and for large illumination angles (θ_i = 50°) the nadir BRF of the field Spectralon deviates by up to 10% and 18% from an ideal reflector. The best agreement to Lambert (BRF = 1) is obtained for an illumination zenith angle of 20°. Except for the typical Spectralon absorption feature at 2150nm no significant wavelength dependency could be detected. The discontinuities, which can be seen in the spectra of the field Spectralon (blue lines in Figure 40), are attributed to the detector channel transitions (an inherent problem with ASD spectroradiometers). However, especially for the field Spectralon that is less homogeneous, they might also be associated with polarization effects or with the spectroradiometer's FOV non-uniformity (refer to Chapter 2.2.1 and Figure 4).

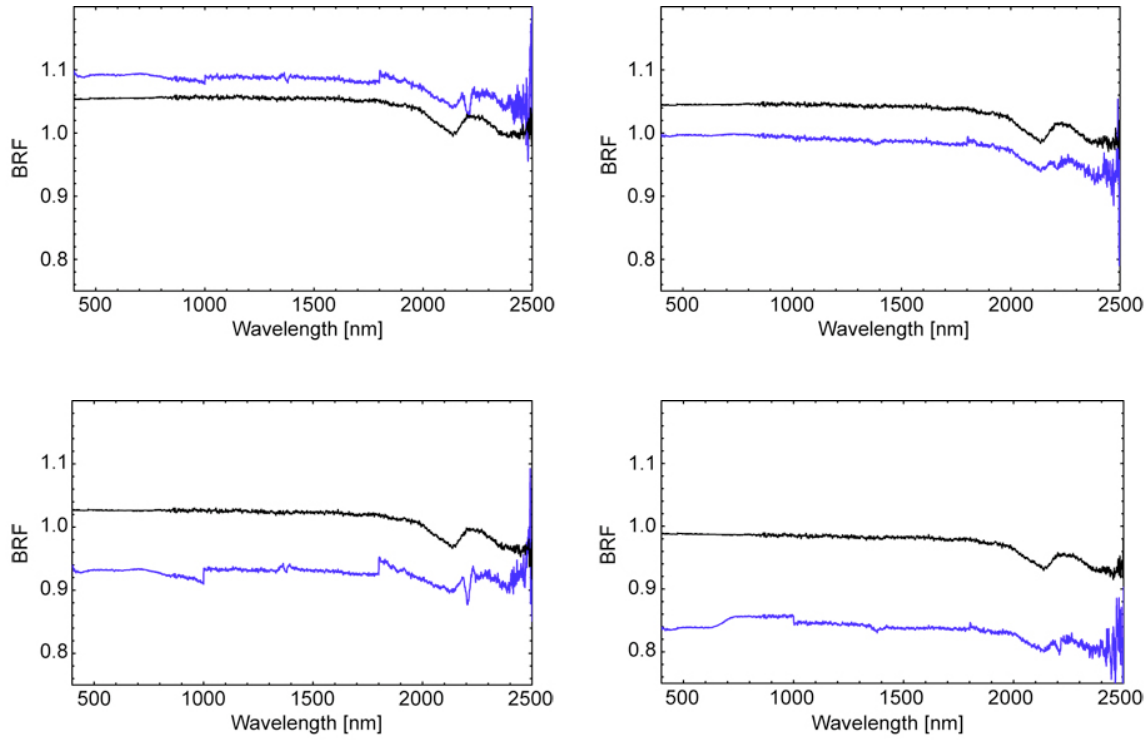

Figure 40: BRF of laboratory Spectralon (black) vs. field Spectralon (blue) illumination zenith angles of 10° (upper left), 20° (upper right), 30° (lower left) and 50° (lower right).

Based on the above results it is seen that both the laboratory Spectralon R_{ref} and the field Spectralon R_{ref} significantly deviate from the ideal reflector assumption. This needs to be considered in the determination of target reflectance values. Not doing so may lead to over- or underestimation of the actual reflectance especially for large illumination zenith angles. Furthermore, the possible assumption

that "Spectralon = Spectralon" when target reflectance measurements e.g. of different measurement campaigns or different research institutions are compared is not acceptable. This is even more important if the respective Spectralon reference panels have already been used in extensive field campaigns and their actual reflectance behaviour is not accurately known. A potential way of tracking such changes consists of integrating the Spectralon reference measurements along with the target reflectance measurements into spectral databases, e.g. SPECCHIO (Hueni et al., 2007).

7 Spectrodirectional Comparison of Spaceborne and Ground-based Reflectance Measurements

In this section a comparison of spaceborne and ground-based spectrodirectional reflectance data will be shown (Schopfer et al., 2007b). The underlying dataset has been obtained during the GonioExp06 field campaign performed in summer 2006 (Schneider et al., 2007). Ground-based bidirectional reflectance factors of a natural target were retrieved over the available spectral range using the field BRF retrieval method presented in Chapter 4 and the spaceborne multiangular dataset, which was obtained by the ESA mission CHRIS (Compact High Resolution Imaging Spectrometer) onboard PROBA-1. Since the same ground-based instrumentation and partly the same algorithms as already discussed earlier have been used, corresponding technical and instrument specific details (e.g. wavelength range, FOV, etc.) are not repeated here unless they differ.

7.1 Introduction

The contrast between the optical properties of surface elements and background and the geometric surface properties of the observed scene lead to individual anisotropic reflectance characteristics for the respective targets. Consequently, directional effects are present in all reflectance data, no matter if they are derived from ground-based or spaceborne sensor systems. Thus, they also occur in biochemistry parameters and in various vegetation indices (VI's) retrieved from multiangular data, as various studies have demonstrated (Huber et al., 2006; Huber et al., 2007a; Huber et al., 2007b; Strub et al., 2002; Verrelst et al., 2006; Verrelst et al., 2007). Such effects can be considered as noise or as a source of additional information, but in any case accurate knowledge about their magnitude and variability is important. However, for many recently developed narrowband indices they are often unknown (Verrelst et al., 2007). Typically, nadir reflectance measurements are used for deriving VI's or empirical and physical correction approaches are developed to deal with the influence of angular effects (Hu et al., 2000; Huete et al., 1992; Qi et al., 1995). In contrast, one way to profit from multiangular data is described by Gemmell et al. (2000) who showed that off-nadir viewing improved the performance of specific indices for discriminating e.g. fractional cover and leaf area index (LAI).
The objectives of this study are focused (1) on the comparison between hemispherical directional reflectance factors (HDRF) of CHRIS and retrieved bidirectional reflectance factors from dual-view goniometer measurements and (2) on the variability of selected vegetation indices for corresponding view angles in both multiangular datasets. The retrieved bidirectional reflectance factor is also compared to the actual ground-based HCRF derived from FIGOS measurements. Directional effects are then investigated for the Normalized Difference Vegetation Index (NDVI) (Tucker, 1979) and the Photochemical Reflectance Index (PRI) (Gamon et al., 1992; Gamon et al., 1997), respectively.

7.2 Data acquisition

The data for this study was acquired in summer 2006 in the framework of an extensive field campaign (Schneider et al., 2007). The study site Gilching (48°05' N, 11°17' E) is located close to the airport Oberpfaffenhofen, Germany, at an altitude of approx. 600 – 700 meters above mean sea level (amsl). Subsequent investigations were carried out using ground-based spectrodirectional dual-view FIGOS measurements and mode 5 data of the spaceborne ESA-mission CHRIS (Compact High Resolution Imaging Spectrometer) on-board PROBA-1 (Barnsley et al., 2004).

The respective field under observation was a flat vegetation area of 200m x 500m and consisted of Triticale, a hybrid between rye and wheat. At measurement time it showed a height of about 90cm with 10 – 20cm spacing among the single plants. Figure 41 shows the Triticale in a nadir view as seen from the goniometer and a lateral view, respectively.

Figure 41: Triticale target from a lateral view (left) and a nadir view (right).

7.2.1 Ground-based spectrodirectional measurements

The dual-view goniometer system FIGOS was used for the first time for spectrodirectional measurements of a vegetation target. A standard angular sampling procedure was chosen and consisted of azimuth angle steps of 30° and zenith angle steps of 15° for both the lower and the upper hemisphere. Additionally, Spectralon reference measurements were collected in the beginning and in the end of each goniometer measurement cycle as well as at every nadir bypass with the downward looking sensor. Due to the target height and in order to assure an accurate reference plane the goniometer system was positioned on 4 wooden boxes, which were covered with black textile. For further specifications of the used ASD FieldSpec 3 spectroradiometers please refer to Chapter 3.2 where the dual-view FIGOS is described in detail. Figure 42 displays the dual-view FIGOS as used for Triticale spectrodirectional measurements.

Figure 42: Dual-view FIGOS setup for acquiring spectrodirectional ground truth data. Note that the goniometer had to be raised by 80cm to assure a constant observation distance for all viewing angles and a reference plane corresponding to the top level of the vegetation canopy.

Simultaneously, an MFR-7 shadowband sunphotometer was used to directly record the total and diffuse illumination in 7 spectral bands. The direct sun irradiance is then calculated as a difference of the two, taking the respective sun zenith angle into account. In total four goniometer datasets at illumination zenith angles ranging from 24.7° to 49.2° were acquired on 24 June 2006, over the same target area as can be seen in Table 6. Unfortunately, only three datasets could be used for the subsequent BRF retrieval, since the upward looking sensor of the dual-view FIGOS produced false readings during the data take of FV3. It is assumed that this malfunctioning is related to a temporary electrical power outage. As can be seen in Figure 43, the highest atmospheric variability was observed during the acquisition of FV4 and the largest overall diffuse irradiance was present for FV1.

ID	DOY	Target	Start LT [h:min]	Period [min]	Start zenith [°]	Delta zenith [°]	Delta azimuth [°]	MFR	FIGOS
FV1	175	Triticale	09:40	23	49.2	3.8	5.1	ok	ok
FV2	175	Triticale	10:56	24	37.2	3.3	7.5	ok	ok
FV3	175	Triticale	11:57	31	29.4	2.9	13.9	ok	incomplete
FV4	175	Triticale	13:12	25	24.7	0.3	13.7	ok	ok

Table 6: Dual-view goniometer dataset of Triticale. For one dataset (FV3) no measurements of the incoming diffuse radiation could be performed.

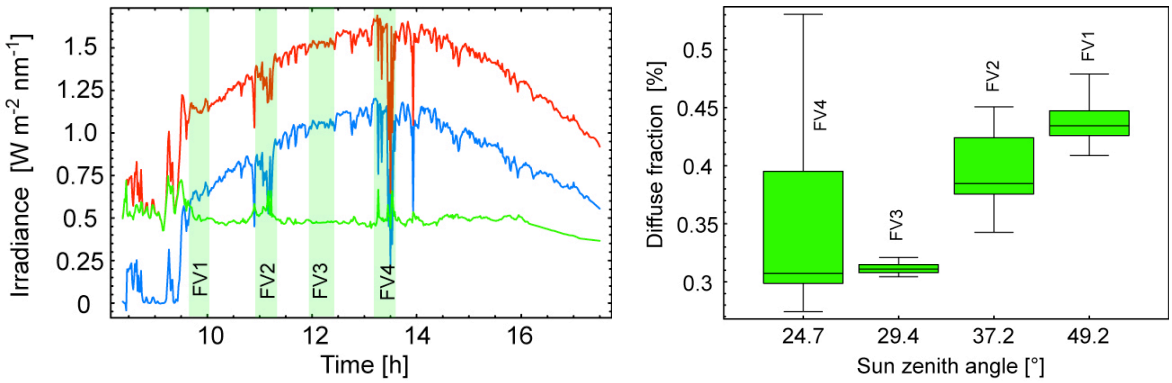

Figure 43: Left: Total (red), direct (blue) and diffuse (green) irradiance as measured with the MFR-7 sunphotometer. The vertical bars represent the time periods of the goniometer data collection. Right: Diffuse fraction calculated for the time period of the respective goniometer datasets. The vertical extent of the box represents the variability of the diffuse irradiance.

7.2.2 Spaceborne data acquisition and pre-processing

The multiangular sensor system CHRIS simultaneously supplies five viewing angles with nominal fly-by zenith angles (FZA's) at +/-55°, +/-36° and 0° (nadir) in 37 bands (mode 5, 447nm to 1035nm) with a spatial resolution of 18m. Unfortunately, only 3 images were acquired at nominal FZA's of +/-36° and nadir on June 21, 2006, over the study site Gilching. The images covered an area of 7 km x 13 km. The actual viewing zenith angles of CHRIS data acquisition rarely represent the nominal FZA's due to uncertainties in pointing. Figure 44 shows the actual view angles for the 3 images. It can also clearly be seen that the acquisition has not occurred in the solar principal plane.

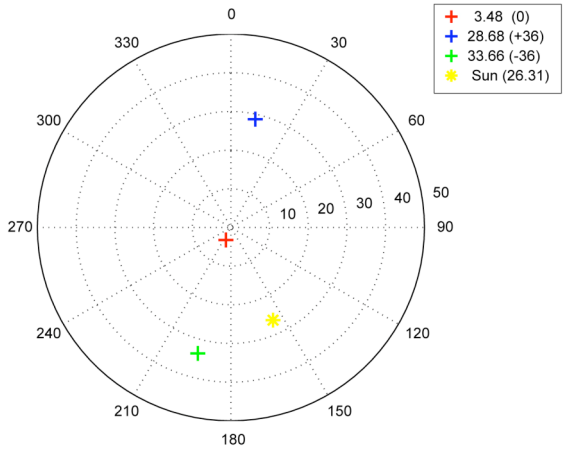

Figure 44: Acquisition geometries and illumination angles for the 3 CHRIS images. The nominal fly-by zenith angles are listed in brackets. The centre of the plot represents the nadir view of the target.

The three CHRIS multiangular acquisitions were orthorectified using a 3D physical model (Kneubühler et al., 2005; Toutin, 2004) and an SRTM derived digital elevation model (DEM), resampled to 18m using bilinear interpolation (Schläpfer et al., 2007). The resulting root mean square errors (RMSE) derived from Ground Control Points (GCP's) were at 0.66 – 0.86 pixel along track and 0.58 – 0.75 pixel across track. Subsequent atmospheric correction of the CHRIS radiance data was

performed using ATCOR-3 (Richter, 1998), which is based on MODTRAN-4. ATCOR-3 enables the processing of data from tilted sensors by accounting for varying path lengths through the atmosphere, varying transmittance and for terrain effects by incorporating digital terrain model (DTM) data and their derivatives such as slope and aspect, sky view factor and cast shadow.

7.3 Method

7.3.1 BRF retrieval for Triticale

The field BRF retrieval for Triticale is performed using the retrieval method as presented in Chapters 4.3 and 4.4 and is not discussed in detail here. The necessary input data consist of the reflected and incoming diffuse radiance measurements of the goniometer datasets FV1, FV2, and FV4, as well as of the corresponding direct irradiance measurements performed with the sunphotometer MFR-7. In order not to restrict the retrieval results to the respective sunphotometer spectral bands (6 spectral bands only), the interpolated direct irradiance values are weighted as described in Chapter 4.4.2. In doing so, a continuous spectral coverage is obtained from 414nm to 936nm. Further extrapolation to longer wavelengths is not possible since the currently used sunphotometer does not provide any interpolation points in that spectral region.

The combined retrieved BRF datasets are then used to derive the spectrodirectional reflectance signatures of Triticale for the respective solar zenith angle of CHRIS data acquisition ($\theta_{i,\ CHRIS}$ = 26.31°). This is done using linear interpolation and is acceptable since $\theta_{i,\ CHRIS}$ is close to the solar zenith angle of FV4 and lies within the range of solar zenith angles for which the BRF retrieval is actually performed. Figure 45 displays the CHRIS path projected onto the respective retrieved BRF. Further analysis of directional effects is done by referring to the CHRIS flight path as the CHRIS azimuth plane.

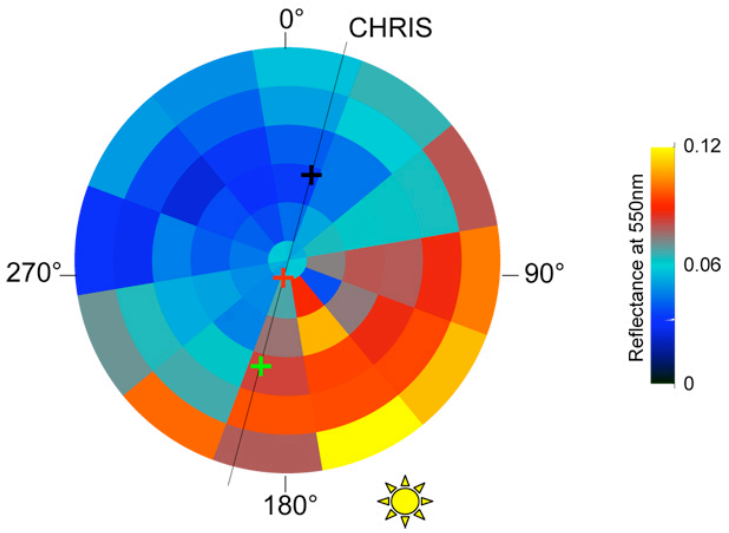

Figure 45: BRF at 550nm and CHRIS flight path (dataset FV4).

7.3.2 Determination of vegetation indices (VI's)

In a first step the retrieved BRF needed to be spectrally convolved with regard to the CHRIS centre wavelength and bandwidths. Subsequently, the BRF data were interpolated over all view angles for the respective wavelengths used for the VI determination. Directional analysis is then performed for the narrowband NDVI calculated from BRF data. The NDVI is determined according to Equation (15) using the reflectances ρ of CHRIS band 7 (661nm) and band 17 (742nm) for RED and NIR, respectively.

$$NDVI = \frac{\rho_{NIR} - \rho_{RED}}{\rho_{NIR} + \rho_{RED}}. \quad (15)$$

As a second VI the photochemical reflectance index PRI was chosen. The PRI belongs to the narrowband greenness indices and gives a measure of the efficiency with which vegetation is able to use incident light for photosynthesis (Gamon et al., 1997). Calculation of the PRI is performed according to Equation (16) using the reflectances ρ of CHRIS band 3 (530) and band 4 (570nm), respectively.

$$PRI = \frac{\rho_{530} - \rho_{570}}{\rho_{530} + \rho_{570}}. \quad (16)$$

Generally, indices were selected for wavelengths fitting within or closely approaching the centre bands of CHRIS mode 5.

Directional analysis was performed for both the total retrieved BRF dataset (observation angles ranging from -75° to 75°) and for the respective azimuth plane corresponding to real CHRIS FZA's.

7.3.3 Target subsetting

Unfortunately, the respective target area where ground-based measurements were taken was only imaged by one CHRIS FZA (-33.66°) and in total only three CHRIS images (of possible five) were available. The latter has to be attributed to the CHRIS performance and is a rather common fact. The first problem was tried to be assessed by looking for other Triticale fields, which show similar reflectance characteristics. Using a land use map of 2006 helped in finding such fields, which were identified in the available three CHRIS images. In total, four other fields consisting of Triticale were determined. However, two of them (field 1 and field 2) could not be clearly identified on the land use map, but showed very similar spectral characteristics in the CHRIS image. Figure 46 (left) indicates a spectral comparison of the four fields under question in relation to the actual Triticale field where ground sampling took place.

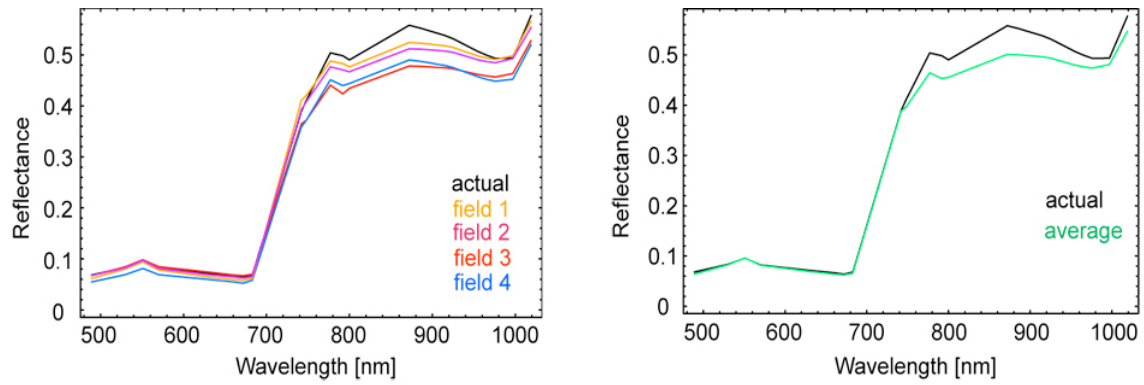

Figure 46: Left: CHRIS spectral signature of the selected Triticale fields. Right: Spectral comparison of the averaged reflectance to the reflectance of the actual Triticale field.

Triticale was knowingly grown on field 3 and field 4 although the reflectances show a remarkable offset in the near infrared range (NIR). Additionally, the spectral signature of field 4 coincides worst in the visual spectral range (VIS) and was consequently dropped. With regard to VI's analysis a good spectral agreement over the respective wavelength region is preferential. Field 1 and field 3 fulfill this criterion. However, field 1 is not proven to be Triticale. Because of that and in order to level out possible errors, an average of the two was calculated for every FZA and used for further investigation. The spectral average of the two fields is shown in Figure 46 (right) in relation to the actual field. The respective reflectance difference amounts to less than 5% for the preferential spectral range from 500nm to 760nm.

7.4 Results

7.4.1 BRF retrieval versus ground-based HCRF

In the following the retrieved BRF and the actually measured HCRF, both obtained from the goniometer dataset FV4, are compared. FV4 was measured at a similar sun position (θ_i = 24.7°) at which the CHRIS overflight took place (θ_i = 26.3°). The comparison is done in the principal plane for a wavelength of 550nm and for a nadir observation direction over the spectral range from 414nm to 936nm. As can be seen in Figure 47 (left) a continuous BRF spectrum is obtained by assessing the originally coarse spectral resolution of the direct irradiance (derived from sunphotometry) using the weight factors determined in Chapter 4.4.2. However, the strong oxygen absorption feature at 760nm could not completely be assessed and is still visible as a very slight peak. The increase in the BRF compared to HCRF consists of about 20% and 10% for the VIS and NIR part of the spectrum, respectively, and the typical spectral vegetation features (green peak at 550nm and red edge) are reproduced well.

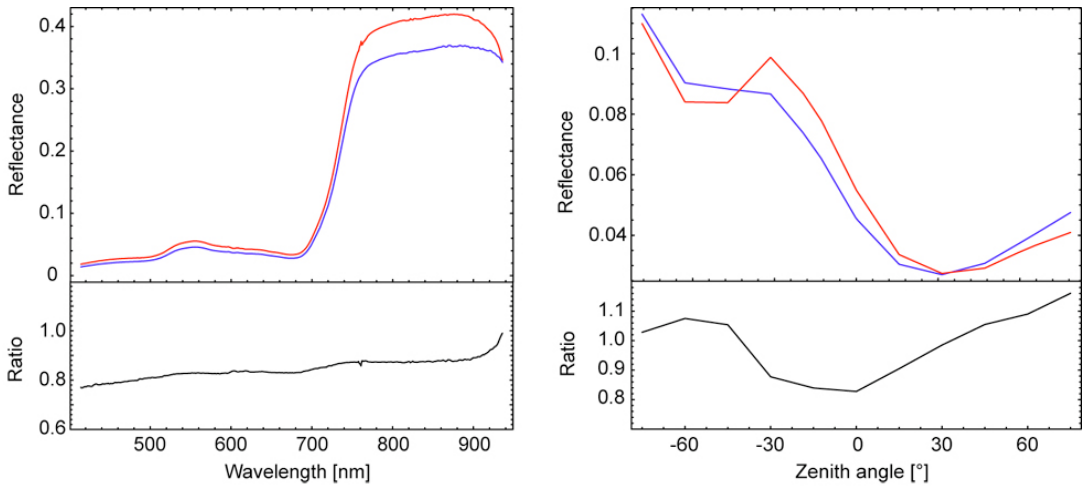

Figure 47: Left: Spectral comparison of the retrieved nadir BRF (red) and the field nadir HCRF (blue) of Triticale. Right: The same results but directionally compared at 550nm.

Figure 47 (right) shows the principal plane for observation zenith angles ranging from -75° (backscattering) to 75° (forward scattering) for a wavelength of 550nm. As already seen for the artificial target, the BRF tends to pronounce directional effects, which are mitigated in the HCRF due to the diffuse irradiance. For backward scattering directions higher BRF values (compared to HCRF) are obtained due to the increased direct irradiance and in the forward scattering lower values are attributed to the absence of the diffuse irradiance. Maximum reflectance values are typically obtained in the backward scattering close to the hotspot configuration. For the exact hotspot configuration no measurements could be taken and the respective HCRF values are interpolated. The vertically oriented (erectophile) structure of the Triticale leads to the fact that largest shadow fractions and consequently minimum reflectances are observed for 20° – 30° forward scattering directions. For larger observation zenith directions the bright ears of the Triticale start to dominate the sensor GIFOV and lead to increased reflectance values.

7.4.2 Comparison of retrieved BRF (FIGOS) and CHRIS HDRF

Figure 48 shows the retrieved BRF from dual-view FIGOS measurements for the three CHRIS FZA'S as well as a comparison to CHRIS HDRF. With respect to nadir the retrieved BRF for the corresponding CHRIS FZA's shows typically higher BRF values in the backward scattering direction and lower BRF values in the forward scattering direction. The percentage difference between backward and forward scattering BRF consists of about 50% in the VIS and 20% in the NIR. This is due to the higher reflectance level at longer wavelengths and consequently leads to less distinct directional effects in the NIR.

Due to the abovementioned target subsetting (cf. Chapter 7.3.3) the direct comparison of CHRIS HDRF and the retrieved BRF (dual-view FIGOS) is only acceptable in the spectral range from 500nm to 760nm. Largest percentage differences between CHRIS HDRF and the retrieved BRF are obtained in the RED for all three viewing directions. For the backward scattering direction CHRIS HDRF and the retrieved BRF differ by about 30% to 40% in the VIS. The nadir direction shows differences of 20% to 30% and for the forward scattering direction the differences reach up to 60% in the VIS. Part

of this disagreement might be related to specific sensor characteristics (spatial resolution) and target scale issues. The dual-view FIGOS is currently operated with a 3° FOV which results in a GIFOV of 10cm at nadir. Therefore, the FIGOS sensor signal is more affected by the small scale distribution of illuminated and shadowed areas within the canopy than this is the case for the CHRIS sensor.

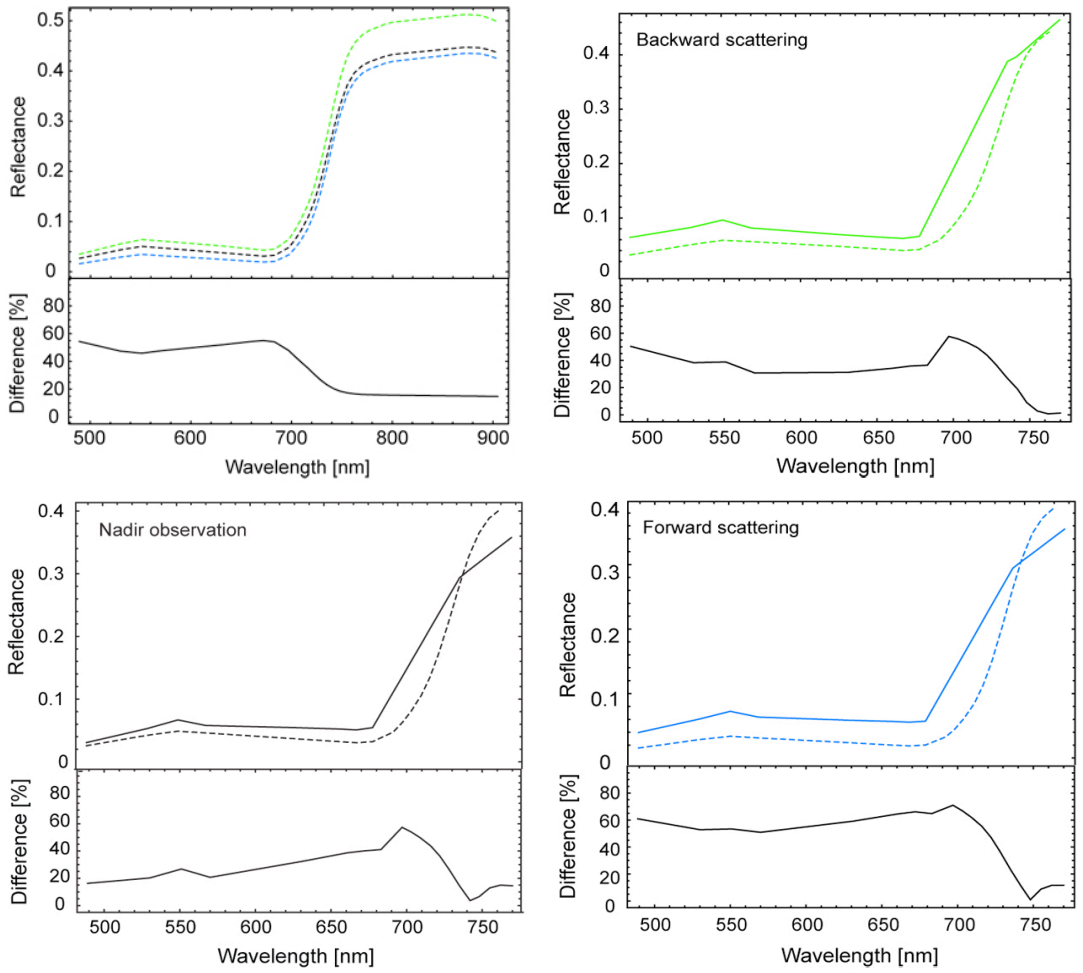

Figure 48: Spectrodirectional comparison of CHRIS HDRF (solid line) and retrieved BRF (dashed line) from FIGOS for the respective CHRIS FZA's. Top left: Retrieved BRF of Triticale for CHRIS FZA's. The colour coding for all plots is: green = backward scattering, black = nadir, blue = forward scattering.

7.4.3 Directional VI's

The NDVI and PRI are analyzed over the whole goniometer dataset for the dual-view FIGOS. For both VI's a directional dependency can be seen. For the NDVI a maximum anisotropy is reached in the forward scattering region (illumination zenith angle was 26.3° for the respective BRF dataset). Maximum directional NDVI may be explained by observing cast shadow, which decreases the RED reflectance and affects NIR reflectances only minimally. NIR reflectances are generally more affected by multiple scattering effects within the canopy. However, in the CHRIS azimuth plane a reasonable agreement with CHRIS NDVI is only obtained for backward scattering reflectances where the difference amount to about 6% only. For the other two observation directions the differences reach

12% and 20%. Figure 49 shows the NDVI distribution interpolated over all goniometer viewing angles (left) and in the CHRIS azimuth plane (right).

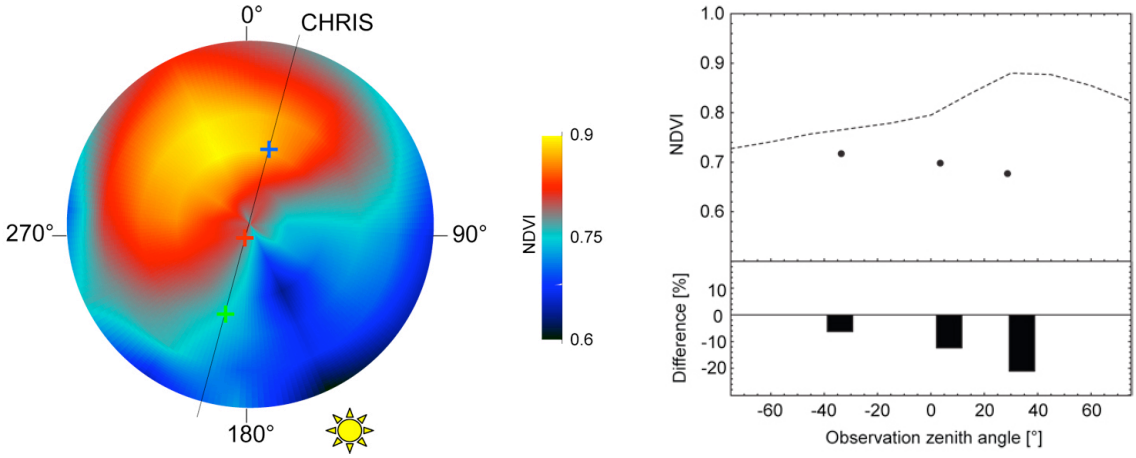

Figure 49: Left: Angular distribution of NDVI retrieved from the BRF dataset. Right: NDVI distribution derived from CHRIS HDRF (points) and from the retrieved BRF (dashed line) along the CHRIS azimuth plane.

The disagreement of CHRIS NDVI values for nadir and forward viewing directions might be related to the same reasons already mentioned above. Since less shadow is affecting the backward scattering the NDVI agreement of CHRIS and the dual-view FIGOS is better for that observation direction.

The angular distribution of the PRI values retrieved from the BRF dataset shows a similar but reverse pattern to the reflectance distribution (see Figure 45) with maximum PRI's at minimum reflectances. CHRIS PRI values reasonably agree for the nadir and the forward scattering directions. The offset for the backward scattering PRI is related to the fact that a higher reflectance value is registered for CHRIS band 3 (530nm) than for band 4 (570nm), respectively, leading to a positive PRI value. This is assumed to be related to a poor atmospheric correction due to the coarse parameterization of the aerosol model. Figure 50 shows the PRI distribution interpolated over all goniometer viewing angles (left) and in the CHRIS azimuth plane (right).

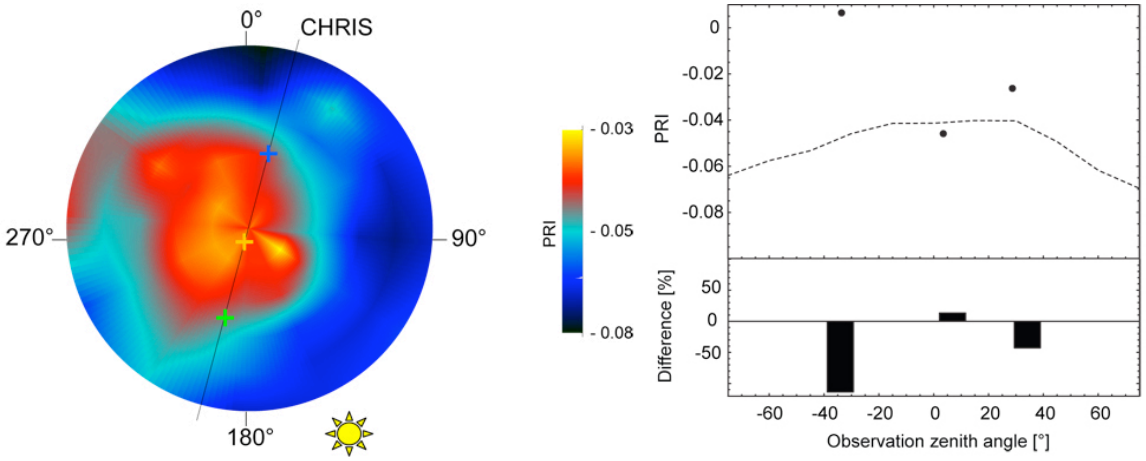

Figure 50: Left: Angular distribution of PRI retrieved from the BRF dataset. Right: PRI distribution derived from CHRIS HDRF (points) and from the retrieved BRF (dashed line) along the CHRIS azimuth plane.

8 Conclusions

8.1 Uniqueness of dual-view FIGOS

The dual-view field goniometer system FIGOS is currently the only instrument which is capable of measuring the reflected and the incoming diffuse radiation at the same angular and at high spectral resolution from 400nm to 2500nm. Another promising multiangular system, GRASS, is being developed at the National Physical Laboratory (NPL) in Teddington (UK), but has not yet reached operational status (Pegrum et al., 2006). Older goniometers such as the PARABOLA series provide a dual-view capability but operate using a limited number of bands only (Bruegge et al., 2000). The simultaneous angular collection of both the sky irradiance and the surface reflectance provides the potential of deriving accurate surface bidirectional reflectance (field BRF retrieval) as demonstrated by Martonchik et al. (1994). In doing so, the measured target reflectance can be corrected for the atmospheric influence present during the data take which also supports field-laboratory comparison studies. Furthermore, retrieved BRF from specific surfaces may serve as input or validation data for existing BRF models. Although various models are compared within the RAdiative transfer Model Intercomparison study (RAMI) no link to the "real truth" could be established so far (Widlowski et al., 2007).

8.2 Qualification of dual-view FIGOS for BRF retrieval

The dual-view goniometer system FIGOS showed a stable and reliable performance for the simultaneous collection of the reflected and incoming diffuse radiation over the respective angular and spectral range. Due to its well-known characteristics it also provides the potential to being used as a reference instrument for various spectrodirectional experiments in future field campaigns. In its present configuration, in conjunction with a sunphotometer, it proved its ability to provide the necessary dataset for a field BRF retrieval of selected targets. Although measurements in both directions are done simultaneously, the critical time to measure a complete goniometer dataset is not increased by having two instruments since both measurements are triggered simultaneously. The need for simultaneous sunphotometer measurements evolves since the direct solar irradiance (a necessary input to the retrieval algorithm) can currently not be obtained from the upward looking FIGOS sensor. Consequently, a complete retrieval dataset consists of measurements from three different instruments (two of them of the same type). This requires the use of instrument intercalibration coefficients. Since the currently used sunphotometer operates using a limited number of bands only, further pre-processing is necessary in order to obtain spectrally continuous information of the direct irradiance. This is achieved by deriving the atmospheric absorption features between the sunphotometer bands from hyperspectral Spectralon reference measurements and leads to a reasonable representation of the BRF for the respective spectral range. However, hyperspectral measurements of the direct irradiance would substantially ease data pre-processing and provide a larger spectral coverage of the retrieved BRF. A possible solution might be to attach a spectroradiometer to a sun-tracking device in order to

continuously collect the solar irradiance. Alternatively, direct irradiance values might also be obtained from simulations using MODTRAN-4 (Berk et al., 1989).

With the addition of an artificial illumination source (currently a 1000W quartz tungsten halogen lamp) the same goniometer system can also be used in a laboratory configuration as LAGOS (without dual-view option). Errors due to inherent system inaccuracies persist but are the same for both goniometer configurations. The usage of an inert, artificial target (for both the field and laboratory experiment) provides the advantage of reducing target related measurement errors and its high angular anisotropy supports FIGOS-LAGOS comparison measurements for e.g. a BRF retrieval. The laboratory setup further provides the possibility of direct comparisons to other goniometer systems currently in use (Bourgeois et al., 2006; Painter et al., 2003; Pegrum et al., 2006; Peltoniemi et al., 2005). At present, no intercalibration between different goniometer systems exists and, therefore, it is not known to what extent spectrodirectional data obtained with other goniometers are comparable. Such knowledge might be important with regard to the generation of large spectrodirectional reference databases (Hueni et al., 2007) used for e.g. model validation purposes.

8.3 Impact of irradiance changes on dual-view FIGOS results

The time period needed to obtain a complete dual-view goniometer dataset is a critical factor since illumination conditions can rapidly change either because of atmospheric changes (e.g. over passing clouds) or changes in the solar zenith angle (for large solar zenith angles the change ratio is typically larger). Short-term atmospheric variability can affect single diffuse radiance measurements differently, leading to an over- or underestimation of the incoming diffuse irradiance. On the other hand, solar zenith angle changes rather seem to affect reflected radiance measurements. Using time resolved total and diffuse sunphotometer measurements substantially improved our ability to correcting for such short-term illumination changes. Therefore, we propose to rely on the combination of dual-view goniometer measurements and continuous total and diffuse irradiance data acquisition. If, in an ideal case, all directional measurements of the two angular datasets (lower and upper hemisphere) were collected at the same time, this correction would not be necessary. Another way to reduce the influence of atmospheric changes during the time period needed would consists of changing the measurement sequence or measuring only half of the upper and lower hemisphere assuming a symmetric distribution of the target reflectance and the incident diffuse irradiance.

The absence of diffuse irradiance (as is the case for laboratory measurements) leads to typically more distinct directional features for both the artificial and the vegetation target. For the vegetation target the diffuse influence leads to a lower backward scattering and a greater forward scattering reflectance (HCRF) compared to the retrieved BRF. The underlying reason is that the backward scattering is rather dominated by the direct irradiance whereas changes in the forward scattering are related to the diffuse irradiance (Lyapustin et al., 1999).
For the artificial target a similar behaviour can partly be identified for the backward scattering reflectances. Although forward scattering reflectances slightly increase for increasing diffuse irradiance conditions, this increase might be superimposed by the strong specular reflectance, which

depends on the direct irradiance component. In laboratory measurements, the specular reflectance might additionally be attenuated by the inhomogeneity of the illuminated area within the GIFOV for corresponding observation zenith angles.

8.4 Conclusions to FIGOS-CHRIS reflectance comparison

The spectrodirectional comparison of ground-based BRF and spaceborne multiangular reflectance revealed that forward scattering reflectances seem to be more sensitive to target heterogeneity and associated canopy element scales, which both strongly affect the distribution of illuminated and shadowed target areas. Such factors are more dominant in the visible range of the spectrum and are emphasized in high absorbing spectral ranges such as the RED due to a reduced multiple scattering in this wavelength range (Sandmeier, 2004). Consequently, large errors are obtained for forward scattering directions when data of sensors with different physical characteristics (e.g. FOV/IFOV) are compared. For backward scattering directions such effects seem to be less distinct. The best agreement between CHRIS HDRF and retrieved BRF for the BLUE and GREEN is obtained for nadir viewing, although differences still reach 12% and 24%, respectively, and increase towards the RED.

The observed reflectance differences are directly influencing the resulting VI's. Since the NDVI incorporates the RED, for which directional effects are most dominant, also the corresponding NDVI values show an angular dependency, which is most distinct for forward scattering directions. Similarly, the largest differences between CHRIS NDVI and ground-based NDVI are obtained for that direction. The backward scattering observation direction provides the best NDVI agreement.

An angular dependency could also be detected for the PRI. However, for small angular deviations close to nadir the PRI seems rather stable. This agrees with Gamon (Gamon et al., 1997) who reports the PRI as well stable as long as the target brightness does not substantially change. Depending on the reflectance differences between CHRIS HDRF and the retrieved BRF for the respective PRI wavelengths, a best agreement is obtained for the nadir direction. However, for the PRI derived from CHRIS special attention has to be paid to the atmospheric correction in the visible spectral range and various aerosol models should be tested.

Since strongest directional effects are usually obtained at large observation angles in the principal plane, the fact that only three CHRIS viewing angle images were available for this study was strongly limiting directional analysis. However, the combination of multiangular spaceborne and ground-based spectrodirectional data does not only support the assessment of directional effects of VI's at various scales. It also bears the potential of improved directional calibration instead of using only nadir-view ground-truth measurements. This might especially be of importance for the forward scattering direction and when rather vertically oriented vegetation targets are observed.

9 Outlook

Comprehensive global, regional and local determinations of atmospheric, hydrological as well as vegetation and soil properties are required in order to reduce uncertainties in predictions for future climate change and associated ecosystem behaviour (Jupp et al., 2006). Progress has been made in determining physical and spectral properties of vegetation and soil surfaces. The potential of multiangular data to support terrestrial ecology research objectives is shown in an increasing number of regional case studies. However, globally applicable algorithms to derive vegetation parameters such as tree height, spatial distribution, vegetation cover, density and understory conditions from multiangular data still need to be improved. Reasons for data uncertainties are related to the challenging assessment of the anisotropic reflectance behaviour of vegetation surfaces and the spatial heterogeneity of terrestrial surfaces. Furthermore, there is still a disagreement of spatial and temporal scales between ground-based, airborne and spaceborne data acquisition and model requirements. Although RT models help understand scattering processes of various surfaces and canopy types they still rely on certain generalizations for each case.

For validation and calibration purposes of air- and spaceborne directional reflectance measurements, as well as for algorithm development and independent RT model validation there is an evolving need for ground-based directional measurements of various surface types. Such ground-based directional data acquisitions must be performed in a standardized and comprehensible way and results as well as metadata need to be well-documented and stored in corresponding functional database facilities. Current ground-based spectrodirectional measurement procedures are not standardized and it is unknown how results obtained from various goniometer systems differ. At the time, the dual-view FIGOS is the only operational hyperspectral goniometer system which is able to collect the necessary datasets in order to retrieve the surface specific BRF. Although it is well suited for such data collection and provides a reliable performance, there are also limitations, which need to be assessed.
In order to address the abovementioned requirements and account for the known gaps, following key issues are identified for future spectrodirectional measurements and research:

a) The dual-view spectrodirectional measurement setup can be further improved with respect to data collection accuracy and ease of use. One possibility consists of assessing the main limitations by reducing the measurement time period, accounting for the changing GIFOV and FOV non-uniformity of the spectroradiometer and collecting the direct irradiance over a continuous spectral range (400nm – 2500nm). However, other drawbacks (e.g. the weight, slight deviations of the zenith arc, pointing accuracy, assembly/disassembly time, etc.) are not accounted for. Another possibility consists of the acquisition of a robotic positioning system as carrier for the dual-view sensors (fibre optics). Such systems are widely used in industry (e.g. car industry, industrial automated painting etc.) and provide characteristics, which are of great usefulness for goniometers. The spatial positioning of the robotic arm is fully automatic, programmable, very fast and highly reproducible. Furthermore, such robotic systems are easy to handle in the field or in the laboratory and their free programmability allows for highly flexible, target specific angular sampling.

b) Dual-view spectrodirectional ground-based data need to be systematically collected (e.g. for CORINE landcover classes) and comprehensively stored in spectral databases. This allows not only for temporal analysis of the directional reflectance behaviour of specific surface types but also supports the long term availability and generation of a priori BRF knowledge. Furthermore, it is proposed to establish a link to the modeling community and incorporate empirically derived BRF for model validation purposes.

c) With regard to the diversity of goniometer systems and their different characteristics and measurement principles, it is a need to perform intercalibration studies with various state of the art goniometers following the example of the modeling community (cf. RAMI). Such studies need to be performed under controlled laboratory conditions using an artificial target. Additionally, it has to be agreed on a common spectrodirectional data format and quality requirements for spectrodirectional measurements have to be defined. Once this is achieved, spectrodirectional measurement results from various campaigns could easily be transferred to such a data standard in order to ensure data comparability between spectrodirectional research groups.

References

Abdou, W. A., Helmlinger, M. C., Conel, J. E., Bruegge, C. J., Pilorz, S. H., Martonchik, J. V. and Gaitley, B. J., 2000: Ground measurements of surface BRF and HDRF using PARABOLA III, *Journal of Geophysical Research*, 106 (D11), 11967-11976.

Analytical Spectral Devices Inc., 1999: Technical Guide, 4th Ed. *Analytical Spectral Devices, Inc.*, Boulder, Colorado, USA.

Anderson, N., Biggar, S., Burkhart, C., Thome, K. and Mavko, M., 2002: Bi-directional Calibration Results for the Cleaning of Spectralon Reference Panels. In: Proc. *SPIE*, Earth Observing Systems VII, W. L. B., 4814, 201-210.

Apel, O., Goerling, C., Leinhos, U., Mann, K. R. and Schaefer, B., 2000: CHARISMA: a new way for angular-resolved scattering measurements. In: Proc. *SPIE*, 4347, 569-578.

Asmail, C. C., Cromer, C. L., Proctor, J. and Hsia, J. J., 1994: Instrumentation at the National Institute of Standards and Technology for bidirectional reflectance distribution function (BRDF) measurements. In: Proc. *Stray Radiation in Optical Systems III*, SPIE, San Diego, CA, USA, 2260, 52-61.

Barnsley, M. J., Settle, J. J., Cutter, M. A., Lobb, D. R. and Teston, F., 2004: The PROBA/CHRIS mission: a low-cost smallsat for hyperspectral multiangle observations of the Earth surface and atmosphere, *IEEE Transactions on Geoscience and Remote Sensing*, 42 (7), 1512-1520.

Bausch, W. C., Lund, D. M. and Blue, M. C., 1989: Robotic data acquisition of directional reflectance factors, *Remote Sensing of Environment*, 30 (2), 159-168.

Beisl, U., 2001: Correction of bidirectional effects in imaging spectrometer data, PhD Thesis, *Department of Geography, Remote Sensing Laboratories RSL*, Zürich, Switzerland.

Berk, A., Bernstein, L. S. and Robertson, D. C., 1989: MODTRAN: A Moderate Resolution Model for LOWTRAN7. Report GL-TR-89-0122, *Air Force Geophysical Laboratory*, Bedford, MA.

Biliouris, D., vom Berge, K., Fleck, S., Nackaerts, K., Dutre, P., Muys, B., Willems, Y. and Coppin, P., 2003: CLabSpeG: A compact laboratory spectro-goniometer system enabling rapid and complete BRDF assessments of forest elements. In: Proc. *Geoscience and Remote Sensing Symposium, 2003. IGARSS '03. Proceedings. 2003 IEEE International*, 7, 4422-4424 vol.7.

Bourgeois, C. S., Ohmura, A., Schroff, K., Frei, H.-J. and Calanca, P., 2006: IAC ETH Goniospectrometer: A Tool for Hyperspectral HDRF Measurements, *Journal of Atmosphere and Oceanic Technology*, 23 (4), 573-584.

Brakke, T. W., 1994: Specular and diffuse components of radiation scattered by leaves, *Agricultural and Forest Meteorology*, 71 (3-4), 283-295.

Brakke, T. W., Wergin, W. P., Erbe, E. F. and Harnden, J. M., 1993: Seasonal variation in the structure and red reflectance of leaves from yellow poplar, Red Oak, and Red Maple, *Remote Sensing of Environment*, 43 (2), 115-130.

Breece, H. T. and Holmes, R. A., 1971: Bidirectional scattering characteristics of healthy green soybean and corn leaves in vivo, *Applied Optics*, 10 (1), 119-127.

Bruegge, C., 2004: Field Measurements of Bidirectional Reflectance. In: Reflection Properties of Vegetation and Soil. Ed(s): Schönermark, M. v., Geiger, B. and Röser, H. P., Wissenschaft und Technik Verlag, Berlin, Germany, 352.

Bruegge, C. J., Helmlinger, M. C., Conel, J. E., Gaitley, B. J. and Abdou, W. A., 2000: PARABOLA III: A sphere-scanning radiometer for field determination of surface anisotropic reflectance functions, *Remote Sensing Reviews*, 19, 75-94.

Camillo, P., 1987: A canopy reflectance model based on an analytical solution to the multiple scattering equation, *Remote Sensing of Environment*, 23, 453-477.

Chopping, M. J., 2000: Testing a LiSK BRDF Model with in Situ Bidirectional Reflectance Factor Measurements over Semiarid Grasslands, *Remote Sensing of Environment*, 74 (2), 287-312.

Coulson, K. L., 1965: Optical Reflection Properties of Natural Surfaces, *Journal of Geophysical Research*, 70 (18), 4601-4611.

Czapla-Myers, J. S., Thome, K. J. and Biggar, S. F., 2002: Optical sensor package for multiangle measurements of surface reflectance. In: Proc. *SPIE*, 4480, 326-333.

Dana, K. J. and Wang, J., 2004: Device for convenient measurement of spatially varying bidirectional reflectance, *Journal of the Optical Society of America*, 21 (1), 1-12.

Dangel, S., Kneubühler, M., Kohler, R., Schaepman, M., Schopfer, J. T., Schaepman-Strub, G. and Itten, K., 2003: Combined Field and Laboratory Goniometer System - FIGOS and LAGOS. In: Proc. *IGARSS*, Toulouse, F, 7, 4428-4430.

Dangel, S., Verstraete, M. M., Schopfer, J., Kneubühler, M., Schaepman, M. and Itten, K. I., 2005: Towards a Direct Comparison of Field and Laboratory Goniometer Measurements, *IEEE Transactions on Geoscience and Remote Sensing*, 43 (11), 2666-2675.

Deering, D. W. and Leone, P., 1986: A sphere-scanning radiometer for rapid directional measurements of sky and ground radiance, *Remote Sensing of Environment*, 19 (1), 1-24.

Demircan, A., Geiger, B., Radke, M. and Schönermark, M. v., 2000a: Bi-directional Reflectance Measurements with the CCD Line Camera WAAC, *Remote Sensing Reviews*, 19 (1-4), 95-110.

Demircan, A., Schuster, R., Radke, M., Schönermark, M. v. and Röser, H. P., 2000b: Use of a wide angle CCD line camera for BRDF measurements, *Infrared Physics & Technology*, 41, 11-19.

Despan, D. and Jacquemoud, S., 2004: Optical Properties of Soil and Leaf: Necessity and problems of modeling. In: Reflection Properties of Vegetation and Soil. Ed(s): Schönermark, M. v., Geiger, B. and Röser, H. P., Wissenschaft und Technik Verlag, Berlin, D, 39-70.

Diner, D. J., Asner, G. P., Davies, R., Knyazikhin, Y., Muller, J. P., Nolin, A. W., Pinty, B., Schaaf, C. B. and Stroeve, J., 1999: New directions in earth observing: Scientific applications of multiangle remote sensing, *Bulletin of the American Meteorological Society*, 80 (11), 2209-2228.

Ehsani, A. R. and Reagan, J. A., 1992: A Microprocessor Based Auto Sun-Tracking Multi-Channel Solar Radiometer System. In: Proc. *Geoscience and Remote Sensing Symposium, 1992. IGARSS '92. International*, Reagan, J. A., 2, 1696-1698.

ESA, 2006: The Changing Earth, New Scientific Challenges for ESA's Living Planet Programme. ESA SP-1304, *European Space Agency*, July 2006, Noordwjik, The Netherlands.

Feingersh, T., Dorigo, W. and Richter, R., 2005: A new model-driven correction factor for BRDF effects in HRS data. In: Proc. *4th EARSEeL Workshop on Imaging Spectroscopy*, Warsaw, Poland.

Gamon, J. A., Penuelas, J. and Field, C. B., 1992: A narrow-waveband spectral index that tracks diurnal changes in photosynthetic efficiency, *Remote Sensing of Environment*, 41 (1), 35-44.

Gamon, J. A., Serrano, L. and Surfus, J. S., 1997: The photochemical reflectance index: an optical indicator of photosynthetic radiation use efficiency across species, functional types, and nutrient levels, *Oecologia*, 112 (4), 492-501.

Gemmell, F. and McDonald, A. J., 2000: View Zenith Angle Effects on the Forest Information Content of Three Spectral Indices, *Remote Sensing of Environment*, 72 (2), 139-158.

GEO, 2005: Global Earth Observation System of Systems GEOSS. 10-Year Implementation Plan. GEO 1000R / ESA SP-1284, *ESA*, Noordwijk, The Netherlands.

Gibbs, D. P., Betty, C. L., Fung, A. K., Blanchard, A. J., Irons, J. R. and Balsam, W. L., 1993: Automated measurement of polarized bidirectional reflectance, *Remote Sensing of Environment*, 43 (1), 97-114.

Gobron, N., Pinty, B., Verstraete, M. M., Martonchik, J. V., Knyazikhin, Y. and Diner, D. J., 2000: Potential of multiangular spectral measurements to characterize land surfaces: Conceptual approach and exploratory application, *Journal of Geophysical Research-Atmospheres*, 105 (D13), 17539-17549.

Govaerts, Y. M., Verstraete, M. M. and Hosgood, B., 1997: Evaluation of a 3D Radiative Transfer Model against Goniometer Measurements on an Artificial Target, *Journal of Remote Sensing*, 1, 131-136.

Grailich, J., 1857: Krystallographische-optische Untersuchungen. *Kaiserliche Akademie der Wissenschaften*, Mai 30, Wien, A.

Hahlweg, C. and Rothe, H., 2005: Classification of optical surface properties and material recognition using multi-spectral BRDF data measured with a semi-hemispherical spectro-radiometer in VIS and NIR. In: Proc. *Optical Fabrication, Testing, and Metrology II*, SPIE, Jena, Germany, 5965, 59650G-12.

Hapke, B., DiMucci, D., Nelson, R. and Smythe, W., 1996: The cause of the hot spot in vegetation canopies and soils: Shadow-hiding versus coherent backscatter, *Remote Sensing of Environment*, 58 (1), 63-68.

Hapke, B. and van Horn, H., 1963: Photometric Studies of Complex Surfaces, with Applications to the Moon, *Journal of Geophysical Research*, 68 (15), 4545-4570.

Hese, S., Lucht, W., Schmullius, C., Barnsley, M., Dubayah, R., Knorr, D., Neumann, K., Riedel, T. and Schroter, K., 2005: Global biomass mapping for an improved understanding of the CO2 balance - the Earth observation mission Carbon-3D, *Remote Sensing of Environment*, 94 (1), 94-104.

Hosgood, B., Piironen, J., Andreoli, G., Koechler, C. and Sandmeier, S., 1999: Wiley Encyclopedia of Electrical and Electronics Engineering: Goniometers. Webster, J. G., John Wiley & Sons, Inc.

Hu, B., Lucht, W., Strahler, A. H., Barker Schaaf, C. and Smith, M., 2000: Surface Albedos and Angle-Corrected NDVI from AVHRR Observations of South America, *Remote Sensing of Environment*, 71 (2), 119-132.

Huber, S., Kneubühler, M., Koetz, B., Schopfer, J., Zimmerman, N. E. and Itten, K., 2007a: The Potential of Spectrodirectional CHRIS/PROBA Data for Biochemistry Estimation. In: Proc. *Envisat Symposium*, Montreux, Switzerland, SP-636, CD-ROM.

Huber, S., Kneubühler, M., Koetz, B., Schopfer, J., Zimmerman, N. E. and Itten, K. I., 2006: Canopy Biochemistry Retrieval using Spectrodirectional Information of CHRIS Data. In: Proc. *2nd International Symposium on Recent Advances in Quantitative Remote Sensing RAQRS*, in press, 24-29 Sept, Torrent (Valencia), Spain.

Huber, S., Kneubühler, M., Koetz, B., Schopfer, J. T., Zimmermann, N. E. and Itten, K. I., 2007b: Estimating Nitrogen Concentration from Directional CHRIS/PROBA Data. In: Proc. *10th International Symposium on Physical Measurements and Signatures in Remote Sensing ISPMSRS*, March 12-14, Davos, Switzerland, XXXVI, Part 7/C50, 462-467.

Hueni, A., Nieke, J., Schopfer, J., Kneubühler, M. and Itten, K., 2007: 2nd Generation of RSL's Spectrum Database SPECCHIO. In: Proc. *10th International Symposium on Physical Measurements and Signatures in Remote Sensing ISPMSRS*, Davos, Switzerland, XXXVI, Part 7/C50, 505-510.

Huete, A. R., Hua, G., Qi, J., Chehbouni, A. and van Leeuwen, W. J. D., 1992: Normalization of multidirectional red and NIR reflectances with the SAVI, *Remote Sensing of Environment*, 41 (2-3), 143-154.

International Charter, 1999: Charter on Cooperation to Achieve the coordinated Use of Space Facilities in the Event of Natural or Technological Disasters. Rev.3 (25/4/2000).2, Paris, France.

Johnson, J. R., Grundy, W. M. and Shepard, M. K., 2004: Visible/near-infrared spectrogoniometric observations and modeling of dust-coated rocks, *Icarus*, 171 (2), 546-556.

Jupp, D. L. B. and Grant, I., 2006: Open Letter. In: Proc. *4th International Workshop on Multiangular Measurements and Models, IWMMM-4*, CSIRO, 20-24 March, Sydney, Australia, CD-ROM.

Kimes, D. S., 1983: Dynamics of directional reflectance factor distribution for vegetation canopies, *Applied Optics*, 22, 1364-1372.

Kimes, D. S. and Kirchner, J. A., 1982: Irradiance measurement errors due to the assumption of a Lambertian reference panel, *Remote Sensing of Environment*, 12 (2), 141-149.

Kneubühler, M., Koetz, B., Richter, R., Schaepman, M. and Itten, K., 2005: Geometric and Radiometric Pre-processing of CHRIS/PROBA Data over Mountaineous Terrain. In: Proc. *3rd CHRIS/PROBA Workshop, Frascati (I)*, ESA Publications Division, Noordwijk, NL, 21-23 March, SP-593, CD-ROM.

Koechler, C., Hosgood, B., Andreoli, G., Schmuck, G., Verdebout, J., Pegoraro, A., Hill, J., Mehl, W., Roberts, D. and Smith, M., 1994: The European optical goniometric facility: Technical description and first experiments on spectral unmixing. In: Proc. *Geoscience and Remote Sensing Symposium, 1994. IGARSS '94. Surface and Atmospheric Remote Sensing: Technologies, Data Analysis and Interpretation*, 4, 2375-2377.

Labsphere, Spectralon Care and Handling Guidelines. *Labsphere*, North Sutton, NH 03260.

Labsphere, 2004: Calibration certificate. Report Number 44110-1-1, *Labsphere Inc.*, 28 December, Sutton, N.H.

Leroux, C., Deuzé, J.-L., Goloub, P., Sergent, C. and Fily, M., 1998: Ground measurements of the polarized bidirectional reflectance of snow in the near-infrared spectral domain: Comparisons with model results, *Journal of Geophysical Research*, 103 (D16), 19721-19732.

Li, Z.-L., Zhang, R., Sun, X., Su, H., Tang, X., Zhu, Z. and Sobrino, J. A., 2004: Experimental system for the study of the directional thermal emission of natural surfaces, *International Journal of Remote Sensing*, 25 (1), 195-204.

Lyapustin, A. I. and Privette, J. L., 1999: A new method of retrieving surface bidirectional reflectance from ground measurements: Atmospheric sensitivity study, *Journal of Geophysical Research-Atmospheres*, 104 (D6), 6257-6268.

Mac Arthur, A. A., MacLellan, C. and Malthus, T. J., 2007: Determining the FOV and Directional Response Field Spectroradiometers. In: Proc. *5th EARSeL Workshop on Imaging Spectroscopy*, 23-25 April, Bruges, Belgium, in print.

Manakos, I. and Schneider, T., 2001: Field spectroscopic measurements for the approximation of the BRDF in the frame of precision farming. In: Proc. *International Workshop on Spectroscopy Application in Precision Farming*, IKB Dürnast, Freising-Weihenstephan, D, 68-73.

Manakos, I., Schneider, T. and Bekakos, M. P., 2004: A Mobile Unit for Field Spectroradiometric Measurements, *International Journal of Neural, Parallel and Scientific Computations*, 12 (4), 525-544.

Martonchik, J. V., 1994: Retrieval of Surface Directional Reflectance Properties Using Ground Level Multiangle Measurements, *Remote Sensing of Environment*, 50 (3), 303-316.

Martonchik, J. V., Bruegge, C. and Strahler, A. H., 2000: A Review of Reflectance Nomenclature Used in Remote Sensing, *Remote Sensing Reviews*, 19 (1-4), 9-20.

Möller, W., Nikolaus, K. P. and Höpe, A., 2003: Degradation of the diffuse reflectance of Spectralon under low-level irradiation, *Metrologia*, 40, 212-215.

Nicodemus, F. E., Richmond, J. C., Hsia, J. J., Ginsberg, I. W. and Limperis, T., 1977: Geometrical Considerations and Nomenclature for Reflectance. *Institute for Basic Standards, National Bureau of Standards*, Washington D.C., USA.

Odermatt, D., Schlaepfer, D., Lehning, M., Schwikowski, M., Kneubühler, M. and Itten, K., 2005: Seasonal Study of Directional Reflectance Properties of Snow, *EARSeL eProceedings*, 4 (2), 203-244.

Oetking, P., 1966: Photometric Studies of Diffusely Reflecting Surfaces with Applications to the Brightness of the Moon, *Journal of Geophysical Research*, 71 (10), 2505-2513.

Painter, T., 2002: The Hyperspectral Bidirectional Reflectance of Snow: Modeling, Measurement and Instrumentation, PhD Thesis, *Department of Geography*, Santa Barbara, USA.

Painter, T. H., Paden, B. and Dozier, J., 2003: Automated spectro-goniometer: A spherical robot for the field measurement of the directional reflectance of snow, *Review of Scientific Instruments*, 74 (12), 5179-5188.

Pegrum, H. M., Fox, N. P., Chapman, M. and Milton, E. J., 2006: Design and testing a new instrument to measure the angular reflectance of terrestrial surfaces. In: Proc. *IEEE International Geoscience & Remote Sensing Symposium & 27th Canadian Symposium on Remote Sensing*, IEEE, Denver, Colorado, CD-ROM.

Peltoniemi, J. I., Kaasalainen, S., Naranen, J., Matikainen, L. and Piironen, J., 2005: Measurement of directional and spectral signatures of light reflectance by snow, *IEEE Transactions on Geoscience and Remote Sensing*, 43 (10), 2294-2304.

Pinty, B., Gobron, N., Widlowski, J.-L., Gerstl, S. A. W., Verstraete, M. M., Antunes, M., Bacour, C., Gascon, F., Gastellu-Etchegorry, J. P., Goel, N., Jacquemoud, S., North, P., Qin, W. and Thompson, R., 2001: Radiation transfer model intercomparison (RAMI) exercise, *Journal of Geophysical Research*, 106 (D11), 11937-11956.

Pinty, B., Widlowski, J.-L., Taberner, M., Gobron, N., Verstraete, M. M., Disney, M., Gascon, F., Gastellu-Etchegorry, J. P., Jiang, L., Kuusk, A., Lewis, P., Li, X., Ni-Meister, W., Nilson, T., North, P., Qin, W., Su, L., Tang, S., Thompson, R., Verhoef, W., Wang, J. M., Wang, J., Yan, G. and Zang, H., 2004: Radiation transfer model intercomparison (RAMI) exercise: results from the second phase, *Journal of Geophysical Research*, 109 (D06210),

Privette, J. L. and Vermote, E., 2004: The impact of atmospheric effects on directional reflectance measurements. In: Reflectance Properties of Vegetation and Soil. Ed(s): Schönermark, M. v., Geiger, B. and Röser, H. P., Wissenschaft und Technik Verlag, Berlin, D, 225-241.

Qi, J., Moran, M. S., Cabot, F. and Dedieu, G., 1995: Normalization of sun/view angle effects using spectral albedo-based vegetation indices, *Remote Sensing of Environment*, 52 (3), 207-217.

Rast, M., 2004: SPECTRA - Surface Processes and Ecosystem Changes Through Response Analysis. SP-1279(2), *ESA*.

Richter, R., 1998: Correction of Satellite Imagery Over Mountaineous Terrain, *Applied Optics*, 37 (18), 4004-4015.

Röser, H. P., Schönermark, M. v. and Radke, M., 1999: Vorrichtung und Verfahren zur Bestimmung der bidirektionalen Reflektanzverteilung, International patent registration number: PCT/DE98/00384.

Sandmeier, S., 2004: Variability of bidirectional reflection properties. In: Reflection Properties of Vegetation and Soil. Ed(s): Schönermark, M. v., Geiger, B. and Röser, H. P., Wissenschaft und Technik Verlag, Berlin, 131-146.

Sandmeier, S., Muller, C., Hosgood, B. and Andreoli, G., 1998a: Physical Mechanisms in Hyperspectral BRDF Data of Grass and Watercress, *Remote Sensing of Environment*, 66 (2), 222-233.

Sandmeier, S., Muller, C., Hosgood, B. and Andreoli, G., 1998b: Sensitivity analysis and quality assessment of laboratory BRDF data, *Remote Sensing of Environment*, 64 (2), 176-191.

Sandmeier, S., Müller, C., Hosgood, B. and Andreoli, G., 1997: Sensitivity studies of bidirectional reflectance data using the EGO/JRC goniometer facility. In: Proc. *7th International Symposium on Physical Measurements and Signatures in Remote Sensing*, Guyot, G. and Phulpin, T., A.A. Balkema Publishing, 7-11 April, Courchevel, F, 1, 357-364.

Sandmeier, S. R., 2000: Acquisition of bidirectional reflectance factor data with field goniometers, *Remote Sensing of Environment*, 73 (3), 257-269.

Sandmeier, S. R. and Itten, K. I., 1999: A field goniometer system (FIGOS) for acquisition of hyperspectral BRDF data, *IEEE Transactions on Geoscience and Remote Sensing*, 37 (2), 978-986.

Schabus, J., 1855: Bestimmung der Krystallgestalten in chemischen Laboratorien erzeugter Produkte. *Kaiserliche Akademie der Wissenschaften*, Wien, A.

Schaepman, M. and Dangel, S., 2000: Solid laboratory calibration of a non-imaging spectroradiometer, *Applied Optics*, 39 (21), 3754-3764.

Schaepman, M. E., 2006: Spectrodirectional remote sensing: From pixels to processes, *International Journal of Applied Earth Observation and Geoinformation JAG*, in press.,

Schaepman-Strub, G., Schaepman, M. E., Painter, T. H., Dangel, S. and Martonchik, J. V., 2006: Reflectance quantities in optical remote sensing--definitions and case studies, *Remote Sensing of Environment*, 103 (1), 27-42.

Schläpfer, D., Nieke, J. and Itten, K. I., 2007: Spatial PSF Nonuniformity Effects in Airborne Pushbroom Imaging Spectrometry Data, *Geoscience and Remote Sensing, IEEE Transactions on*, 45 (2), 458-468.

Schneider, T., Schopfer, J., Oppelt, N., Dorigo, W., Vreeling, W. and Gege, P., 2007: GonioExp06 - A Field Goniometer Intercomparison Campaign, in Support of Physical Model Inversion and Upscaling Methods for Hyperspectral, Multispectral RS Data. In: Proc. *Envisat Symposium*, ESA, Montreux, Switzerland, SP-636, CD-ROM.

Schneider, T., Zimmermann, S. and Manakos, I., 2004: Field Goniometer System for Accompanying Directional Measurements. In: Proc. *2nd CHRIS/Proba Workshop*, ESA/ESRIN, Frascati, Italy, SP-578, 12.

Schönermark, M. v., Geiger, B. and Röser, H. P., 2004: *Reflection Properties of Vegetation and Soil*, Berlin (Germany), Wissenschaft und Technik Verlag, 352.

Schopfer, J., Dangel, S., Kaiser, J. W., Kneubühler, M., Nieke, J., Schaepman-Strub, G., Schaepman, M. and Itten, K., 2004: Comparison of Field and Laboratory Spectrodirectional Measurements Using a Standard Artificial Target. In: Proc. *SPIE*, Maspalomas, Spain, 5570, 626-633.

Schopfer, J., Dangel, S., Kneubühler, M. and Itten, K., 2006: Spectrodirectional assessment of incoming diffuse radiation in field BRDF retrieval. In: Proc. *4th International Workshop on*

Multiangular Measurements and Models IWMMM-4, CSIRO, 20-24 March, Sydney, Australia, CD-ROM.

Schopfer, J., Dangel, S., Kneubühler, M. and Itten, K., 2007a: Dual Field-of-View Goniometer System FIGOS. In: Proc. *10th International Symposium on Physical Measurements and Signatures in Remote Sensing*, M.E. Schaepman, S. L., N.E. Groot, and M. Kneubühler, Intl. Archives of the Photogrammetry, Remote Sensing and Spatial Information Sciences ISPRS, Davos, Switzerland, XXXVI, Part 7/C50, 493-498.

Schopfer, J., Huber, S., Odermatt, D., Schneider, T., Dorigo, W., Oppelt, N., Koetz, B., Kneubühler, M. and Itten, K., 2007b: Towards a Comparison of Spaceborne and Ground-Based Spectrodirectional Reflectance Data. In: Proc. *Envisat Symposium 2007*, ESA, 23-27 April, Montreux, Switzerland, SP-636, CD-ROM.

Schröder, G., 1998: Technische Optik. 8th edition, Vogel Publishing.

Serrot, G., Bodilis, M., Briottet, X. and Cosnefroy, H., 1998: Presentation of a new BRDF measurement device. In: Proc. *EUROPTO Conference on Optics in Atmospheric Propagation and Adaptive Systems IV*, September 1998, Barcelona, Spain.

Snyder, W. C. and Wan, Z. M., 1996: Surface temperature correction for active infrared reflectance measurements of natural materials, *Applied Optics*, 35 (13), 2216-2220.

Spectra Vista Corporation, GER 3700 User Manual, Revision 3.2. New York, USA.

Steffen, K., 1987: Bidirectional reflectance of snow at 500-600nm. In: Large Scale Effects of Seasonal Snow Cover. Ed(s): Goodison, B. E., Barry, R. G. and Dozier, J., IAHS Publication, 166, 415-425.

Stockton, P. H. and Deering, D. W., 1994: PARABOLA II: a field sphere-scanning radiometer for radiance measurements of sky and ground. In: Proc. *NASA/SPIE Conference on Spin-Off Technologies from NASA for Commercial Sensors and Scientific Applications*, SPIE, San Diego, CA, USA, 2270, 115-122.

Strub, G., Beisl, U., Schaepman, M., Schlaepfer, D., Dickerhof, C. and Itten, K., 2002: Evaluation of diurnal hyperspectral HDRF data acquired with the RSL field goniometer during the DAISEX'99 campaign, *Journal of Photogrammetry and Remote Sensing*, 57 (3), 184-193.

Strub, G., Schaepman, M. E., Knyazikhin, Y. and Itten, K. I., 2003: Evaluation of spectrodirectional Alfalfa canopy data acquired during DAISEX '99, *IEEE Transactions on Geoscience and Remote Sensing*, 41 (5), 1034-1042.

Suhr, B., Gege, P., Strobel, P., Kaiser, J. W., Nieke, J., Itten, K. I. and Ulbrich, G., 2005: The Calibration Homebase for the Airborne Imaging Spectrometer APEX. In: Proc. *4th EARSeL Workshop on Imaging Spectroscopy: Imaging Spectroscopy; New Quality in Environmental Studies*, B. Zagajewski, M. S., 27-29 April, Warsaw (Poland), 577-584.

Suomalainen, J., 2006: Multiangular Spectrometry and Optical Properties of Debris Covered Surfaces, Master Thesis, *Department of Physical Sciences*, Helsinki, Finland.

Susaki, J., Hara, K., Kajiwara, K. and Honda, Y., 2004: Robust estimation of BRDF model parameters, *Remote Sensing of Environment*, 89 (1), 63-71.

Tanikawa, T., Aoki, T., Hori, M., Hachikubo, A. and Aniya, M., 2006: Snow Bidirectional Reflectance Model Using Non-Spherical Snow Particles and its Validation with Field Measurements, *EARSeL eProceedings*, 5 (2), 137-145.

Toutin, T., 2004: Review article: Geometric processing of remote sensing images: models, algorithms and methods, *International Journal of Remote Sensing*, 25 (10), 1893-1924.

Tucker, C. J., 1979: Red and photographic infrared linear combinations for monitoring vegetation, *Remote Sensing of Environment*, 8 (2), 127-150.

Turner, M. and Brown, J., 2000: The Sandmeier Field Goniometer: A Measurement Tool for bidirectional reflectance. In: Proc. *34th Aerospace Mechanisms Symposium AMS*, NASA Goddard Space Flight Center, Greenbelt, USA.

UN, 1971: Convention on Wetlands of International Importance especially as Waterfowl Habitat. In: UN Treaty Series No. 14583, Ramsar, Iran.

UN, 1994: Convention to Combat Desertification in those Countries experiencing serious Drought and/or Desertification, particularly in Africa. In: UN Treaty Series No. 33480, Paris, France.

UN Millenium Project, 2005: Investing in Development: A Practical Plan to Achieve the Millennium Development Goals. *United Nations Development Programme*, New York, USA.

UNEP, 2002: Decisions Adopted by the Conference of the Parties to the Convention on Biological Diversity at its Sixth Meeting. UNEP/CBD/6/20, April 2002, The Hague, The Netherlands.

Vanderbilt, V. C. and Grant, L., 1985: Plant Canopy Specular Reflectance Model, *Geoscience and Remote Sensing, IEEE Transactions on*, GE-23 (5), 722-730.

Verrelst, J., Koetz, B., Kneubühler, M. and Schaepman, M., 2006: Directional Sensitivity Analysis of Vegetation Indices from Multiangular CHRIS/PROBA Data. In: Proc. *ISPRS Mid-term Symposium 2006*, May 2006, Enschede, The Netherlands.

Verrelst, J., Schaepman, M. E., Koetz, B. and Kneubühler, M., 2007: Angular sensitivity analysis of vegetation indices derived from CHRIS/PROBA data, *Remote Sensing of Environment*, In Press, Corrected Proof,

Walter-Shea, E. A., Hays, C. J., Mesarch, M. A. and Jackson, R. D., 1993: An improved goniometer system for calibrating field reference-reflectance panels, *Remote Sensing of Environment*, 43 (2), 131-138.

Weiss, M., Baret, F., Myneni, R. B., Pragnere, A. and Knyazikhin, Y., 2000: Investigation of a model inversion technique to estimate canopy biophysical variables from spectral and directional reflectance data, *Agronomie*, 20 (1), 3-22.

Widlowski, J.-L., Taberner, M., Pinty, B., Bruniquel-Pinel, V., Disney, M., Fernandes, R., Gastellu-Etchegorry, J. P., Gobron, N., Kuusk, A., Qin, W., Robustelli, M., Rochdi, N., Ruiloba, R., Soler, C., Thompson, r., Verhoef, W., Verstraete, M. M. and Xie, D., 2007: The third Radiative transfer Model Intercomparison (RAMI) exercise: Documenting progress in canopy reflectance modeling, *Journal of Geophysical Research*, 112 (D09111),

WMO, 2006: Systematic Observation Requirements for Satellite-Based Products for Climate. GCOS-107 (WMO/TD No. 1338), *WMO*, September 2006, Geneva, Switzerland.

Yankee Environmental Systems, 2000: MFR-7 Rotating Shadowband Radiometer: Installation and User Guide, Version 2.10. *Yankee Environmental Systems, Inc.*, Turner Falls (MA), USA.

Acknowledgements

This thesis was supported by research grants of the Swiss National Science Foundation projects 200020-101517 and 200020-112626.

I would like to acknowledge all the contributors for their highly appreciated support, dedication and interest to accomplish this PhD thesis.
My gratitude goes especially to my promoter and supervisor Klaus Itten for his confidence, commitment and generous support during the past years to make this work possible. I would like to express my appreciation to Stefan Dangel, who supported me with the physical background and inspired the work by providing valuable thoughts and scientific ideas. He always raised the right questions at the right moment to keep me on track. I deeply acknowledge my team leader Mathias Kneubühler for sharing know-how, supporting day-to-day work of the thesis and taking care of many organizational and financial issues. I greatly appreciate the willingness of Thomas Schneider (Technical University of Munich, Germany) to review this thesis and contribute an external expertise of the work.
Special thanks go to Silvia Huber, with whom I shared up's and down's during our dissertation projects and spent many hours with scientific discussions and motivating personal conversations; Andy Hüni, who brought in interesting perspectives (let's say: observation angles) to spectrodirectional measurements and research and definitely eased spectrodirectional data handling with SPECCHIO; Ben Kötz, whose support was very valuable in the beginning of the thesis and opened the doors to the complex matters in spectroradiometer measurements and data analysis; Daniel Nüesch for his helpful motivation from a distance which initiated the writing process; Daniel Odermatt, who contributed to the success of the main field campaign in 2006 with his goniometer experience and shared many late-night working sessions; Stefan Rey for his valuable work to the goniometer systems review; Daniel Schläpfer, whose expertise was very helpful for CHRIS data processing and in many BRDF discussions and, of course, FIGOS and LAGOS for all the challenges but also their reliable performance. Further, I would like to thank all my colleagues in the SpectroLab group, at the Remote Sensing Laboratories and at the Department of Geography of the University of Zurich for the manifold support and the pleasant and motivating atmosphere.
I express my thanks to Kurt Bösiger and his team of the Physics Workshop of the University of Zurich. They significantly contributed to the construction of the dual-view FIGOS and were always available for short-term requests. Without you this would not have been possible.
I would also like to thank the people of the Limnological Station in Iffeldorf, Germany, for their great hospitality during the GonioExp06 campaign, and acknowledge the scientists from the Technical University of Munich and the DLR, Germany, who supported us in various ways.

Finally, with gratitude, I would like to thank my family and my friends, who contributed to my overall wellbeing and provided me always a change to scientific work.

Zurich, March 2008 Jürg Schopfer

Personal Bibliography

2007

Schopfer, J., Huber, S., Odermatt, D., Schneider, T., Dorigo, W., Oppelt, N., Koetz, B., Kneubühler, M. and Itten, K., 2007: Towards a Comparison of Spaceborne and Ground-Based Spectrodirectional Reflectance Data. In: Proc. Envisat Symposium 2007, ESA, 23-27 April, Montreux, Switzerland, SP-636, CD-ROM.

Schopfer, J., Dangel, S., Kneubühler, M. and Itten, K., 2007: Dual Field-of-View Goniometer System FIGOS. In: Proc. 10th International Symposium on Physical Measurements and Signatures in Remote Sensing, M.E. Schaepman, S. L., N.E. Groot, and M. Kneubühler, Intl. Archives of the Photogrammetry, Remote Sensing and Spatial Information Sciences ISPRS, Davos, Switzerland, XXXVI, Part 7/C50, 493-498.

Schneider, T., **Schopfer, J.**, Oppelt, N., Dorigo, W., Vreeling, W. and Gege, P., 2007: GonioExp06 - A Field Goniometer Intercomparison Campaign, in Support of Physical Model Inversion and Upscaling Methods for Hyperspectral, Multispectral RS Data. In: Proc. Envisat Symposium, ESA, Montreux, Switzerland, SP-636, CD-ROM.

Hueni, A., Nieke, **J., Schopfer**, J., Kneubühler, M. and Itten, K., 2007: 2nd Generation of RSL's Spectrum Database SPECCHIO. In: Proc. 10th International Symposium on Physical Measurements and Signatures in Remote Sensing ISPMSRS, Davos, Switzerland, XXXVI, Part 7/C50, 505-510.

Hueni, A., Nieke, **J., Schopfer**, J., Kneubühler, M. and Itten, K., 2007: Metadata of Spectral Data Collections. In: Proc. 5th EARSeL Workshop on Imaging Spectroscopy, Bruges, Belgium, CD-ROM.

Huber, S., Kneubühler, M., Koetz, B., **Schopfer, J.T.**, Itten, K.I., & Zimmerman, N.E. (2007). Contribution of Directional CHRIS/Proba Data for Estimating Canopy Biochemistry in Forest. Journal of Applied Remote Sensing, Under Review.

Huber, S., Kneubühler, M., Koetz, B., **Schopfer, J. T.**, Zimmermann, N. E. and Itten, K. I., 2007: Estimating Nitrogen Concentration from Directional CHRIS/PROBA Data. In: Proc. 10th International Symposium on Physical Measurements and Signatures in Remote Sensing ISPMSRS, March 12-14, Davos, Switzerland, XXXVI, Part 7/C50, 462-467.

Huber, S., Kneubühler, M., Koetz, B., **Schopfer, J.**, Zimmerman, N. E. and Itten, K., 2007: The Potential of Spectrodirectional CHRIS/PROBA Data for Biochemistry Estimation. In: Proc. Envisat Symposium, Montreux, Switzerland, SP-636, CD-ROM.

Koetz, B., Kneubühler, M., Huber, S., **Schopfer, J.** and Baret, F., 2007: Radiative Transfer Model Inversion Based on Multi-Temporal CHRIS/PROBA Data for LAI Estimation. In: Proc. 10th International Symposium on Physical Measurements and Signatures in Remote Sensing ISPMSRS, Davos, Switzerland, XXXVI, Part 7/C50, 344-349.

Malenovsky, Z., Bartholomeus, H. M., Acerbi-Junior, F. W., **Schopfer, J. T.**, Painter, T. H., Epema, G. F. and Bregt, A. K., 2007: Scaling dimensions in spectroscopy of soil and vegetation, International Journal of Applied Earth Observation and Geoinformation, 9 (2), 137-164.

2006

Schopfer, J., Dangel, S., Kneubühler, M. and Itten, K., 2006: Spectrodirectional assessment of incoming diffuse radiation in field BRDF retrieval. In: Proc. 4th International Workshop on Multiangular Measurements and Models IWMMM-4, CSIRO, 20-24 March, Sydney, Australia, CD-ROM.

Schopfer, J., Dangel, S., Kaiser, J. W., Kneubühler, M., Nieke, J., Schaepman-Strub, G., Schaepman, M. E. and Itten, K. I., 2006: Correction of the diffuse influence in spectrodirectional measurements. In: Proc. International Radiation Symposium (IRS) 2004: Current Problems in Atmospheric Radiation, Fischer, H. and Sohn, B. J., Depaak Publishing (Hampton, Virginia), 23-28 August, Busan, Korea, 371-374.

Kneubühler, M., Koetz, B., Huber, S., **Schopfer, J.**, Richter, R. and Itten, K. I., 2006: CHRIS/PROBA Data Analysis at the Swiss Midlands Testsite. In: Proc. 4th CHRIS/PROBA Workshop, 19-21 Sept, Frascati, I, CD-ROM.

Kneubühler, M., Koetz, B., Huber, S., **Schopfer, J.**, Richter, R. and Itten, K. I., 2006: Monitoring Vegetation Growth using Multitemporal CHRIS/PROBA Data. In: Proc. IEEE Geoscience and Remote Sensing Symposium (IGARSS 2006), Denver, Colorado, 2677-2680.

Huber, S., Kneubühler, M., Koetz, B., **Schopfer, J.**, Zimmerman, N. E. and Itten, K. I., 2006: Canopy Biochemistry Retrieval using Spectrodirectional Information of CHRIS Data. In: Proc. 2nd International Symposium on Recent Advances in Quantitative Remote Sensing RAQRS, in press, 24-29 Sept, Torrent (Valencia), Spain.

2005

Schopfer, J., Dangel, S., Verstraete, M. M., Kneubühler, M., Schaepman, M. and Itten, K., 2005: Intercomparison of Field and Laboratory Goniometer Measurements. In: Proc. 9th Int. Symposium on Physical Measurements and Signatures in Remote Sensing (ISPMSRS), Shunlin Liang, J. L., Xiaowen Li, Ronggao Liu, Michael Schaepman, ISPRS WG VII/1, 17-19 October, Beijing, China, XXXVI (7/W20), 465-467.

Schopfer, J., Dangel, S., Rodriguez, T., Kneubühler, M. and Itten, K., 2005: Spectrodirectional Field and Laboratory Measurements of an Artificial Target. In: Proc. 4th EARSeL Workshop on Imaging Spectroscopy, 27-29 April, Warsaw, Poland, 573-582.

Huber, S., **Schopfer, J.**, Kneubühler, M., Nieke, J. and Itten, K., 2005: A New Approach Using Various Remote Sensing Data for Vegetation Parameter Retrieval as Input to Ecosystem Models. In: Proc. CEReS International Symposium on Remote Sensing, 13-14 December, Chiba University, Japan, 209-212.

Dangel, S., Verstraete, M. M., **Schopfer, J.**, Kneubühler, M., Schaepman, M. and Itten, K. I., 2005: Towards a Direct Comparison of Field and Laboratory Goniometer Measurements, IEEE Transactions on Geoscience and Remote Sensing, 43 (11), 2666-2675.

Koetz, B., Kneubühler, M., **Schopfer, J.**, Schaepman, M. and Itten, K., 2005: Influence of Changing Background on CHRIS/PROBA Data over a Heterogeneous Canopy. In: Proc. 4th EARSeL Workshop on Imaging Spectroscopy, 27-29 April, Warsaw, 273-281.

2004

Schopfer, J., Dangel, S., Kaiser, J. W., Kneubühler, M., Nieke, J., Schaepman-Strub, G., Schaepman, M. and Itten, K., 2004: Comparison of Field and Laboratory Spectrodirectional Measurements Using a Standard Artificial Target. In: Proc. SPIE, Maspalomas, Spain, 5570, 626-633.

Huber, S., **Schopfer, J. T.**, Kneubühler, M., Nieke, J. and Itten, K., 2004: A New Approach Using Various Remote Sensing Data for Vegetation Parameter Retrieval as Input to Ecosystem Models. In: Proc. Envisat & ERS Symposium, ESA-ESTEC, 6-10 September, Salzburg, Austria, SP-572, CD-ROM.

Dangel, S., Kneubühler, M., Kohler, R., Schaepman, M., **Schopfer, J. T.**, Schaepman-Strub, G. and Itten, K., 2004: Combined Field and Laboratory Goniometer System FIGOS and LAGOS. In: Proc. 2nd SPECTRA Workshop, Rast, M., ESA/ESTEC, Noordwijk, NL, WPP-225.

2003

Dangel, S., Kneubühler, M., Kohler, R., Schaepman, M., **Schopfer, J. T.**, Schaepman-Strub, G. and Itten, K., 2003: Combined Field and Laboratory Goniometer System - FIGOS and LAGOS. In: Proc. IGARSS, Toulouse, F, 7, 4428-4430.

2002

Schaepman, M., Dangel, S., Kneubühler, M., Schlaepfer, D., Bojinski, S., Brazile, J., Koetz, B., Strub, G., Kohler, R., Popp, C., **Schopfer, J.** and Itten, K., 2002: Quantitative Field Spectroscopic Measurement Instrumentation and Techniques. In: Proc. 1st Workshop on Field Spectrometry, NERC, Southampton, UK, CD-ROM, 13.